Available online at www.sciencedirect.com

ScienceDirect

Advances in Space Research xxx (xxxx) xxx

ADVANCES IN SPACE RESEARCH (a COSPAR publication)

www.elsevier.com/locate/asr

Overview, progress and next steps for our understanding of the near-earth space radiation and plasma environment: Science and applications

Yihua Zheng [a,*], Insoo Jun [b], Weichao Tu [c], Yuri Y. Shprits [d,e,f], Wousik Kim [b], Daniel Matthiä [g], Matthias M. Meier [g], W. Kent Tobiska [h], Yoshizumi Miyoshi [i], Vania K. Jordanova [j], Natalia Y. Ganushkina [k,l], Valeriy Tenishev [m], T.P. O'Brien [n], Antoine Brunet [o], Vincent Maget [o], Jingnan Guo [p,q], Dedong Wang [d], Richard B. Horne [r], Sarah Glauert [r], Bernhard Haas [d,e], Alexander Y. Drozdov [f]

[a] *NASA Goddard Space Flight Center, Greenbelt, MD 20771, USA*
[b] *Jet Propulsion Laboratory, California Institute of Technology, Pasadena, CA 91109, USA*
[c] *Department of Physics and Astronomy, West Virginia University, Morgantown, WV 26506, USA*
[d] *GFZ German Research Centre for Geosciences, Potsdam D-14473, Germany*
[e] *Institute of Physics and Astronomy, University of Potsdam, Potsdam 51147, Germany*
[f] *Department of Earth, Planetary, and Space Sciences, University of California, Los Angeles, CA 90095, USA*
[g] *German Aerospace Center (DLR), Institute of Aerospace Medicine, Cologne, Germany*
[h] *Space Environment Technologies, Pacific Palisades, CA 90272, USA*
[i] *Institute for Space-Earth Environmental Research, Nagoya University, Graduate School of Engineering, Nagoya 464-8601, Japan*
[j] *Los Alamos National Laboratory, Los Alamos, NM 87545, USA*
[k] *University of Michigan, Ann Arbor, MI 48109, USA*
[l] *Finnish Meteorological Institute, Helsinki 00560, Finland*
[m] *NASA Marshall Space Flight Center, Huntsville, AL 35812, USA*
[n] *The Aerospace Corporation, Chantilly, VA 20151, USA*
[o] *ONERA/DPHY, Université de Toulouse, Toulouse, 31013, France*
[p] *Deep Space Exploration Laboratory/School of Earth and Space Sciences, University of Science and Technology of China, Hefei, 230026, China*
[q] *CAS Center for Excellence in Comparative Planetology USTC, Hefei 230026, China*
[r] *British Antarctic Survey, Natural Environment Research Council, Cambridge, CB3 0ET, UK*

Received 28 May 2023; received in revised form 5 May 2024; accepted 8 May 2024

Abstract

The Near-Earth Space Radiation and Plasma Environment falls within the realm of G3 Cluster (G3 refers to 'Near-Earth Radiation and Plasma Environment' of the 'Coupled Geospace System') under the COSPAR (Committee On Space Research)/International Space Weather Action Teams (ISWAT) Initiative. The diverse and dynamic particle populations from this region pose challenges from both science and space weather-impact perspectives. The G3 cluster has intimate connections with solar, heliosphere clusters, and the other Geospace ones (G1, G2) through a chain of physical processes. This paper reviews recent scientific advances in understanding this complex space environment, identifies gaps in research and space weather applications, and maps out our recommendations on priorities for the next 5–10 years.

* Corresponding author.
E-mail address: yihua.zheng@nasa.gov (Y. Zheng).

https://doi.org/10.1016/j.asr.2024.05.017
0273-1177/Published by Elsevier B.V. on behalf of COSPAR.

Keywords: Near-Earth Radiation and Plasma Environment; Space Weather Impacts on space hardware and humans; Space radiation effects at aviation altitudes; Gaps and recommendations

1. Introduction

The G3 Cluster under the COSPAR/ISWAT initiative (https://www.iswat-cospar.org/g3) mainly refers to the near-Earth radiation and plasma environment. The goal of the Cluster is to perform impact-driven model assessment; to advance scientific understanding and modeling capability of the region related to radiation impact assessment; to stay connected with other relevant clusters' progress and seek collaborative inter-cluster efforts; and to help end users with better tools and products. Five action teams have been organized under this cluster: 1. Radiation Effects at Aviation Altitudes (Lead: Kent Tobiska, Matthias M. Meier); 2. Surface Charging Effects and the Relevant Space Environment (Lead: Vania Jordanova, Natalia Ganushkina, Joseph Minow, Dave Pitchford); 3. Total dose effects (Lead: Insoo Jun, Timothy Guild); 4. Internal Charging Effects and the Relevant Space Environment (Lead: Yuri Shprits, Paul O'Brien); 5. Solar Energetic Particle Population in Geospace (Lead: Valeriy Tenishev).

The near-Earth radiation and plasma environment consists of diverse particle populations of different origins that often evolve dynamically over time and space and span a broad energy range. Such an environment poses challenges from both science and space weather-impact perspectives. It brings about deleterious effects on spacecraft electronics, materials, and it can pose a significant health challenge for life in space. End users include those involved in satellite design, launch, operations, and anomaly resolution; flight crew and passengers (aviation); emergency management personnel (dealing with radio communication problems due to polar cap absorption during large solar energetic particle events); astronauts and space travelers; stakeholders and policymakers.

Fig. 1 summarizes the major space weather impacts and their environmental sources for the G3 Cluster. Ring current, aurora and plasma sheet particles can be potential space environmental sources for surface charging (e.g., Ganushkina et al., 2017). Electrons with energy greater than 100 keV and up to several MeV (mainly from radiation belt electrons) are responsible for internal charging. Strict energy limits for surface charging and internal charging can be ambiguous as the effects are highly dependent on the materials. Galactic Cosmic Rays (GCRs) are high-energy particles, ranging from tens of MeV to many GeVs and beyond, that originate outside our solar system from e.g., supernova explosions. Solar Energetic Particles (SEPs), on the other hand, are energized during solar eruptive events or from the interaction of the suprathermal proton population with CME (Coronal Mass Ejection) −driven shocks, with energies ranging from a few keV up to tens GeV. These particles can reach the near-Earth region depending on their energy and the strength/variations of fields they propagate through. GCRs, SEPs, and trapped protons in the inner radiation belt are the three main sources of radiation hazards for space hardware, avionics, and human activities in space and at aviation altitude. These sources can cause single-event effects (SEEs) and total dose (TD) effects, which can have detrimental effects on equipment and cause radiation impacts on humans (Dyer et al., 2023). Another significant source of radiation exposure in Low Earth Orbit (LEO) is albedo protons (also albedo neutrons). These protons are produced by the interaction of high-energy SEP and GCR particles with the Earth's atmosphere. This constitutes a prime source of high-energy protons trapped in the Earth radiation belts (e.g., Selesnick et al., 2014; Combier et al., 2017), especially during solar minimum. Energetic electrons (>100 keV), protons (>10 MeV), heavy ions, and neutrons can lead to TD effects over time. The intricacies of radiation effects from neutrons are shown in the handbook of European Cooperation for Space Standardization ECSS-E-HB-10-12A, but not the focus of this review. Polar Cap Absorption (PCA) has also been recognized since the early days of short-wave communication during which SEPs from solar eruptive events produce intense ionization in the lower ionosphere and give rise to heavy absorption of radio waves, which results in a complete disruption of radio communications in the High Frequency (HF) band at high latitudes (e.g., Rose and Ziauddin, 1962; Bailey, 1964; Fiori et al., 2022). PCA led to the brief HF communication outage experienced by Air Force One enroute to China during the 25–27 April 1984 solar/SEP event (National Research Council, 2008). PCA also affects satellite communications and operations of Global Navigation Satellite Systems (GNSS). Usually unrecognized, SEPs and GCRs have a significant impact on the composition of the Earth's atmosphere. These particles enhance the atmospheric concentration of NOx (Nitrogen Oxides) and HOx (Hydrogen Oxides), which play a crucial role in the ozone balance (e.g., Andersson et al., 2014; Maliniemi et al., 2022) in the middle atmosphere by catalytically destroying odd oxygen.

The G3 cluster has intimate connections with clusters of solar, heliosphere and others in the coupled geospace domain. The circles in Fig. 2 indicate such connections and G3's direct space weather impacts. Please see Reiss et al. (2023) for Cluster S2 (Ambient solar magnetic field: heating and spectral irradiance) review; Linton et al. (2023) titled 'Recent Progress on Understanding Coronal Mass Ejection/Flare Onset by a NASA Living with a Star Focused Science Team' that is relevant to Cluster S3 (Solar eruptions); Guo et al. (2024) for the review of Cluster H3 (Radiation environment in heliosphere); Temmer et al.

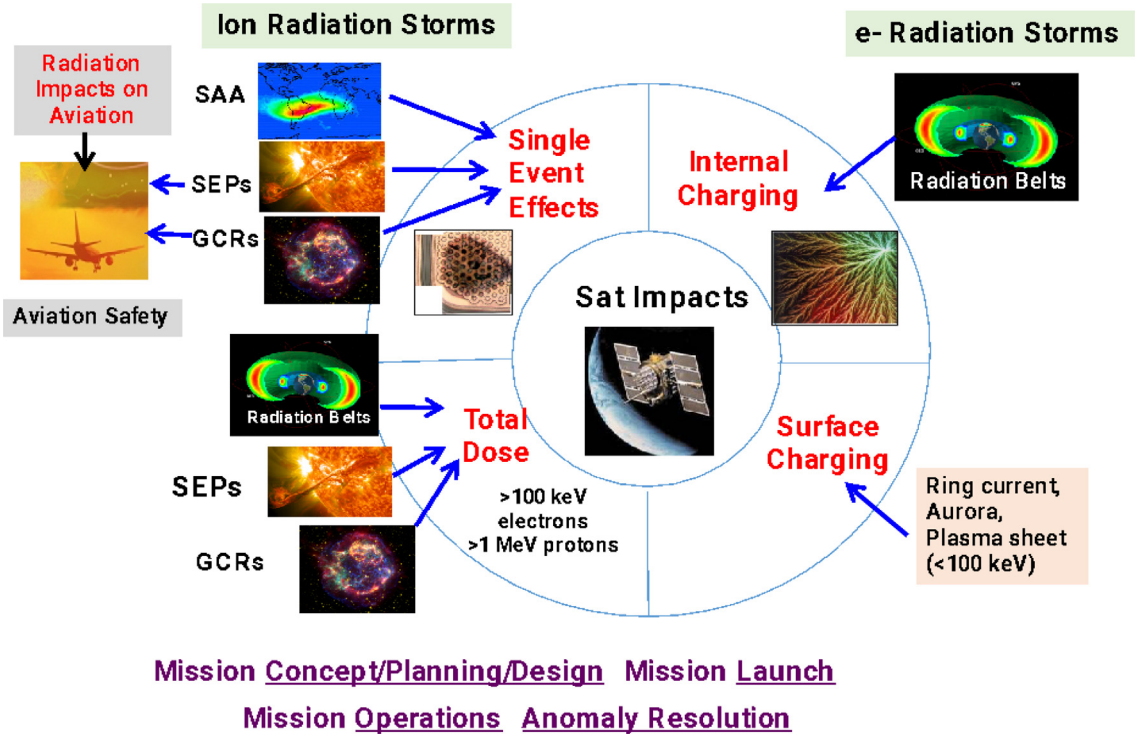

Fig. 1. The main space weather impacts and their environmental sources for the G3 Cluster (Zheng et al., 2019).

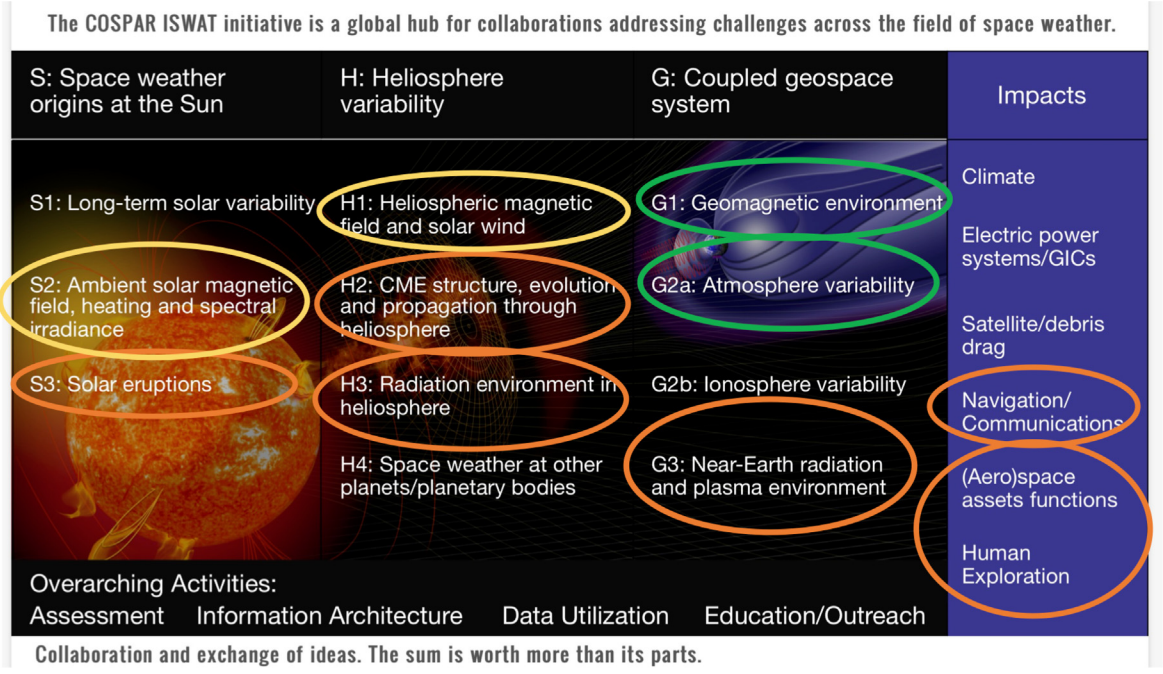

Fig. 2. G3's connection with other clusters in the overall ISWAT initiative and G3's direct space weather impacts.

(2023) for the review of H1 and H2; and Georgoulis et al. (2024) for 'Prediction of solar energetic events impacting space weather conditions'. Through energetic particle precipitation (from SEPs, GCRs, radiation belt electrons and ring current particles, an illustration of such impact on the atmosphere is provided in Fig. 3 (Baker et al., 2012; Mironova et al., 2015; Sinnhuber and Funke, 2020) and magnetic field variations brought about by the ring current, G3 has influences on G1 and G2, therefore contributing to other impacts such as geomagnetically induced currents.

Due to the complexities of cluster G3, the diverse populations of particles involved, and its rich and far-reaching space weather impacts (e.g., Allen, 2010; Koons et al.,

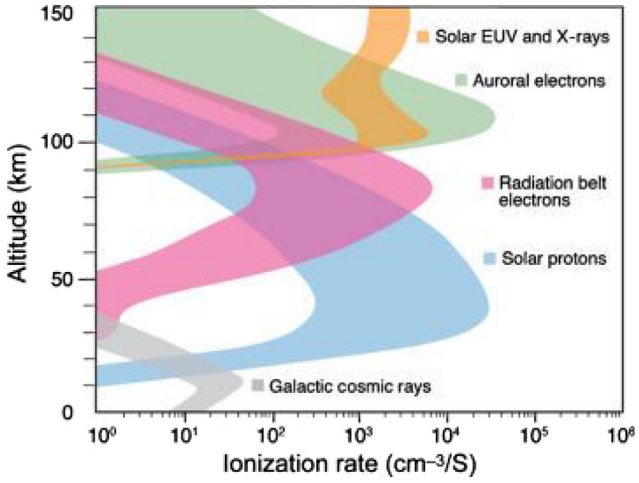

Fig. 3. Sketch showing how different particle precipitation (plus solar irradiance) affects the ionization rate of the atmosphere. From Mironova et al. (2015) that was based on the original figure by Baker et al. (2012).

2000), this review reflects the limited yet unique views of this important region of space, focusing on recent progress, gaps in research and applications, and our recommendations on priorities for the next 5–10 years by taking heed of both science and space weather operational needs. For the mission design, technological and engineering aspects of the G3 cluster where climatological/empirical models are utilized and more appropriate, please see the review by Jun et al., 2024 (titled 'A Review on Radiation Environment Pathways to Impacts: Radiation Effects, Relevant Empirical Environment Models, and Future Needs', this issue).

The discussion is roughly grouped by different impacts. Section 2 provides a short introduction to the impacts; Section 3 describes relevant environment and environment models including current scientific understanding of each population. Section 4 identifies gaps in each impact area and makes recommendations for the next steps that need to be taken. Summary is provided in Section 5.

2. Short introduction of the space weather impacts in the near-earth space

In this section, a brief introduction is provided regarding the common radiation and plasma impacts that space missions could experience in near-Earth space. The following table shows a snapshot of the impact types and which section of the relevant radiation environments are covered in this paper (Table 1).

Note that as can be seen in the table, some of the environments are common denominators for two or more impacts. Therefore, the review of those environments will be covered only in one section.

2.1. Surface charging

Spacecraft surface charging is the accumulation of net electric charge, and therefore potential, on the exterior surface(s) of a spacecraft. The fundamental physical process for surface charging is that of current balance: at equilibrium (typically achieved in milliseconds for the overall spacecraft, seconds to minutes on isolated surfaces relative to vehicle ground, and up to hours between surfaces), all currents sum to zero.

As emphasized in a companion paper (Minow et al., 2024, this issue), there is no clear dichotomy between surface charging and internal charging just from the electron energy range point of view. When the term 'surface charging' is used in the scientific and engineering community, generally, it is used to imply that the effect is caused by the lower energy part (without being specific about what 'the lower part…' actually means) of electrons and ions from space environment perspective (other contributing sources are secondary electrons, ions, backscattering electrons and photoelectrons (Minow et al., 2024)). On the contrary, 'internal charging' implies the relevance of the higher energy part of the electron spectrum, with an electron energy of some 100's keV often identified for the lower electron energy limit for internal charging. In fact, much like there is continuous electron energy spectrum, there exists a continuous spectrum of charging effects. Electron range and material thickness is also a consideration for what is surface and internal charging. Charging of a thick material by electrons with energies of only 10's to a few 100's keV may be considered surface charging when the material thickness is much greater than the electron range. In contrast, charging of thin materials such as the polymer substrate in a thermal blanket layer, paint on the surface of a spacecraft, or dielectric optical coatings by electrons of a few 10's of keV may be considered internal charging when the concern is the buildup of charge density within the volume of the thin materials. A 'better' approach might be to describe 'surface charging' as being the situation where illumination (photoelectron

Table 1
Impact types, their corresponding environment and section.

Impact Type	Relevant Environments	Sections
Surface Charging	Electron and ion plasma	2.1
Internal Charging	Trapped electrons (fluence)	2.2
Single Event Effects	Trapped protons, Galactic cosmic rays, solar energetic particles	2.3
Aviation	Galactic cosmic ray and solar protons (fluence) Geomagnetic cutoff	2.4
Total Dose	Trapped electrons and protons, solar protons (fluence), and albedo neutrons	2.5

contribution in Equation 1 in Minow et al., 2024) is an important factor and then to describe 'shallow charging' and 'deep charging'' (or 'internal charging') as the situations where electron energy is the sole discriminator and illumination is not relevant. Another way to distinguish them is that surface charging is governed by the current balance on a surface while internal charging is governed by the charge balance in a material volume.

This said, we still can say the radiation environment mostly relevant with surface charging would be low energy electron/ion plasma covering energies from a few tens of eV to a few tens of keV.

A detailed review of different aspects of surface charging can be found in Minow et al. (2024). The official NASA handbook NASA-HDBK-4002B (NASA, 2022), the European documents ECSS-E- ST-20-06C (ECSS 'A', 2019) and ECSS-E-HB-20-06A (ECSS 'B', 2019), and the JAXA document JERG-2-211A (JAXA, 2012) including wealth of information on charging and discharging design standard and mitigation measures.

2.2. Internal charging

Spacecraft encounter electron environments with a broad spectrum. Electrons with sufficient energies may penetrate the spacecraft structure or electronics chassis and deposit their charge within dielectrics or floating conductors. Electrons can be accumulated in dielectrics over time due to dielectrics' very low conductivity. The accumulation of charge in dielectrics such as circuit boards can result in arcing (electrostatic discharge) when the electric field becomes larger than the dielectrics' breakdown threshold electric field, and in turn, directly damage sensitive components in circuit boards. Indeed, numerous spacecraft anomalies and failures have been attributed to this internal charging (Koons et al., 2000), which is also interchangeably called internal electrostatic discharge (IESD), deep dielectric charging, or bulk dielectric charging.

As stated in Section 2.1, often, internal charging and surface charging are distinguished by the electron energies causing these effects, however, there are no strict energy limits for these effects. Another main difference between internal charging and surface charging is the time scale. Typically, the time scale of surface charging is less than one second and that of internal charging is longer than one hour. Surface discharges occur on or near the outer surface of a spacecraft and discharges often have to be coupled to sensitive electronics, which usually accompanies large attenuation. Internal charging, by contrast, may be caused by energetic particles that can penetrate and deposit charge very close to a victim site, and cause a discharge directly to a victim pin or wire with very little attenuation. As such, internal charging represents a potentially more severe threat to spacecraft systems. IESD is a result of a complex interplay of many different factors including the specific mission design, the mission's radiation environment, material properties, material geometry, and shielding. Among all these factors, the radiation environment is mostly relevant to the scope of this paper. Therefore, this review focuses on the physics and modeling of the high-energy electron environment relevant to IESD. They are mainly trapped electrons in the Earth's radiation belt.

2.3. Single event effects

Single Event Effect (SEE) is a transient effect in which a single particle with relatively high Linear Energy Transfer (LET) can cause an ionization trail along the particle path in the sensitive volume within an electrical, electronic, or electromechanical (EEE) device, sufficient to cause temporary changes in a circuit state or catastrophic system failures. The most directly relevant radiation sources for SEE are: GCRs, SEPs, Earth's inner radiation belt, and atmospheric secondary neutrons.

Composed of protons and heavy ions, GCRs exhibit low-intensity levels. The GCR environment in near-Earth space is subject to solar cycle modulation, anticorrelated with the sunspot number. GCRs also exhibit Forbush decreases associated with magnetic activity due to passage of interplanetary CMEs and/or high speed streams. For the GCR component that causes SEE, there are no large dynamic effects. The far more episodic, dynamic, and highly unpredictable source of protons (and heavy ions) for space missions is SEP events. During these events, the SEE hazard to space assets can increase many orders of magnitude over GCR levels. Finally, trapped protons contribute to the SEE risk for satellites, especially those that traverse the inner Van Allen belt called the South Atlantic Anomaly (SAA). The recent PAMELA (Payload for Antimatter Matter Exploration and Light-nuclei Astrophysics) results extend the observational range for the trapped radiation down to lower L-shells (~1.1 RE) and up to the highest kinetic energies (4 GeV), significantly improving the specification of the low-altitude radiation environment where current models suffer from the largest uncertainties (e.g., Adriani et al., 2015). How neutron fluxes associated with the SAA region evolve with geomagnetic conditions and altitudes need further investigations. The recent 'Atlantic Kiss' measurement campaign indicates that no additional radiation exposure could be detected for commercial flights (at an altitude of ~13 km) traveling through the geographical region of the SAA during a geomagnetically quiet period (Meier et al., 2023). Research results of the SAMADHA (South Atlantic Magnetic Anomaly Dosimetry at High Altitude) collaboration have not shown unambiguous evidence of neutron flux enhancement during geomagnetic storms (Vigorito et al., 2023).

There are many different categorizations of SEE. Some examples of SEEs are listed in Table 2.

2.4. Aviation

The interactions of cosmic particles of galactic and solar origin with the constituents of the Earth's atmosphere gen-

Table 2
Examples of Single Event Effects.

Soft Errors (no permanent damage)	
Single Event Upset	Non-permanent change of state of a "bit" caused by creation of free charge by passage or interaction of radiation
MBU/MCU	Multiple Bit/Cell Upset: in an MBU/MCU, multiple bits or memory cells can flip their states simultaneously, leading to a more significant error in the data stored in the device.
Single Event Transients	Single strike on a logic element can induce a pulse on output line that may not be adequately filtered and so propagate, introducing logic errors
Single Event Functional Interrupt	In complex logic devices (e.g., ASICS (Application Specific Integrated Circuits)), a strike inducing a logic change can disrupt the program execution in unpredictable ways
Hard Errors (permanent damage to device/circuit)	
Single Event Latchup	Permanent (but protectable) damage to a component through creation of parasitic current path by passage or interaction of radiation
Single Event Hard Errors	They are unexpected and typically rare events that can occur in electronic devices, particularly in integrated circuits, due to various types of radiation-induced disturbances.
Single-Event Dielectric Rupture	Can cause the insulating layers to break down and create a conductive path between adjacent conductors, which can lead to permanent damage or failure of the device.
Single Event Burnout (SEB)	Can occur in power transistors, such as MOSFETs (Metal-Oxide-Semiconductor Field-Effect Transistors). SEB can cause the transistor to become permanently conducting and thus causing a short circuit between the source and drain terminals of the device.
Single Event Gate Rupture	Occurs when the energy deposited by the particle causes the formation of a conductive path through the gate oxide, which can result in a high current flow through the device and eventual failure.

erate a complex secondary radiation field that results in an increased radiation exposure at flight altitudes in comparison with ground level (Meier et al., 2020; Mertens and Tobiska, 2021). While the influence of the magnetosphere and the atmospheric depth on the radiation exposure due to the galactic cosmic radiation can be modelled with reasonable accuracy, the assessment of the impacts of strong solar particle events (SPEs) on the atmospheric radiation environment poses a challenge and is subject to unknown uncertainties as well. The magnetic shielding effects from dynamically varying Earth's magnetic fields during storm times add additional complexities and modeling uncertainties.

The International Commission on Radiological Protection (ICRP) already recommended treating the exposures of aircrew due to cosmic radiation as occupational radiation exposures in 1990 (ICRP, 1990). This recommendation was adopted by the European Union (EU) in 1996 and became effective as legal regulation within the member states of the EU in 2000 (EURATOM, 1996). An amendment from 2013 further ameliorated the radiation protection standards of aircrew in the EU EURATOM, 2014) based on the most recent recommendations of the ICRP from 2007 (ICRP, 2007). Although the ICRP recommendations have not been implemented in binding U.S. legislation yet, U.S. aircrews are also considered occupationally exposed to ionizing radiation. The U.S. Federal Aviation Administration (FAA) has actively supported research into the unique ionizing radiation environment of aviation since the 1960s and the FAA has adopted a mostly advisory role for airmen and air-carriers, publishing Advisory Circulars, e.g., (FAA, 2014), educational documents (Friedberg and Copeland, 2003, 2011), and technical reports, e.g., (Copeland, 2018). The interested reader is referred to (Meier et al., 2020) for more detailed information.

Furthermore, the interaction of radiation with matter may lead to malfunctions in avionics, active implanted medical devices of passengers, aircraft power electronics due to the increasing trend of MEA (More Electric Aircraft) (Dobynde et al., 2023), and the disruption of radio communications due to ionospheric effects. According to the U.S. Code of Federal Regulations, Title 14, Part 121, Subpart E § 121.99 it is mandatory for U.S. aircraft operators to "show that a two-way communication system, or other means of communication approved by the responsible Flight Standards office, is available over the entire route" (Meier et al., 2020).

2.5. Total dose

Total dose effects in material, electronic, and photonic parts is a cumulative, long-term degradation due to ionizing or non-ionizing radiation—mainly primary protons and electrons but secondary particles arising from interactions between these primary particles and spacecraft materials can also contribute. For the case of Total Ionizing Dose (TID), the concern is mainly its effects in surface materials, insulating regions of metal-oxide semiconductors (MOS), and bipolar devices, most composed of SiO_2 (Silicon Dioxide).

]Displacement Damage Dose (DDD) is also a cumulative effect caused when the incident radiation displaces atoms in surface material, a semiconductor lattice or optical material. This produces defects that result in material property changes such as darkening, carrier lifetime shortening, mobility decreases, and degradation of optical transmission. DDD effects are commonly observed in components such as bipolar devices, solar cells, charge-coupled devices (CCDs), focal planes, and optocouplers.

The near-Earth radiation environments that are relevant to total dose include trapped particles in the Earth's radiation belts and the proton "fluence" of SEP events.

3. Recent advances in near-earth plasma and radiation environment

3.1. Relevant to surface charging

Environmental sources for surface charging include the ring current and aurora region. Auroral charging is discussed in Minow et al. (2024). Another reason why we focus on the ring current population for surface charging is that aurora and aurora physics are under G1 cluster (Opgenoorth et al., 2024) based on the ISWAT structure although a counter argument is that ring current, aurora, plasmasphere, and radiation belt have intimate connections (Goldstein et al., 2005; Brandt et al., 2013; Pierrard et al., 2021; Wang et al., 2020; Thaller et al., 2022).

Ring current (including electrons and ions of different species), radiation belts, and cold plasma of a few eVs in the plasmasphere coexist and interact with each other via field variations, wave-particle interactions and different cross-scale and cross-energy coupling processes. This interconnected system and its coupling to the surrounding regions including ionosphere-thermosphere-mesosphere and the plasma sheet/tail has been studied and recognized for many years (e.g., Zheng et al., 2009; Yu et al., 2019a, Miyoshi et al., 2018). How different ring current particles (ions and electrons) and radiation belt electrons respond to different types of solar wind or its substructures have also been investigated (e.g., Mouikis et al. (2019); Pandya et al. (2022); Miyoshi and Kataoka (2005); Kilpua et al. (2015, 2019); Kepko and Viall (2019); Koskinen and Kilpua (2022) and references therein). Fig. 4 (Yu et al., 2019a) illustrates the cross-region, cross-energy, cross-scale coupling and interconnections of the near-Earth region.

Even though ring current electrons only carry 10–25 % of plasma pressure in the near-Earth region, they are the primary source of surface charging in the region. From the energy content perspective, Zhao et al. (2016) found that the electron energy content is usually much smaller than that of ions, and that the enhancement of ring current electron energy content during the moderate storm can increase to ~30 % of that of ring current ions, indicating a more dynamic feature of ring current electrons and important role of electrons in the ring current buildup. When we summarize the recent accomplishment in our understanding of ring current dynamics, ions and electrons will be discussed together as they are intimately linked.

Recent successful missions such as Van Allen Probes (a dedicated mission to studies of radiation belts with unprecedented high-quality instrument suites), THEMIS (Time History of Events and Macroscale Interactions during Substorms), MMS (Magnetospheric MultiScale), Arase, together with measurements from ground assets, small satellites, cubesats, and balloons, have brought enhanced understanding of radiation belts, ring current and plasmasphere. It is impossible to include an exhaustive

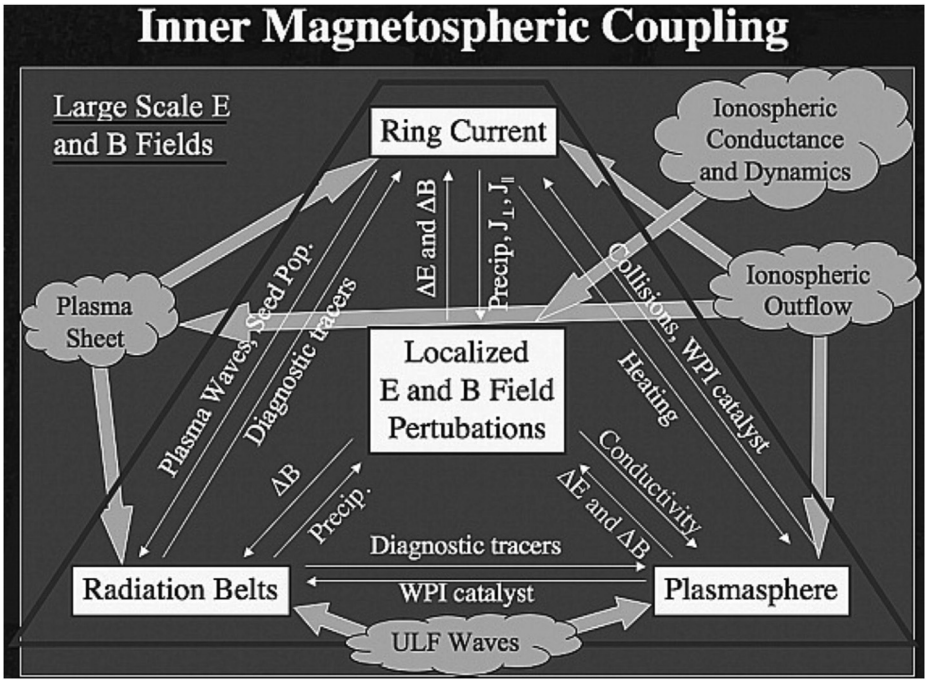

Fig. 4. Showing the tightly coupled inner magnetosphere and its connection to the ionosphere-thermosphere system and the plasma sheet (from Yu et al., 2019a). Impacts of energetic particle precipitation on mesosphere and stratosphere are not included here but shown separately in Fig. 3. Note WPI: Wave Particle Interaction.

list of recent findings. This paper only highlights some of them relevant to the goals of the G3 cluster (or a reflection of limitations of the authors' views/knowledge).

3.1.1. Recent progress in scientific understanding of ring current dynamics

Motion/drift of 1–300 keV charged particles results in the major current system in the magnetosphere: the so-called ring current, which controls the variations and distribution of magnetic field and couples the inner magnetosphere and the ionosphere. The source of ring current includes particles of ionospheric and solar wind origins. An in-depth coverage of the dynamics of energetic particles forming the ring current populations, from theoretical, observational, and modeling perspectives, may be found in a recent book "Ring Current Investigations: The Quest for Space Weather Prediction" (edited by Jordanova, Ilie, and Chen, 2020).

Here are some of the recent highlights, which are tabulated in Table 3 as a quick summary.

3.1.1.1. Complexities in energy-dependent source locations. Gkioulidou et al. (2019) showed <1 keV O+ ion outflow can directly get into the heart of the ring current. Kistler et al. (2016) showed that there are two different O + populations in the plasma sheet during the storm-time ring current: a hot and relatively more isotropic population and a low-energy and more field-aligned population, with the former mostly likely coming from the cusp and the latter from auroral outflow. It is the former contributing more to the ring current during storm times. Global consequences of these will affect ring current electron behaviors and particles of other energies/species.

3.1.1.2. Energy dependent dynamics and transport. Gkioulidou et al. (2016) showed that the low-energy component of the protons (<80 keV) is more convection dominated and is strongly governed by convective timescales. It correlates well with the absolute value of SYM-H index (a proxy of the axially symmetric magnetic field disturbance at low and middle latitudes on the Earth's surface, similar to the Dst index. The high-energy component (>100 keV) varies on much longer timescales and is more diffusion dominated. It shows either no correlation or anticorrelation with the absolute value of SYM-H index. Their study also shows that the contributions of the low- and high- energy portion protons to the inner magnetosphere energy content are comparable. Fig. 5 serves as the summary.

The dynamics of ring current electrons due to radial transport from an outside source and local interactions with plasma waves were simulated by Jordanova et al. (2016) with a kinetic ring current model called RAM-SCB (Ring current-Atmosphere interactions Model (RAM) with Self-Consistent B field (SCB)) and compared with Van Allen Probes observations. The low-energy electron fluxes increased significantly by convective transport during the storm main phase and decreased during the recovery phase, in agreement with observations, but this mechanism underestimated the injection of high-energy (>100 keV) electrons. However, adding local acceleration by plasma waves led to the intensification of electron fluxes at energies as low as 50 keV, and RAM-SCB considerably overestimated the observed trapped fluxes. This energization effect was unexpected since the energy diffusion coefficients are much smaller than the pitch angle diffusion coefficients at ~50 keV. The presence of large energy gradients that developed in the electron phase space distribution at the particle injection front enhanced this energization effect. These results indicated that either including additional loss mechanisms or improving the accuracy of wave-particle interactions, are needed to better reproduce the ring current electron populations.

3.1.1.3. Species dependence and solar wind driver response difference. It is well known that different ring current ion species and ring current electrons exhibit different dynamics during the course of a geomagnetic storm. Yue et al. (2019) shows abundant O+ ions are always present during large storms when SYM-H < −60 nT without exception, while having the pressure ratio between O+ and proton (H+) larger than 0.8 and occasionally even larger than 1 when L < 3. Simultaneously, the pressure anisotropy decreases with decreasing SYM-H and increasing L shell. The pressure anisotropy decrease during the storm main phase is likely related to the pitch angle isotropization pro-

Table 3
Summary of recent advances in understanding the environment of ring current that is relevant to surface charging.

Source	Complexities in energy-dependent source locations	Gkioulidou et al., 2019; Kistler et al., 2016
Dynamics and transport	Energy dependent dynamics and transport	Gkioulidou et al., 2016; Jordanova et al., 2016; Shprits et al., 2015; Aseev et al., 2019; Haas et al., 2023
Response to solar wind driving	Particle species dependence and solar wind driver response difference	Yue et al., 2019; Miyoshi and Kataoka, 2005; Mouikis et al., 2019; Pandya et al., 2022
Connections to tail and substorm activities	Effects of dipolarization, substorm activity and injections, and tail and transition region dynamics on ring current	Sandhu et al., 2018; Jang et al., 2021; Gabrielse et al., 2019; Keesee et al., 2021
Connections to other regions	Ring current's influence on/connections with other surrounding regions	Welling et al., 2011; Zhang and Brambles, 2021; Antonova et al., 2018; Pulkkinen et al., 2013; Ebihara et al., 2021; Krall et al., 2023; Merkin et al., 2019; Sorathia et al., 2021; Lin et al., 2021b; Yu et al., 2022.

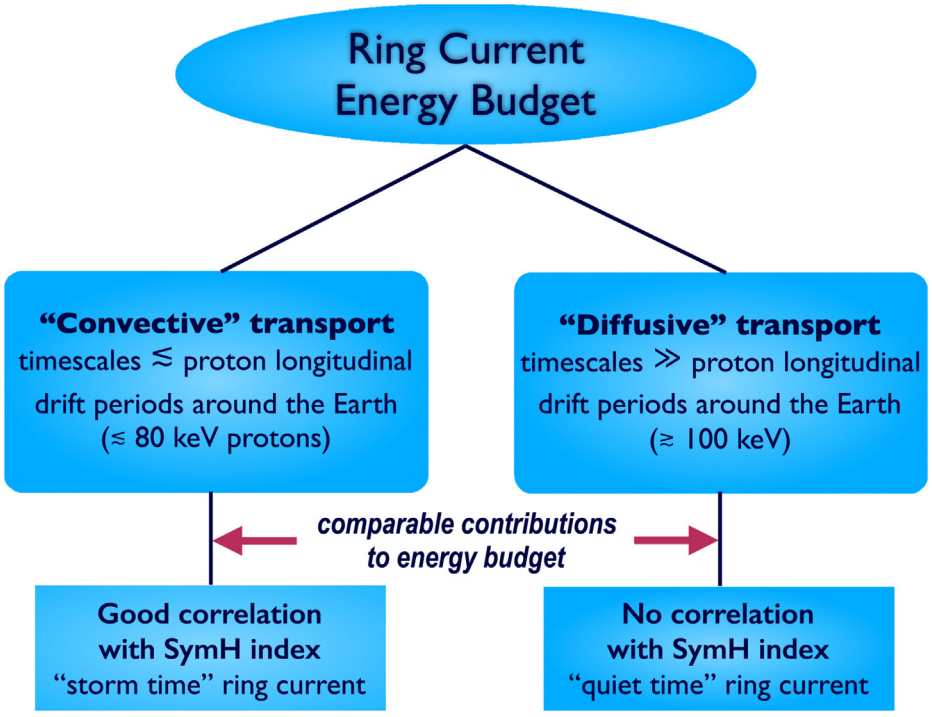

Fig. 5. Energy dependent transport and dynamics (from Gkioulidou et al., 2016).

cesses. In addition, they find that the O+ and H+ pressure ratio increases during the storm main phase and then decreases during the storm recovery phase, suggesting faster buildup and decay of O+ pressure compared to H+ ions, which are probably associated with some species dependent source and/or energization as well as loss processes in the inner magnetosphere.

Ring current particles also differ in response to different solar wind driving (e.g., Miyoshi and Kataoka, 2005, Swiger et al., 2022) such as during the influence of a CME storm or a CIR/SIR (Corotating Interaction Region/Stream Interaction Region) storm (there will be added complexities with a geomagnetic storm resulting from a mixture of both solar wind drivers). Recent Van Allen Probe measurements have added further understanding in this aspect. Mouikis et al. (2019) and Pandya et al. (2022) studied how different ring current behave differently in response to CME and CIR storms. Mouikis et al. (2019) finds the H+ pressure response shows similar source and convection patterns for CME and CIR storms while the O+ pressure from the <~55 keV O+ particles is significantly stronger for CME storms and peaks at lower L values than H+. Pandya et al. (2022) finds ions with ≥1 keV energies show more variability in response to the solar wind changes, while the lower energy (<1 keV) ions are relatively stable. They also find O+ ions show more pronounced flux enhancement during CME storms than CIR storm intervals. But the duration of enhanced flux is longer for CIR storms.

3.1.1.4. Effects of dipolarization, substorm activity and injections, and tail and transition region dynamics on ring current. Sandhu et al. (2018) showed that the ring current energy is significantly higher in the expansion phase of substorms compared to the growth phase, with the energy enhancement persisting into the substorm recovery phase. Jang et al. (2021) shows that a non-storm time supersubstorm may also have a significant contribution to the ring current. Utilizing measurements from a suite of satellites and ground-based assets, Gabrielse et al. (2019) attempted to connect particle injections at different spatial-sizes and temporal scales together into a cohesive picture. Their case study led them to interpret that fast earthward flows with embedded small-scale dipolarizing flux bundles transport both magnetic flux and energetic particles earthward, resulting in minutes-long injection signatures. As these narrow flows/magnetic flux propagate towards Earth, the flux piles up and subsequently contributes to the large-scale energization region. What follows is that a large-scale injection propagates azimuthally and poleward/tailward, observed in situ as enhanced flux and on the ground in the riometer signal. The large-scale dipolarization is the source for the large-scale electron injection. By combining ENA (Energetic Neutral Atom) imaging observations from TWINS, in-situ observations by MMS, and simulation results from a global MHD (Magnetohydrodynamics) code, Keesee et al. (2021) demonstrated that mesoscale structures in Earth's magnetotail are a primary feature of particle transport to the inner magnetosphere during storms and substorms.

3.1.1.5. Ring current's influence on/connections with other surrounding regions. The two-way coupling of the ring current to the plasmasphere, radiation belts, the underlying

ionosphere-thermosphere (Welling et al., 2011; Zhang and Brambles, 2021), and the tail (Antonova et al., 2018) has been further studied and emphasized. One aspect is through current closure such as ring current and field-aligned current connections, the modification of inner magnetosphere-ionosphere-thermosphere coupling via changes of conductance due to particle precipitation. Careful treatment and inclusion of ring current dynamics is crucial in correct modeling/forecasting of geomagnetically induced currents (GICs) (e.g., Pulkkinen et al., 2013; Ebihara et al., 2021). Krall et al. (2023) shows that ring current can heat the plasmasphere and contribute to O+ ion outflow. To the contrary, the heating of the ionosphere only produces small effects.

There has been progress on modeling the tail/transition region connections with the inner magnetosphere physics.

Plasma sheet injections associated with low flux tube entropy bubbles have been found to be the primary means of mass transport from the plasma sheet to the inner magnetosphere. Using a test particle approach, Yang et al. (2015) finds that the contribution of plasma sheet bubbles to the ring current energy increases from ~20 % for weak storms to ~50 % for moderate storms and levels off at ~61 % for intense storms, while the contribution of trapped particles decreases from ~60 % for weak storms to ~30 % for moderate and ~21 % for intense storms.

Utilizing high-resolution Lyon-Fedder-Mobarry (LFM) model (Lyon et al., 2004; Merkin and Lyon, 2010), Merkin et al. (2019) showed that the azimuthally localized structures/plasma sheet flows (Bursty Bulk Flows BBFs) are the sole contributor to the global dipolarization of inner magnetosphere after the onset of a substorm and the characteristics of BBFs/Dipolarization Fronts (DFs) are distinctively different from those occurred prior to the onset. By combining a global magnetosphere model GAMERA (Grid Agnostic MHD for Extended Research Applications) (Zhang et al., 2019; Sorathia et al., 2020), a test particle code called CHIMP (Conservative Hamiltonian Integrator for Magnetospheric Particles) (Sorathia et al., 2018), Sorathia et al. (2021) was able to model the influence of transition region dynamics on ion transport into the inner magnetosphere. The modeling results show mesoscale bubbles, localized depleted entropy regions, and particle gradient drifts are critical for ion transport. Li et al. (2021a) investigated the connection between fast flow injections from the tail plasma sheet and the inner magnetosphere under a southward IMF (interplanetary magnetic field) using the combined AuburN Global hybrId codE in 3-D (ANGIE3D) and the Comprehensive Inner Magnetosphere-Ionosphere (CIMI) model. The one-way coupling from ANGIE3D to CIMI (there is no feedback from CIMI to ANGIE3D) was able to reproduce localized fast flows, the braking of fast flows from dipole-like magnetic fields as they move inward and the resulting perpendicular heating in injection sources. Multiple fast flow injections lead to multiple peaks in the particle fluxes in the inner magnetosphere as well as fine structures of upward and downward field- aligned currents at the ionosphere, and low-energy particles penetrate deeper radially than the high-energy particles. Their results show the combined ANGIE3D-CIMI model is capable of simulating the global kinetic physics that contains both Region-1 and Region-2 field-aligned currents.

Progress has been made in modeling the coupled magnetosphere-ionosphere-thermosphere system in terms of mesoscale structures (Lin et al., 2021a, 2022). Fast flows at mid-latitude trough regions in the form of SAPS (Sub-Auroral Polarization Streams)/SAID (Sub-Auroral Ion Drift) are manifestations of the tight coupling of the ring current, the tail, electron precipitation and the internal structures of the ionosphere-thermosphere system though mechanisms of SAPS/SAID formation remain topics of active debate. In the recent review by Yu et al. (2022), three major mesoscale coupling processes within the magnetosphere-ionosphere system were emphasized: (1) coupling via transient and localized field-aligned currents (FACs), which could be intrinsically connected to bursty flows in the tail; (2) coupling via mid-latitude convection; (3) coupling via particle precipitation/conductance.

3.1.2. Environment modeling of ring current dynamics

There are several ring current models existing in the community. The Rice Convection Model (RCM) is an established physical model of the inner and middle magnetosphere that includes coupling to the ionosphere (e.g., Jaggi and Wolf, 1973; Wolf et al., 1982, 2016; Toffoletto et al., 2003). It has been further developed and improved over the years and has been coupled with different models including a few global MHD models of the magnetosphere (De Zeeuw et al., 2004; Pembroke et al., 2012; Bao et al., 2021) and models of the ionosphere-thermosphere system (Maruyama et al., 2005; Huba et al., 2017).

The Multiscale Atmosphere-Geospace Environment (MAGE) is a newly developed geospace modeling system (e.g., Wu et al., 2022) that was designed specially to resolve and study mesoscale structures during storms, such as SAPS (Lin et al., 2021b), traveling ionospheric disturbances (Pham et al., 2022), and plasma sheet bursty bulk flows (Sorathia et al., 2021). It is one of the main goals of the NASA DRIVE Science Center called Center for Geospace Storms (CGS, https://cgs.jhuapl.edu/Models/). The MAGE configuration couples several model components together to address outstanding questions regarding atmosphere-geospace interactions and dynamics. The model includes the GAMERA global MHD model of the magnetosphere (Sorathia et al., 2020; Zhang et al., 2019), RCM of the ring current (Toffoletto et al., 2003), Thermosphere Ionosphere Electrodynamics General Circulation Model (TIEGCM) of the upper atmosphere (Qian et al., 2014; Richmond et al., 1992), and the RE-developed Magnetosphere-Ionosphere Coupler/Solver (REMIX) (Merkin and Lyon, 2010). MAGE is in the development and improvement stage, mainly used for science research at present (see Section 4 in the accompanying paper on

the geomagnetic environment by Opgenoorth et al., 2024 in this special issue).

Other ring current models such as the MSM (Magnetospheric Specification Model)/MSFM (Magnetospheric Specification and Forecast Model), the CIMI model, RAM-SCB, VERB-4D (Versatile Electron Radiation Belt-4D), and IMPTAM (Inner Magnetosphere Particle Transport and Acceleration model) have realtime running capabilities. These models have been described in the surface charging review paper by Minow et al. (2024) in this special issue. Therefore, minimal descriptions of each model are provided here.

Models of Realtime Capability

- MSM/MSFM

The Magnetospheric Specification and Forecast Model (MSFM) (Freeman et al., 1994)/Magnetospheric Specification Model (MSM) (Hilmer and Voigt, 1995; Hilmer and Ginet, 2000) are partly based on RCM. Both MSM and MSFM have been used operationally by the US Air Force for predicting the ring current electron fluxes at GEO (geostationary orbit). MSFM was sufficient to make realistic electron flux predictions. However, it didn't include substorm-related injections which was dominated by injection of keV electrons in *meso*-scale fast flow channels.

- CIMI

The Comprehensive Inner Magnetosphere-Ionosphere (CIMI) model (e.g., Fok et al., 2014; 2021) was developed to study the dynamic variations of the ring current, radiation belts, and plasmasphere as well as the coupling between these populations and with the ionosphere. The CIMI model and its predecessors, such as Fok Ring Current (Fok-RC) Model (e.g., Fok and Moore, 1997 and references therein) and Fok Radiation Belt Environment (Fok − RBE) Model (Zheng et al., 2003; Fok et al., 2008) have been used widely for both science and space weather application purposes (Fok et al., 2008; Zheng et al., 2015). The Fok-RC and Fok-RBE models driven by Space Weather Modeling Framework (SWMF) have been running in realtime for nearly two decades. Their simulation outputs/products have been available at the integrated Space Weather Analysis (iSWA) system (https://iswa.gsfc.nasa.gov/IswaSystemWebApp/) developed by the Community Coordinated Modeling Center (CCMC) since 2010. Zheng et al. (2015) describes the Fok-RC and Fok-RBE products that are relevant to surface charging and internal charging and shows the realtime simulation results capturing the formation and injection of a new electron population from the tail (substorm related processes) that is likely to be responsible for the failure of Galaxy 15 on 5 April 2010 (e.g., Allen, 2010; Ferguson et al., 2011).

- IMPTAM

The IMPTAM in its various versions (Ganushkina et al., 2013, 2014, 2015, 2019; Ganushkina, 2022) has been operating online since March 2013 (imptam.fmi.fi and imptam.engin.umich.edu). IMPTAM follows distributions of electrons and ions in the drift approximation with arbitrary pitch angles from the plasma sheet to the inner regions with energies reaching up to hundreds of keVs in time-dependent magnetic and electric fields. Liouville's theorem is used to gain information of the entire distribution function with losses taken into account. For the obtained distribution function, radial diffusion is applied by solving the radial diffusion equation on the distribution function. IMPTAM is driven by the solar wind and IMF parameters and geomagnetic indices. The model provides the low energy electron (and proton) flux at all L-shells and at all satellite orbits, when necessary. IMPTAM output can serve as an input to assess surface charging levels of spacecraft immersed in severe environments and as an input to radiation belts models as distributions of electron seed population for further acceleration to MeV energies.

- VERB-4D

The VERB-4D code is based on the one-grid method of Subbotin and Shprits (2012), which possesses numerical stability and accuracy required to combine convection and diffusion processes. VERB-4D solves the modified Fokker Planck equation with two additional advection terms accounting for azimuthal and radial motion. As a result, VERB-4D allows for diffusion including radial, pitch-angle, energy and mixed terms, and convection simulations of radiation belt and ring current electrons. The model's numerical schemes have been thoroughly tested and validated (Aseev et al., 2016), while VERB-4D has been used to study the electron ring current dynamics during the March 2013 St. Patrick's Day storm (Assev et al., 2019, Haas et al., 2023). In comparison to VERB-3D that is used for modeling relativistic radiation belt electrons, the main difference is the inclusion of the convective transport that determines the dynamics of lower energy electrons in VERB-4D, which adds one more dimension in magnetic local time.

The code can be run on multiple processors of a computer cluster and computes diffusion coefficients in a non-dipole field. The code includes diffusion coefficients for hiss and chorus waves using the most recent state-of-the-art statistical wave models. The plasmapause location that is used to separate regions of hiss and chorus wave propagation can take from different models (e.g. the statistical model of Carpenter and Anderson (1992); a machine learning model of Zhelavskaya et al. (2017); or from a physics-based calculation in Zhelavskaya et al., 2021).

Aseev and Shprits (2019) performed data assimilation with Kalman filtering applied to the log of electron fluxes, using a simplified version of the VERB-4D code for fixed first and second adiabatic invariants. A comparison of the model with and without data assimilation showed that data assimilation can significantly improve the results of the simulations.

VERB-4D's capabilities are shown in the Europe Horizon 2020 PAGER (Prediction of Adverse effects of Geomagnetic storms and Energetic Radiation) project, where it provides data-assimilative nowcasts and ensemble forecasts of the surface charging environment in realtime.

- RAM-SCB

The RAM-SCB (Jordanova et al., 1997; 2010; Engel et al., 2019) was designed to simulate the dynamics of ring current ions and electrons inside of geosynchronous orbit by carefully tracking transport, energization, and loss processes including those from wave-particle interactions. The model was further developed during the SHIELDS (short for "Space Hazards Induced near Earth by Large, Dynamic Storms") project (Jordanova et al., 2018). Godinez et al. (2016) have demonstrated that implementing an Ensemble Kalman Filter (EnKF) algorithm in RAM-SCB could improve the characterization of charged particle fluxes, significantly reducing the root mean square (RMS) error depending on the time and location but at a high cost of computational resources. For operational applications, a robust version of RAM-SCB that performs simulation faster than real time with limited resources (e.g., it takes less than 24 h to run a 24-hour time window simulation), and predicts energy spectra of particle fluxes along specified satellite trajectories has been developed (Jordanova et al., 2022). The output from RAM-SCB could be used as input to post-processing tools designed to calculate the surface charging for specific spacecraft geometry (Delzanno and Camporeale, 2013; Meierbachtol et al., 2017). Such diagnostics, evaluating anomalies' relation to space environment dynamics, are critically important when performing analyses of space-system failures (Table 4).

3.2. Radiation environment and environment models relevant to internal charging

As discussed in Section 2.2, the high energy electrons (generally > 100 keV) such as ones trapped in Earth's radiation belt are the major contributors to internal charging. In this section, we provide a review on: (1) the recent scientific advances in understanding the radiation belt dynamics, particularly those aspects that are crucial for further improvement of models and model forecast; and (2) a list of some of the physics-based radiation belt models available in the international community that are related to the internal charging phenomenon. Although these physics-based models are not actually being used by the spacecraft design community (see Jun et al., 2024 for those models that are used for mission design purpose) to define the internal charging environment specification during mission design, they can be still useful to understand the state of the internal changing environment (i.e., high energy electron environment) when anomalies or failures happen that could be attributed to internal charging.

It is worth noting that *the time scale of the internal charging is longer than one hour (typically much longer, days or weeks),* the temporal variation of a high-energy electron environment with a time scale longer than one hour is important for internal charging dynamics.

3.2.1. Recent scientific advances in radiation belts physics

The Van Allen Probes mission (together with observations from other assets and with the advancement in modeling and theory) has radically changed our understanding of the radiation belts and inner magnetosphere, local particle energization, particle loss, the ring current, plasmasphere, and radiation belt connections, and other important phenomena. The dynamics in the belts result from a complex of source and loss mechanisms. Bortnik and Thorne (2007), Shprits et al. (2008a,b), Li and Hudson (2019), Thorne (2010), Tu et al. (2019a), Zhao et al. (2019a), Ripoll et al. (2020), Li et al. (2020, 2021a), Kanekal and Miyoshi (2021), Miyoshi et al. (2022), Lejosne and Kollmann (2020), Lejosne et al. (2022),

Table 4
A list of Ring Current Models.

Name	Model Feature	Realtime capability	References
RCM	kinetic	n	Jaggi and Wolf, 1973; Wolf et al., 1982, 2016; Toffoletto et al., 2003
MSM/MSFM	kinetic	y	Freeman et al., 1994; Hilmer and Voigt, 1995; Hilmer and Ginet, 2000
CIMI	convection–diffusion	y	Fok et al., 2014; 2021
RAM-SCB	convection–diffusion	y	Jordanova et al., 1997; 2010; 2018; 2022
IMPTAM	test particle	y	Ganushkina et al., 2013; 2014; 2015; 2019
VERB- 4D	convection–diffusion	y	Shprits et al., 2015
BAS-RBM (details in Section 3.2.2.1)	diffusion	y	Horne et al., 2013,2021
MAGE	Suite of models	n	Lin et al., 2021a; Pham et al., 2022

Camporeale et al. (2022a), and Kryakunova et al., (2023) provide detailed accounts of the wide-ranging progress. Baker et al. (2018) provides a comprehensive review of the radiation belt dynamics, its relationship to solar wind drivers, and its connections to many important regions of the Earth's magnetosphere, ionosphere, mesosphere and stratosphere system via energetic electron precipitation. It also describes its potential deleterious space weather impacts.

Some of the highlights of the progress are provided in Table 5 and detailed in the following subsections.

3.2.1.1. Energy dependent radiation belt electron dynamics. During the Van Allen Probes lifetime, the outer zone multi-MeV electrons extend inward toward the Earth to about L around 2.8, but rarely closer. This was termed "the impenetrable barrier" by Baker et al. (2014). But electrons around 1 MeV and below have been found to penetrate to the slot region/the inner belt due to two largest geomagnetic storms of solar cycle 24 (see Fig. 1 of Claudepierre and O'Brien, 2020 for the pronounced energy dependence). Such an impenetrable barrier has also been reported by others (e.g., Foster et al., 2016; Hogan et al., 2021). It is worth noting that 'the impenetrable barrier' here refers to relativistic electrons above 1 MeV and for the Van Allen Belt period where no superstorms occurred.

When investigating multi-MeV electron dynamics near the inner edge of the outer radiation belt, Hogan et al. (2021) found that ~3 MeV electrons behave very differently from ~7 MeV electrons with the former showing flux enhancement over a wide range of L shells and the latter showing rapid depletions over a narrow L shell range.

Wave-particle interactions also exhibit energy dependent characteristics. When simulating the storm of 25 October 2016 driven by whistler-mode chorus waves in Hua et al. (2022a), during which the maximum fluxes were observed during the 2013–2018 period, they discovered that the electrons below ~1 MeV reached the upper limit of chorus acceleration within ~1 day and then remained at a stable level, whilst the multi-MeV electrons were subject to the continuous acceleration process. Energetic electron precipitation is also energy dependent. In Zhang et al. (2022a), it shows that microbursts with energies up to 150 keV are due to near-equatorial electron scattering by chorus wave packets with peaks well above the threshold for nonlinear resonant interaction while the rare microbursts exceeding 500 keV are observed preferentially near dawn during disturbed periods – evidence of scattering by intense ducted chorus waves propagating from the equator up to middle latitudes with little attenuation.

The complex energy-dependence (e.g., Reeves et al., 2016) resulting from a variety of physical processes poses challenges for radiation belt forecasting/modeling.

3.2.1.2. Rapid acceleration and loss of energetic electrons. It is well-known that radiation belt electron flux levels are highly dynamic – increasing or decreasing on time scales from minutes to years. Recently, a lot of progress has been made in further understanding of the underlying physical causes of these rapid flux variations. Thorne et al. (2013) demonstrate more definitively that rapid acceleration of multi-MeV electrons observed by Van Allen Probes can be explained by acceleration via the concurrent magnetospheric chorus waves. Hogan et al. (2021) shows that rapid loss can occur to ~7 MeV electrons. Multisatellite observation of MeV electron fluxes of Kurita et al. (2018) shows that ~2.5-MeV electron fluxes substantially decreased within a few tens of minutes where the EMIC (Electromagnetic Ion Cyclotron) waves were present. Similarly, Drozdov et al. (2022) finds that fast localized loss by interactions with EMIC waves are a common and crucial process for ultrarelativistic electron populations.

Recent studies have analyzed the fundamental effect of magnetopause shadowing on rapid losses induced in the outer region of the radiation belts, both for electrons and protons. Using a Superposed Epoch Analysis (SEA) with NOAA (National Oceanic and Atmospheric Administration) Polar-orbiting Operational Environmental Satellite (POES) 15 measurement over more than one solar cycle, Herrera et al. (2016) showed that their developed model of magnetopause location fits well with their SEA results. This magnetopause model has been included in the Salammbô code which includes both electrons and protons. The model results showed good agreement when being compared to Van Allen Probes MAGEIS measurements. By analyzing seven years of Van Allen Probes data, Olifer et al. (2021) find that electron radiation belt losses (over very short temporal scales) in reference to the pre-storm level becomes more organized using the last-closed drift shell plus an energy-dependent ULF (Ultra Low Frequency) wave radial diffusion model. Tu et al. (2019b) modeled the magnetopause shadowing loss of energetic electrons during the intense CME driven storm in June 2015 and reproduced the fast dropout of relativistic and ultrarelativistic electrons observed by Van Allen Probes. Zhang et al. (2022b) show superfast precipitation is caused by nonlinear electron interactions with intense plasma waves and such type of superfast precipitation has a high occurrence rate. Ozeke et al. (2020) finds both rapid acceleration and loss during the March 2015 and 2013 geomagnetic storms. Both rapid loss and flux enhancement of MeV and ultrarelativistic (>3MeV) electrons were discussed in Shprits et al. (2022). The morphological structures and the dynamics of this population is different from the bulk of the radiation belts. A number of studies have also demonstrated that these particles are accelerated predominantly by the local acceleration and only in the presence of density depletions (Allison et al., 2021; Allison and Shprits, 2020; Shprits et al., 2022). Several recent studies have also shown that EMIC waves can very effectively scatter the >3 MeV electrons, while not significantly affecting the lower energy population (Shprits et al., 2013; 2016; 2018a; 2019; Drozdov et al., 2017, 2020; Qin et al., 2019a). Prompt acceleration can be also produced by

Table 5
Summary of recent advances in understanding the environment of radiation belts that is relevant to internal charging.

Dynamics	Energy Dependent Radiation Belt Electron Dynamics	e.g., Baker et al., 2014; Foster et al., 2016; Hogan et al., 2021; Hua et al., 2022a; Zhang et al., 2022a
Dynamics	Rapid Acceleration or Loss of Energetic Electrons	e.g., Hogan et al., 2021; Kurita et al., 2018; Drozdov et al., 2022; Olifer et al., 2021; Tu et al., 2019b; Zhang et al., 2022b; Ozeke et al., 2020; Shprits et al., 2022
Influences of substorm activities	Roles of Substorms on Radiation Belt Dynamics	e.g., Jaynes et al., 2015; Hua et al., 2022b; Ma et al., 2023; Mann and Ozeke, 2016; Rodger et al., 2022
Waves	Better Understanding of Waves and Wave-Particle Interactions	e.g., Baker, 2021; Zong et al., 2017; Zhao et al., 2019b; Drozdov et al., 2020; Gu et al., 2020; Li et al., 2017; Takahashi et al., 2021; Wang and Shprits, 2019
Response to solar wind driving	Influence of Solar Wind Drivers	e.g., Miyoshi and & Kataoka, 2011; Miyoshi and Kataoka, 2005; Kilpua et al., 2015, 2019; Kepko & Viall, 2019; Murphy et al., 2020; Turner et al., 2019
Impacts on atmosphere	Energetic Particle Precipitation and Contribution to Radiation Effects on Aviation	e.g., Robinson et al., 1987; Newell et al., 2009; Yu et al., 2016; Randall et al., 2005; Andersson et al., 2014; Tobiska et al., 2018; Sadykov et al., 2020; Xu et al., 2021; Aryan et al., 2023

shocks, which have been known for years. Recent published work, such as Foster et al., 2015; Hudson et al., 2017; Hao et al., 2019, has shed new light on the involved physical processes.

3.2.1.3. Roles of substorms on radiation belt dynamics. Substorms are thought to be the reservoir of the electron source and seed population and the source of the wave growth that provides the acceleration of these particles to relativistic energies (e.g., Baker et al., 2014; Jaynes et al., 2015; Tu et al., 2014). Hua et al. (2022b) demonstrates the importance of substorms in modulating radiation belt electron fluxes. The study reveals that maximum fluxes strongly correlate to cumulative effects of substorms instead of storms, with the strongest dependence on the time-integrated AL (an index measuring the intensity of auroral currents and it is usually used as an indicator for substorm activity level). When investigating two GEM (Geospace Environment Modeling) Challenge flux enhancement events on 18 March 2013 (storm time) and 19 September 2013 (non-storm time), Ma et al. (2023) found that the acceleration of electron flux at higher L-shell was contributed dominantly by clusters of AL peaks. When examining how the total radiation belt content responds to substorm and quiet-time intervals, Forsyth et al. (2016) shows the situation can be complicated and nuanced. There is a 50 % chance of an increase or decrease in the radiation belt content up to 33 h following a substorm interval. There is up to a 75 % chance of a decrease in radiation belt content following a quiet interval. Since particle injections associated with substorm activities provide seed population for radiation belt dynamics (also ring current), their accurate specification is a critical component/boundary condition for improved radiation belt modeling. Mann and Ozeke (2016) emphasizes the importance of high temporal-cadence boundary conditions in modeling radiation belt physics. Rodger et al. (2022) show the distribution (in MLT (magnetic local time), magnetic shell L, etc) of energetic participle precipitation of >30 keV bears similarities with the lower band whistler mode chorus during substorms, indicating substorm induced chorus waves serve as an active agent (scattering particles into loss cone via wave-particle interactions) for energetic electron precipitation.

3.2.1.4. Better understanding of waves and wave-particle interactions. Recent advancements in research, particularly through the analysis of measurements from Van Allen Probes alongside other complementary assets, have significantly deepened our understanding of various types of waves influencing the dynamics of the inner magnetosphere (e.g., Mann et al., 2016; Zhao et al., 2019b; Zhou et al., 2022). Baker (2021) provides a summary of many of the wave modes and particle interactions that have been studied in recent years. Zong et al. (2017) reviewed interactions of ULF pc3-5 waves with charged particles in Earth's magnetosphere. Zhao et al. (2019b) identified the previously unknown feature of a reversed relativistic electron energy spectra due to plasmaspheric hiss interactions following geomagnetic storm events. Gu et al. (2020) performed a statistical study (over 68 geomagnetic storms in the period of 2012–2017) on the correlation of electron flux at different energies to the chorus and plasmaspheric hiss activities and found chorus waves act as a critical candidate for relativistic electron acceleration and plasmaspheric hiss as a viable cause for relativistic electron loss, from a statistical sense. But details can be complex, and the involved physical processes are energy-dependent and also vary with each individual storm. There are great complexities with wave-particle interactions. For example, interactions with VLF (Very Low Frequency) and ULF waves energize some part of the trapped population while de-energizing and/or contributing to the loss of another part of the population (e.g., Li et al., 2007; Shprits et al., 2008b; Drozdov et al., 2020; Wang and Shprits, 2019). Also, different types of waves can exist simultaneously and affect particle behaviors either in concert or in competition (e.g., Takahashi et al., 2021; Li et al., 2017; Drozdov et al., 2020, Drozdov et al., 2022). Sometimes waves can affect particle dynamics within a limited time and region. The loss of electrons from the radia-

tion belts remains to be not well quantified. It is known that the loss to the magnetopause (Shprits et al., 2008b; Tu et al., 2019b), plasmapheric hiss (Lyon et al., 2004; Li et al., 2015) and chorus (Thorne et al., 2005) can all significantly contribute to scattering of MeV particles while contribution of the EMIC waves to this energy scattering is not fully understood (Denton et al., 2019; Shprits et al., 2022; Usanova et al., 2014). Recent missions such as Lomonosov (Shprits et al., 2018b), ELFIN (Electron Losses and Fields Investigation), operating at LEO and capable of resolving the loss cone, will help observe and quantify the precipitation in the future.

3.2.1.5. Influence of solar wind drivers. There have been a lot of studies (e.g., Miyoshi and Kataoka, 2005, 2011; Kilpua et al., 2015, 2019; Kepko and Viall, 2019; Murphy et al., 2020; Turner et al., 2019) looking into how different solar wind drivers/substructures (CME, CIR/SIR, substructure of a CME (shock, sheath and ejecta, and regions of shock-compressed ejecta), periodic density structures within SIR) affect radiation belt dynamics. Naturally, the response of radiation belts to different solar wind drivers and their mixture differs as they could trigger/favor generation of different types of waves and different plasma sheet conditions which provide the 'seed' population. While during CIR/SIR led geomagnetic storms, ~1 MeV radiation belt electron fluxes tend to peak in the outer edge of the outer belt while CME-led geomagnetic storms tend to push the flux peak further inward. Murphy et al. (2020) proposes a framework to help understanding and quantifying the loss and acceleration of relativistic electrons in the outer radiation belt during different types of geomagnetic storms. When measured by total radiation belt content (RBC), radiation belt dynamics can be divided into two sequential phases. Their analysis shows that during the initial phase, radiation belt loss is organized by the location of the magnetopause and the strength of Dst and ultralow frequency wave power. During the second phase, radiation belt enhancements are well organized by the amplitude of ultralow frequency waves, the auroral electrojet index, and solar wind energy input. Overall, their results demonstrate that storm time dynamics of the RBC is repeatable and well characterized by solar wind and geomagnetic driving regardless of solar wind drivers (CME or CIR/SIR) during the two phases of a storm. Such insightful understanding is crucial for improvement of radiation belt modeling and prediction.

3.2.1.6. Radiation belt electron precipitation and contribution to radiation effects on aviation. Energetic particle precipitation and its impacts on the ionosphere and atmosphere has been the focus of many discussions. Energetic particle precipitation is an important input of ionospheric conductance (e.g., Robinson et al., 1987; Newell et al., 2009), which will directly affect the ionospheric convection electric field that drives the plasma transport in the magnetosphere. The plasma and field in the magnetosphere control the wave excitation and particle scattering, which then have a feedback effect on particle precipitation (e.g., Raeder et al., 1996; Yu et al., 2016). Therefore, understanding and accurately quantifying the particle precipitation is critical to magnetosphere-ionosphere coupling. Precipitation of energetic particles has also been shown to have a strong impact on atmospheric chemistry (e.g., Andersson et al., 2014; Maliniemi et al., 2022; Randall, 2005). Precipitating radiation belt electrons are one important source population (see Fig. 3). In addition, a third radiation source has been suggested to contribute (Tobiska et al., 2018) to the total dose at aviation altitudes even though not at a dominant percentage, which results from photons due to bremsstrahlung from precipitating particles of the Van Allen radiation belts. However, this is an active area of study (Sadykov et al., 2020; Xu et al., 2021; Aryan et al., 2023) and conclusive experimental evidence of such a contribution is still missing.

3.2.2. List of radiation belt models (relevant to internal charging)

3.2.2.1. Physics-based models with realtime capabilities.

- CIMI and Its Variants

It has been discussed in Section 3.3.2 regarding ring current models. The CIMI is also capable of simulating radiation belt electron dynamics.

- VERB

Similar to VERB-4D, the VERB-3D model has been validated against observations for 100 days (Subbotin et al., 2011; Kim et al., 2011), a year (Wang and Shprits, 2019), individual storms (Kim and Shprits, 2013; Wang et al., 2020), and superstorms (Shprits et al., 2011). The model is capable of reproducing the general dynamics of the radiation belts and can be used to predict the values of averaged fluences for deep dielectric charging. Moreover, the performance of the VERB code can be further improved by using data assimilation. The VERB-3D code can resolve small pitch angles near the edge of the loss cone, and can model fluxes at LEO (e.g., Shprits et al., 2012). The non-uniform pitch-angle grid used in the VERB-3D code also allows for accurate calculation of precipitating fluxes. The code has been recently used to model the dynamic evolution of the ultra-relativistic particle populations (Shprits et al., 2013a,b, 2016).

Satellite observations are often restricted to a limited range of radial distances and energies and have different observational errors. Data assimilation allows for the combination of measurements from different spacecraft with varying uncertainties according to the underlying errors of each of the instruments. The VERB-3D model has developed data assimilative capabilities providing a link between data sampled in different orbits (e.g., THEMIS, Arase or Van Allen Probes) and low-altitude particle measurements (e.g., POES, SAMPEX, Proba-V or Lomonosov) (Cervantes et al., 2020; Castillo Tibocha et al., 2021). The

VERB code has been used to reconstruct radiation belt dynamics for the period of 8 solar cycles, which is almost 90 years (Saikin et al., 2021).

- BAS-RBM

The British Antarctic Survey Radiation Belt Model (BAS-RBM) is described in Glauert et al. (2014a,b). The BAS model simulates changes in the high-energy electron population of the radiation belts taking into account effects such as the changing solar activity and wave-particle interactions. The BAS-RBM is a three-dimensional, time-dependent diffusion model for phase-space density based on the solution of the Fokker-Planck equation. This will help to improve our understanding of the processes involved and help us develop warning and forecasting capabilities. The BAS-RBM has been used to reconstruct 30 years of the radiation belts (Glauert et al., 2018).

The BAS-RBM is now used to provide real-time forecasts via the European Space Agency web portal. These are the SaRIF (Satellite RIsk prediction and radiation Forecast) suite of products which include forecasts of the electron radiation belts and risk indicators for internal charging and total ionising dose for selected satellite orbits. The electron flux spectrum is also provided. It also includes a searchable reconstruction of the radiation belts going back years (Horne et al., 2021, Glauert et al., 2021).

- BAS-PRO

The BAS-PRO model is designed for simulating the dynamic proton radiation belt. It includes radial diffusion, CRAND source, Coulomb collisions, and nuclear scattering loss processes. It is primarily focused on the 1–10 MeV energy range protons which cause most of the solar array degradation (Lozinski et al., 2021a,b).

- DREAM and DREAM3D

The Dynamic Radiation Environment Assimilation Model (DREAM) (Koller et al., 2007, Reeves et al., 2012), represents a 1-D radial diffusion model that uses an Ensemble Kalman filter method for data assimilation. The model extension to three dimensions (DREAM3D) includes radial, pitch angle, and momentum diffusion and mixed pitch angle-momentum diffusion, which are driven by dynamic wave databases from the statistical CRRES (Combined Release and Radiation Effects Satellite) wave data, including plasmaspheric hiss, lower-band, and upper-band chorus (Tu et al., 2013). DREAM3D has been shown to better reproduce strong enhancement of radiation belt electrons during an intense geomagnetic storm using event-specific inputs of chorus wave and electron seed population (Tu et al., 2014).

- Li's radiation belt electron model

The >2 MeV daily electron flux at GEO is forecast with up to 2-day lead time in Li's radiation belt electron model. The model solves 1-D radial diffusion equation and uses only solar wind velocity and IMF as inputs (Li et al., 2001; Li, 2004). The model has been running in realtime/-forecast mode for over a decade (https://lasp.colorado.edu/space_weather/xlf3/xlf3.html). The results of the model prediction are also available at the CCMC (https://iswa.gsfc.nasa.gov/iswa_data_tree/model/magnetosphere/LiX_RB/3.X/) along with the model description (https://kauai.ccmc.gsfc.nasa.gov/CMR/view/model/SimulationModel?resourceID=spase://CCMC/SimulationModel/Li%20Radiation%20Belt%20Prediction%20%20Model/3.0).

- Salammbô

Salammbô is a set of physics-based models for the simulation of the electron and proton radiation belts creation and dynamics (Beutier and Boscher, 1995; Varotsou et al., 2008). While it was first developed to understand and reproduce the radiative environment around Earth, it has also been applied to simulate the radiation belts of Jupiter (Nénon et al., 2018) and Saturn (Lorenzato et al., 2012). It solves the classical Fokker-Planck diffusion equation in the three-dimensional phase space, written in terms of particle energy, the sine of the equatorial pitch angle, and the Roederer L* parameter. It is also used as a data assimilative model (Bourdarie and Maget, 2012) using the formalism of EnKF.

As some physical mechanisms, such as radial diffusion, magnetopause shadowing, or Coulomb interactions with the atmosphere, are shared between the electron and proton descriptions, the dual capability of Salammbô, which can simulate both species, provides insights on these physical processes.

Thanks to these capabilities, the Salammbô model is currently used for climatological and meteorological applications, such as for the development of environment specification models (Sicard et al., 2022; Brunet et al., 2021), and space weather forecasting in operational pipelines such as European Funded Project SAFESPACE (Dahmen et al., 2023) and ESA Space Situational Awareness RB-FAN (Radiation Belt-Forecast And Nowcast) (Maget et al., 2022).

3.2.2.2. Machine-learning based/empirical models. There have been many empirical and/or machine-learning based radiation belt models. Here we focus on those that have realtime/forecasting capabilities or those that have been used in space weather applications/tools.

- REFM

The Relativistic Electron Forecast Model (REFM) predicts the >2 MeV 24-hour electron fluence at GEO. It is based on a linear prediction filter (Baker et al., 1990) that uses average solar wind speed as its input. An offset is used to help account for additional physical processes that can dramatically affect the electron fluence (the fluence can experience rapid variations without a corresponding change in solar wind speed). REFM is the operational model used at NOAA SWPC (Space Weather Prediction Center). It provides forecasts of the 24-hour fluence with +1 to +3 days of lead-time (https://www.swpc.noaa.gov/products/relativistic-electron-forecast-model).

- NICT Radiation Belt Model

The radiation belt model used by NICT (National Institute of Information and Communications Technology) in Japan is based on Sakaguchi et al. (2013,2015). The model outputs daily fluence forecasts up to 3-day lead time (https://radi.nict.go.jp/en/). Predictions are calculated by multivariate autoregressive models and Kalman filter based on realtime observations.

- ORIENT-R and ORIENT-M

The Outer RadIation belt Electron Neural net model for Relativistic electrons (ORIENT-R) (>1.8 MeV) (Chu et al., 2021) and the Outer Radiation belt Electron Neural net model for Medium (ORIENT-M, Ma et al., 2022, 2023) energy electrons (50 keV–1 MeV). The most important quantities for determining outer radiation belt dynamics are found to be AL, solar wind flow speed and density, and SYM-H indices. The ORIENT model does not need any other in situ data (e.g., fluxes from LEO satellites) to provide boundary conditions as inputs into the model, and thus the model is capable of reconstructing energetic electron fluxes (covering a wide energy range) for periods both deep in the past (hindcast) and into the future (forecast), as long as the geomagnetic indices and solar wind parameters are available. The model has been running in realtime/forecast mode at Space Environment Technologies (https://spacewx.com/).

- SNB^{3}GEO

The Sheffield SNB^{3}GEO (Balikhin et al., 2016) online forecast tool has been operating continually since 2012 (https://ssg.group.shef.ac.uk/ssg2013/UOSSW/2MeV_EF.html). The Sheffield SNB^{3}GEO model was derived using the NARMAX (Nonlinear AutoRegressive Moving Average models with eXogenous input) system identification algorithm. Performance of the model over a 4-year period in comparison with measurements from GOES-13 or those from LANL satellites was carried out by Geletaw et al. (2023). Measurements from GOES-13 give more favorable model performance, which may reflect the bias that GOES data is the primary data source during the model building process.

- SHELLS

Taking advantage of measurements available at LEO, SHELLS (Specifying High Altitude Electrons using Low Altitude LEO Systems) is a radiation belt model (Claudepierre and O'Brien, 2020) utilizing artificial neural network technique. The geomagnetic activity index Kp and LEO electron flux measurements from the NOAA POES operational spacecraft are used as model training inputs. SHELLS is to be used to improve specification of the internal charging radiation hazard at satellites to improve capabilities of an anomaly diagnostic tool called SEAES-FC (Space Environment Anomalies Expert System – Flow Chart) (O'Brien, 2009).

- RB-Daily-E model

The Radiation Belt Daily Average Electron flux model (RB-Daily-E) built on Van Allen Probes and THEMIS data is consistent with GPS CXD (Combined X-ray Dosimeter) and Arase data (Gabrielse et al., 2022). It provides daily fluxes covering a broad energy range (33–7,700 keV) and L shell (L: 2–7). The RB-Daily-E Model has applications for when daily fluxes are required for post-anomaly investigations, including long-term radiation environment effects such as solar cell and solar array degradation.

- The Model by Kalegaev et al. (2022)

The machine-learning based model can provide up to 4-days forecast of >2 MeV daily electron fluence at GEO. Forecast of the solar wind speed is based on solar EUV images during the influence of coronal holes (details can be found in Kalegaev et al., 2022). Introduction of solar wind speed as an additional input parameter to this daily electron fluence model improves the model's performance. The Space Monitoring Data Center of Skobeltsyn Institute of Nuclear Physics of Moscow State University (SINP MSU) provides access to near real-time satellite data and operational forecasting models related to space weather. The model result can be found here (https://swx.sinp.msu.ru/).

3.2.2.3. Climatological models. Here we focus on recent development of climatological models of radiation belt environment. More details of these models can be found in Jun et al. (2024).

- IRENE (AE9/AP9/SPM)

The IRENE (International Radiation Environment Near Earth)-AE9/AP9/SPM is a new set of models for the fluxes of radiation belt and plasma particles in near-Earth space for use in space system design, mission plan-

ning, and other applications of climatological specification. The AE9 (0.04–10 MeV e−), AP9 (0.1 – 400 MeV H+), and SPM (1–40 keV e−, 1.15–164 keV H+, 1.15–164 keV He+, and 1.15–164 keV O+) models were developed by the Air Force Research Laboratory and the Aerospace Research Corporation (Ginet et al., 2013; Johnston et al., 2015; O'Brien et al., 2018a). This model is to replace AE8/AP8 (Vette, 1991). Model details can be found here (https://www.vdl.afrl.af.mil/programs/ae9ap9/).

- GREEN

The GREEN (Global Radiation Earth Environment) model is an ONERA's model providing fluxes at any location between $L^* = 1$ and $L^* = 8$, all along the magnetic field lines, for all local times and for any energy between 0.1 keV and 10 MeV for electrons (GREEN-e) and between 0.1 keV and 800 MeV for protons (GREEN-p) depending on the solar cycle (Sicard et al., 2018, 2019). GREEN-e is composed of global models (AE8 and SPM for low energies) and local models (SLOT model, OZONE and IGE-2006). GREEN model is accessible for space industry in the OMERE tool: https://www.trad.fr/en/space/omere-software/.

GREEN is a mean model therefore not suitable for conservative internal charging assessment. However, the GREEN "Upper Envelope" model (Sicard et al., 2022), which considers the solar cycle variation and gives the maximum flux for each year of the solar cycle, are newly developed and will be included in the newer version of GREEN.

- The 5DRBM-e (5 Dimensional Radiation Belt Model for electrons)

The 5DRBM-e model (Métrailler et al., 2019) is a global, data-driven model of the radiation belts for trapped electrons. The model is based on years of in-situ measurements of electrons by the radiation monitors on board the INTEGRAL (16 years of operation) and XMM-Newtonn (19 years of operation) satellites along their long elliptical orbits. The "5D" in the name refers to the fact that the model takes into account five dimensions: the energy, pitch angle, and location of the charged particles, as well as the temporal and spatial variations in the Earth's magnetic field. The "e" in the name indicates that the model is specifically focused on the electron population within the radiation belts. This model outputs the integral flux for trapped electrons within energies ranging from 0.7 to 1.75 MeV. Cross-validation of the 5DRBM-e with the well-known AE8min/max and AE9mean models for a low eccentricity GPS orbit shows excellent agreement and demonstrates that the new model can be used to provide reliable predictions along widely different orbits around Earth for the purpose of designing, planning, and operating satellites with more accurate instrument safety margins (Table 6).

3.3. Recent progress related to SEE

Single Event Effect is a transient effect, as such the flux (not fluence) environment is pertinent. Environment sources for SEEs include peak fluxes of SEPs, background fluxes of GCRs, and peak fluxes of energetic protons trapped in the Earth radiation belt. GCRs are produced outside the solar system in high-energy explosive events and consist mostly of energetic protons that penetrate the heliosphere. They are slowly modulated by the strength of the Sun's interplanetary magnetic field (Simpson, 1983). SEPs come from solar activity such as coronal mass ejections related to flaring events or from interplanetary magnetic field shocks (Gopalswamy et al., 2022; Reames, 2013). In the latter case, fast coronal mass ejections propagate through the ambient solar wind and create a shock front that produces accelerated energetic protons/ions. Geomagnetic cutoff models are used for the SEE evaluation within the magnetosphere. In this section, we first provide a summary of commonly used GCR models. Then we provide reviews on the peak flux SEP models used for assessing SEEs. Lastly, we provide SEP modeling status within Earth's magnetosphere (with consideration of geomagnetic shielding through rigidity cutoff).

3.3.1. Commonly used GCR models

The GCR environment in near-Earth space is subject to solar cycle modulation, anti-correlated with the sunspot number. GCRs also exhibit Forbush decreases associated with magnetic activity resulting from CMEs and/or high speed solar wind streams.

The CREME96 (Cosmic Ray Effects on Micro-Electronics) GCR model is the Nymmik cosmic ray model which has been adopted by the International Standards Organization (ISO) (ISO 15390, 2004). The recommended model is the Badhwar-O'Neill Model (O'Neill et al., 2015) which fits the measured cosmic ray spectra more accurately than previous models. The Badhwar-O'Neill 2020 (BON 2020) GCR model is further calibrated using AMS (Alpha Magnetic Spectrometer) −02 and PAMELA data. Solar activity is described using ACE/CRIS (Cosmic Ray Isotope Spectrometer) daily integral flux measurements. Another recently developed model, called HelMod (Boschini et al., 2022), provides modulated spectra for protons and nuclei during high and low solar activity periods, in the inner and outer heliosphere, at Earth location and outside the ecliptic plane, as well as at different distances from Sun in the inner and outer heliosphere (Table 7).

3.3.2. Empirical SEP peak flux or worst-case event models for SEE evaluation

The commonly used models and references are provided in Table 8. More details can be found in Jun et al. (2024) and the associated references.

3.3.3. Physics-based SEP nowcast/forecast models

Whitman et al. (2023) provides a thorough review of SEP models available in the community. However, SEP models often stop at L1 (Lagrangian 1 point) or outside the magnetic shielding of Earth's magnetic field. A global model of SEP intensity for the near-Earth region is yet to be developed. Limited recent efforts include applying AMPS (Adaptive Mesh Particle Simulator) (Tenishev et al., 2018, 2021) to studying the access and transport of SEPs throughout the near-Earth region; developing a model by mapping GOES measurements to other L shells (Young and Kress, 2016; Young et al., 2021); the data-based SPAM (Solar Particle Access to the Magnetosphere) Model that maps real-time low altitude measurements from POES/MetOp 35 to high altitudes to estimate access regions of the SEPs (Green et al., 2021). The validity of mapping methods remains to be tested. SEP modeling efforts for the near-Earth region remain woefully inadequate.

3.3.4. Models of SEP within the earth magnetosphere: Geomagnetic cutoff

The specification of SEPs in the magnetosphere requires modeling the magnetic shielding effects. This is typically done in terms of the minimum value of the particle's rigidity that is required for the particle to reach a specific location in the geospace. A commonly used quantity to describe magnetic shielding is called cutoff rigidity. Rigidity is defined as momentum per unit charge which is useful in characterizing charged particle access in magnetic fields. Cutoff rigidity usually increases with decreasing geomagnetic latitudes where only particles with high rigidity (energy) can have access to the lower latitudes. The higher energy SEP particles are, the lower L shell they are able to penetrate/access. SEPs result from large solar eruptions. They are episodic in nature and hard to predict. SEPs span a broad energy range (from 10^6 to 10^{10} eV/nucleon) and pose as radiation hazards for space hardware/electronics, avionics, and humans in space. Guo et al. (2024) in this

Table 6
A list of Radiation Belt Electron Models.

Physics Based Models				
Name	Feature	Realtime	References	Other info
REFM	Linear filter	y	Baker et al., 1990	Running at NOAA/SWPC
CIMI	Fokker-Planck equation	y	Fok et al., 2014, 2021	Running at CCMC
VERB 3D	Fokker-Planck equation	y	Shprits et al., 2012, 2013a,b, 2016	Running at CCMC
BAS-RBM	Fokker-Planck equation	y	Glauert et al., 2014a,b	Running at BAS
BAS-PRO	Fokker-Planck equation	y	Lozinski et al., 2021a,b	Running at BAS
DREAM3D	Radial diffusion	y	Koller et al., 2007, Reeves et al., 2012; Tu et al., 2014	Realtime at LANL
Li's RB model	Radial diffusion	y	Li et al., 2001; Li, 2004	Realtime at CU/Boulder and CCMC
Salammbô	Fokker-Planck equation	y	Beutier and Boscher, 1995; Boscher et al., 2018; Bourdarie and Maget, 2012	Running realtime at ONERA for electrons and protons
Machine-Learning Based/Empirical Models				
ORIENT-R/ ORIENT-M	Neural net	y	Chu et al., 2021; Ma et al., 2022, 2023	Running realtime at Space Environment Technologies, soon at CCMC
SNB^{3}GEO	NARMAX	y	Balikhin et al., 2016; Geletaw et al. (2023)	Running at the University of Sheffield
NICT model	Multivariate Autoregressive (AR) Model	y	Sakaguchi et al., 2013; 2015	Running at NICT
The model by Kalegaev et al. (2022)	Artificial neural networks (ANNs).	y	Kalegaev et al. (2022)	Running at SINP MSU
SHELLS	Random forest	y	Claudepierre and O'Brien, 2020	Running at Aerospace corp.
RB-Daily-E model:	Empirical via mapping	n	Gabrielse et al., 2022	For anomaly resolution
Climatological Models				
IRENE-AE9/AP9/ SPM	Data from variety of source	n	Ginet et al., 2013; Johnston et al., 2015; O'Brien et al., 2018a	https://www.vdl.afrl.af.mil/programs/ae9ap9/
GREEN	Consists of multiple models	n	Sicard et al., 2018, 2019	https://www.trad.fr/en/space/omere-software/ publicly available
The 5DRBM-e model	Data from INTEGRAL (>16 years) and XMM-Newton (>18 years)	n	Métrailler et al., 2019	

special issue provides a detailed account of the latest research, current scientific understanding, modeling status of SEPs, and recommendations for future activities/efforts. In comparison to free space that is outside the influence of Earth's magnetic field (resulting in magnetic shielding) and atmosphere (resulting in atmospheric interactions), specification of SEPs in the magnetosphere is even more challenging.

Earth's magnetic field shields its environment from energetic ions such as SEPs, the degree of shielding varies with magnetic field strengths and particle energies (or rigidities). Therefore, accurate specification of SEPs' spatial- and energy-distribution and intensity in near-Earth space requires knowledge of SEPs' characteristics (occurrence, source, intensity, spectrum, etc.) and the influence of the varying magnetic field of Earth.

In contrast to copious amounts of research done on ring current and radiation belt electrons, work on SEPs' access to the near-Earth region, their spatial distribution, energy dependence, and temporal occurrence/evolution in the magnetosphere, is rather limited. The limitation can be seen both in numbers of researchers working in the field and the number of publications and/or operational models. Taking advantage of measurements from numerous platforms/spacecraft (e.g., GOES, POES, SAMPEX, GPS, Van Allen Probes, PAMELA, AMS-02), progress has been made in characterizing rigidity cutoffs due to geomagnetic storms and SEPs' dynamic behavior and anisotropy in the near-Earth region (Leske et al., 2001; Neal et al., 2013; Tyssøy and Stadsnes, 2015; Adriani et al., 2016; Aguilar et al., 2021; Bruno et al., 2018, 2021; Chen et al., 2020; O'Brien et al., 2018b). Modeling efforts include Kress et al., 2010; Qin et al., 2019b; Li et al., 2021b; Tenishev et al., 2018. Recent results show that rigidity cutoffs of SEPs can be highly dynamic both in space and time (e.g., O'Brien et al., 2018b; Filwett et al., 2020). Small substructures of SEPs in interplanetary space can penetrate to the near-Earth region down to L values of $\leq$4.

Rigidity Cutoff Models

Störmer (1955) provided a theoretical prediction of the cutoffs under the influence of a dipole magnetic field. Since then, test particle approach has been applied to modeling the rigidity cutoffs (Kress et al., 2010, 2015; Maget et al., 2013; Smart and &Shea, 2009; Smart and Shea, 2001, 2003). Other rigidity calculation code includes Planetocosmics (https://cosray.unibe.ch/~laurent/planetocosmics/; https://www.spenvis.oma.be/help/models/planetocosmics.html; Desorgher et al., 2006) particle trajectory simulation based on the Geant4 toolkit (https://www.spenvis.oma.be/help/background/geant4/geant4.html) and the general-purpose AMPS which utilizes the Monte Carlo approach. AMPS's capability goes well beyond the rigidity calculation, one of which is to track and trace propagation and transport of energetic particles in geospace. There are also empirical models/empirical relationships based on particle flux measurements (e.g., Ogliore et al., 2001; Leske et al., 2001; van Hazendonk et al., 2022).

3.4. Radiation environment and models relevant to aviation

Air safety has improved significantly over the past decades except for effects from space weather, which includes ionizing radiation. Radiation exposure is a natural hazard faced by aircrew, high-altitude pilots, frequent flyers, and commercial space travelers to altitudes as high as the International Space Station (ISS). Their avionics can also be affected.

Multiple sources of ionizing radiation contribute to the radiation exposure in the aerospace environment that reaches from Earth's surface into space. GCRs and SEPs are the dominant ionizing radiation sources.

This is especially true for travel at commercial aviation altitudes starting at 8 km (26,000 ft.) and above (Friedberg and Copeland, 2003, 2011; Tobiska et al., 2016; Meier et al., 2020). The presence of ionizing radiation from GCRs and/or SEPs in the aerospace environment causes concern for the effects of this environment on human health, e.g., radiation exposure effects and effects on Cardiac Implanted Devices (CIDs), on vehicle avionics, and on aircraft power electronics.

The geomagnetic field provides a form of momentum shielding, or attenuation, by deflecting the lower energy charged particles back out to space via the Lorentz force. This spectral filtering effect is quantified in terms of geomagnetic cutoff rigidity (Mertens et al., 2010), Rc., which has been discussed in Section 3.3.4, along with cutoff models. The subgroup of SEP events called GLEs (Ground Level Enhancements) are of particular interest to aviation and human safety in space (e.g., Shea and Smart, 2012; Mishev et al., 2023). GLEs represent an extreme type of SEP events with energies high enough to trigger the enhancement of ground-level detectors and to present elevated risks. The factors that drive a solar eruptive event into a Ground Level Enhancement (GLE) are still not fully understood. The question of whether GLEs and extreme SEP events represent the high-energy, low-probability end of the continuous distribution of SEP events or if they are distinct events with unique acceleration mechanisms and prerequisites remains a subject of ongoing investigation (e.g., Nitta et al., 2012; Usoskin and Kovaltsov, 2021; McCracken et al., 2023). Therefore, forecasting GLEs is even more challenging.

There are multiple components to modeling radiation effects at aviation altitudes: (1) energy spectra of the source population (GCR or SEP); or (2) magnetic shielding effects; (3) radiation transport; (4) interactions with Earth's atmosphere.

Table 7
Commonly used GCR models.

Model	Reference
CRÈME 96/the Nymmik cosmic ray model (ISO 15390, 2004)	ISO 15390, 2004; Nymmik et al., 1996
BON 2010, BON 2014, BON 2020	O'Neill, 2010; O'Neill et al., 2015; Slaba and Whitman, 2020
DLR (German Aerospace Center) GCR model	Matthiä et al., 2013
HelMod	Boschini et al., 2022

Table 8
Commonly used SEP Peak Flux or Worst-Case Event Models for assessment of SEEs.

Model	Reference
CRÈME 96	Tylka et al., 1997
ESP (Emission of Solar Protons) Peak Flux/Worst-Case Event Model	Xapsos et al., 1998, 1999
MSSREM (Mission Specific Solar Radiation Environment Model)	Robinson et al., 1987
SAPPHIRE (Solar Accumulated and Peak Proton and Heavy Ions Radiation Environment)/VESPER (Virtual Enhancements-Solar Proton Event Radiation)	Jiggens et al., 2018a,b; Aminalragia-Giamini et al., 2018

3.4.1. Models of radiation effects at aviation altitudes

- **CARI-7A**

Development of the CARI (Civil Aeromedical Research Institute) program for calculating doses of cosmic radiation on aircraft flights began in the late 1980 s. Development of version 7 began in 2009 with calculations of needed fluence to dose conversion coefficients for light ions and alpha particles (e.g., Copeland et al., 2010, 2012). CARI-7A development and validation are described in Copeland (2017). It was first made widely available in February 2017 and has been improved continuously by user feedback since it was released. The Monte Carlo program MCNPX (Monte Carlo N-Particle Extended) 2.7.0 (Oak Ridge National Laboratory, 2011) was used for radiation transport. The primary cosmic ray spectrum model and handling of cutoff rigidities are all user-selectable at runtime. The International Standard Organization (ISO) GCR model (ISO, 2004) is used in CARI-7's implementation at NOAA/SWPC. Alternative option for the GCR modeling is to use Badhwar-O'Neill models (2011, 2014). Vertical cutoff rigidities as calculated by interpolation from tables calculated by Smart and Shea (2005) and Shea and Smart (2012) are usually used as whole-sky effective cutoff rigidities. Other alternatives for the cutoffs include the empirical ones from Ogliore et al. (2001); Leske et al. (2001), O'Brien et al. (2018b). The primary radiation field includes nuclei from H to Fe, while the secondary radiation field also includes neutrons, photons, e−, e+, μ−, μ+, π−, π+, kaons (no dosimetry), neutrinos (no dosimetry), deuterons, tritons, and helions.

- **WASAVIES**

A physics-based radiation dose estimation model called WASAVIES (WArning System for AVIation Exposure to Solar Energetic Particles) has been developed in Japan (Kataoka et al., 2014; Sato et al., 2008; Sato et al., 2014; Yasuda et al., 2011). It consists of three numerical components: (1) transport of SEPs in interplanetary space; (2) transport of SEPs in the magnetosphere; (3) nuclear reaction of SEPs in atmosphere. Its input data sources are neutron monitors and GOES proton measurements. The air shower is a Monte-Carlo-based method called PHITS (Particle and Heavy Ion Transport code System). More on the model and its realtime implementation details can be found in Sato et al. (2018). The model is running realtime at Japan/NICT (https://wasavies.nict.go.jp/index_e.html).

- **NAIRAS**

The Nowcast of Aerospace Ionization RAdiation System (NAIRAS) model predicts biologically hazardous radiation exposure to crew and passengers onboard aircraft or spacecraft from the ever-present GCRs, inner radiation belt trapped protons (TRP) in LEO, and the episodic, transient SEPs originating from solar eruptive events. The NAIRAS model also predicts the radiation flux and fluence quantities for the assessment of microelectronic single event effects to avionic and spaceflight electronic systems.

The NAIRAS model is composed of coupled physics-based models that transport cosmic radiation through the heliosphere, Earth's magnetosphere, the neutral atmosphere, and aircraft or spacecraft shielding. GCR are propagated from outside the heliosphere to 1 AU (astronomical unit) by solving a steady-state, convective-diffusive transport equation including adiabatic energy loss. A hybrid version of the Badhwar and O'Neill 2010 model, denoted H-BON10, was developed for NAIRAS to solve GCR heliospheric transport. The GCR composition in H-BON10 was also extended to include primary nuclei from hydrogen through uranium for predicting LET spectra out to 100 MeV*cm^2/mg for SEE assessment. Transport through the magnetosphere incorporates the dynamical response of the geomagnetic field to space weather variability in the interplanetary medium using the CISM (Center for Integrated Space weather Modeling) −Dartmouth vertical geomagnetic cutoff rigidity model (Kress et al., 2004,

2010). Transport of cosmic radiation through material media – i.e., the atmosphere and/or aircraft or spacecraft shielding – is calculated with the deterministic HZETRN (High charge (Z) and Energy TRaNsport) code.

The NAIRAS model computes ionizing radiation particle flux spectra from the primary sources (GCR, TRP, SEP) and the secondary radiations produced from nuclear interactions between the radiation source ions and the constituents of the intervening material media. The secondary particles consist of heavy-ion fragments from GCR ions and protons, alphas, pions and muons, and electromagnetic cascade particles (electrons, positrons, and gamma ray photons) produced by interactions with the radiation source ions. The particle flux spectra are the fundamental physical quantities from which important response functions are calculated, such as dosimetric quantities and the various flux and fluence quantities useful for characterizing SEE.

Two independent modes of NAIRAS version 3.0 are available for users: (1) real-time global predictions of the atmospheric radiation environment, which are updated hourly, and (2) Run-on-Request (RoR) capability allowing the user to select a specific time-period for the global dosimetric calculations, or to upload an aircraft, balloon, or spaceflight trajectory file to provide simulations of the dosimetric and radiation flux and fluence quantities along the flight path. Both realtime modeling results/products and RoR outputs/capabilities are available at CCMC (https://ccmc.gsfc.nasa.gov/models/NAIRAS~3.0/).

- **PANDOCA**

The PANDOCA (Professional AviatioN DOse CAlculator) code was developed at the Institute of Aerospace Medicine of the German Aerospace Center (DLR). Different versions of the model exist which are capable of calculating ambient dose equivalent, ambient dose and effective dose according to the recommendations given in ICRP Report 60 (ICRP, 1991) and ICRP Report 103 (ICRP, 2007), respectively. The latest version approved for the dose assessment of aircrew in Germany calculates the ambient dose equivalent H*(10) and the effective dose after ICRP, Report 103. The impact of updated weighting factors with respect to the definitions of ICRP Report 60 was investigated and published in Meier and Matthiä (2019).

The radiation exposure is calculated using the Geant4 version 4.9.1 Monte Carlo code (Agostinelli et al., 2003; Allison et al., 2006; Allison et al., 2016) in combination with the model of the atmosphere (Picone et al., 2002) and the magnetic field of the Earth (Maus et al., 2005) provided by the PLANETOCOSMICS tool. Galactic cosmic hydrogen and helium are considered as primary particles in the energy range from 100 MeV to 1.5 TeV (hydrogen) and 100 MeV to 850 GeV (helium). The primary particle energy spectra as described by Matthiä et al. (2013) are used. The Geant4 interface to the JAM (Jet AA Microscopic Transport Model)/JQMD (Jaeri Quantum Molecular Dynamics) model by Koi et al. (2003) is used to calculate the helium transport at energies larger than 10 GeV/n. The resulting energy spectra of secondary protons, neutrons, photons, electrons, positrons, muons and pions at a given altitude are converted to effective dose and ambient dose equivalent using fluence-to-dose conversion factors (for ambient dose equivalent: https://inf.infn.it; for effective dose: ICRP (2010)).

The geomagnetic shielding was considered using the effective vertical cut-off rigidity calculated with PLANETOCOSMICS on a two-times-three-degree grid in geographic latitude and longitude. The calculations of effective cut-off rigidity are based on the IGRF (International Geomagnetic Reference Field) model of the geomagnetic field. The geographic location is converted to cut-off rigidity and the corresponding cut-off energy by interpolating between the calculated values on the coordinate grid. For a given flight profile, the model provides the effective dose rate and the ambient dose equivalent rate at each waypoint and the resulting flight-integrated values. Details about the PANDOCA model are published in Matthiä et al. (2014).

In case of a ground level enhancement, data from the neutron monitor network are used to derive the temporal evolution of the primary spectrum of the solar energetic particles. Using asymptotic viewing directions of the different neutron monitor stations, the angular distribution of the event is described. Typically, data of about 30 neutron monitor stations are used for this analysis. For the calculation of the radiation exposure on a specific flight route, the asymptotic viewing direction at each waypoint is calculated, the primary energy spectrum is derived and the dose rates at the given location are calculated. The procedure is described in detail in Matthiä et al. (2009a, 2009b). During solar events without sufficient information from ground-based neutron monitors, data from satellite (e.g. GOES) measurements are used.

- **SIEVERT/SiGLE**

To address the needs for assessing aviation radiation impact, the SIEVERT system (Clairand et al., 2009a,b), developed in France, is used for evaluating exposure to cosmic radiation in air transport. More information can be found at https://www.sievert-system.org. SiGLE computes radiation doses due to GLEs onboard aircrafts within the SIEVERT system. The SIEVERT and SiGLE codes have been in operational use for many years in France for monitoring of radiation doses from GCRs and SEPs. The EPCARD (**E**uropean **P**rogram Package for the **C**alculation of **A**viation Route **D**oses) tool package is used for computing dose contributions from GCRs. SiGLE is an empirical model based on four previous GLE events. The updated SiGLE model and its real time version SiGLE_RT (SiGLE, 2020: https://previ.obspm.fr/index.php?page=SiGLEevolves) use the full potential of the worldwide net-

work of neutron monitors to account for the North/South anisotropy of SEPs. More details can be found in A 1.9 of EURADOS Report 2021–03 (Beck et al., 2021).

- **AVIDOS**

Another aviation radiation impact model in Europe is AVIDOS (Aviation Dosimetry – Software Package for European Accredited Aviation Dosimetry). AVIDOS (Latocha et al., 2009) is used for the dose assessment of aircraft crew exposed to cosmic radiation. The code employs a multiparameter model built upon simulations of cosmic radiation exposure done using the FLUKA Monte Carlo code (Ferrari et al., 2005). AVIDOS calculates both ambient dose equivalent H*(10) and effective dose E for flight routes over the whole world at typically used altitudes and for the full range of solar activity. The dose assessment procedure using AVIDOS is accredited by the Austrian office for accreditation according to European regulations and is valid in the whole Europe. An online version of AVIDOS with user friendly interface is accessible to public under the internet address: https://swe.ssa.esa.int/avidos-federated. SOLARDOS (Assessment of the Radiation Exposure due to Solar Particle Events at Aircraft Altitude) is a module for real-time assessment of radiation exposure at aviation altitudes due to strong solar energetic particles that lead to enhanced radiation levels on ground (GLE). This module together with AVIDOS forms the software package AVIDOS 2.0.

- **MAIRE+**

The new Model for Atmospheric Ionising Radiation Effects (MAIRE+) has been developed under the UK Space Weather Instrumentation, Measurement, Modeling and Risk programme (Hands et al., 2022). The model provides nowcasts of the aviation radiation environment, including both the galactic cosmic ray (GCR) background and during GLE (ground level enhancements) events. MAIRE+ uses multiple data sources to characterize primary GCR and GLE particle spectra and combines these with precalculated geomagnetic and atmospheric response matrices to predict particle fluxes from ground level to 20 km altitude across the entire globe. Two neutron monitors, with one located at Oulu in Finland and the other one located at Dourbes in Belgium, are used as the primary indicators of GLE intensity to maximize accuracy over UK airspace. Model outputs are compared to data from a solid-state detector carried on board Concorde during ground level enhancements in 1989. The model is hosted in the UK at the Met Office Space Weather Operations Centre (MOSWOC) and is also available at https://spaceweather.surrey.ac.uk/.

MAIRE+ improves on its predecessors MAIRE (Hands et al., 2017 and https://maire.uk/maire/), and QARM (the QinetiQ Atmospheric Radiation Model, Lei et al., 2004, 2006; Dyer et al., 2007) by adding SEP/GLE calculations in real-time whereas the previous models used major historical events as examples.

- **ARMAS (Automated Radiation Measurements for Aerospace Safety) Model**

A global, statistical model of the ARMAS measurement database has been created to specify and predict effective dose rates. The model is based on the ARMAS decade-long science-driven technology demonstration program that provides a pathway for cost-effective identification and management of radiation risks created by space weather. This program directly supports monitoring while obtaining valuable science data; it lays the basis for continual data assimilative nowcasting and forecasting of the aviation radiation environment.

The background to the ARMAS measurement database upon which the model is based uses calibrated instruments to provide real-time TID and dose rates in low latency, high cadence, high time resolution, and globally relevant locations (Tobiska et al., 2015, 2016, 2018; Gersey et al., 2020). Thus, based on a decade of ARMAS measurements between 2013 and 2023, a large, global database has been acquired for nearly all magnetic latitudes and many magnetic longitudes. By early 2023, there are a half million science quality 1-minute dosimetric data records associated with time, location, and a variety of space weather drivers parameters including the state of the Earth's magnetic field between the surface and 500 km altitude. Using this database, Tobiska et al. (2018) developed the ARMAS statistical model for specifying effective dose rate that is driven by location (geographic latitude, longitude, and pressure altitude) and the NOAA G-scale value for a given time epoch. The ARMAS statistical model results are available for every flight at the ARMAS data archive located at https://spacewx.com/radiation-decision-aids/ and the model is described in Tobiska et al. (2018) (Table 9).

3.4.2. Datasets of radiation effects at aviation altitudes

The lack of continuous 24/7 measurements, especially above regions with a large percentage of the world's air traffic, is one of the most pressing problems our community faces. High-quality measurements are needed to build statistical databases, to support data assimilative and physics-based models, and to provide data sets against which models are compared (Meier et al., 2018). Radiation sensors for both, LET and TID, are needed to address different needs for science and operations, respectively. There are needs to:

(1) characterize the dynamic and variable primary particle radiation environment due to all sources, including the way it represents changing cutoff rigidities, by measuring the radiation environment from Low Earth Orbit (LEO) down to commercial aviation altitudes and ground level;

Table 9
List of Models Providing Aviation Radiation Exposure Assessment.

Model	Geomagnetic shielding	Atmospheric interactions	Use	References	Other info
CARI-7	y	y	ICAO (International Civil Aviation Organization), FAA	Copeland et al., 2010, 2012	https://www.faa.gov/data_research/research/med_humanfacs/aeromedical/radiobiology/cari7
WASAVIES	y	y	ICAO	Sato et al., 2008, 2014, 2018; Kataoka et al., 2014; Yasuda et al., 2011	https://wasavies.nict.go.jp/index_e.html
AVIDOS	y	y	ICAO	Latocha et al., 2009	https://swe.ssa.esa.int/avidos-federated
SiGLE	y	y	ICAO	A 1.9 of Beck et al., 2021	https://previ.obspm.fr/index.php?page=SiGLEevolves
NAIRAS	y	y	NASA	Mertens et al., 2013, 2023	https://ccmc.gsfc.nasa.gov/models/NAIRAS~3.0/
PANDOCA	y	y	DLR	Matthiä et al. (2014)	One of the official models in Germany. Used by Lufthansa
MAIRE+	y	y	ICAO, UK Met Office	Hands et al., 2022	Official UK model
ARMAS	y	y	Sub-orbital, business jet, South Korean industry	Tobiska et al., 2018	Statistical model of ARMAS measurement database

(2) demonstrate COTS (Commercial-Off-The-Shelf) – based technology for top-of-the-atmosphere ionizing radiation monitoring simultaneous with atmospheric aviation altitude measurements;
(3) compare measurements between different types of radiation sensors;
(4) demonstrate integrated systems for ground-to-orbit management of the radiation exposure;
(5) aid space exploration by using measurements to specify the radiation environment consistently from the Earth's surface to LEO; and.
(6) provide radiation observations for validation of and assimilation into the radiation models that can be applied to the radiation safety protocols by using industry and agency partnerships.

Mature measurement capabilities exist for providing real-time radiation monitoring. For example, capabilities include ARMAS (Tobiska et al., 2018) and Liulin (Dachev et al., 2015) radiation detectors that are externally mounted on the ISS's Japanese Experiment Module (JEM) Exposure Facility (EF). These detectors provide primary radiation measurements at the top of the atmosphere. In the atmosphere there exists some capabilities. Since 1988, the UK CREAM (Cosmic Radiation Effects and Activation Monitor) and its successors (e.g. the Smart Atmospheric Ionizing RAdiation (SAIRA) Monitoring Network) have obtained data from some 2000 flights covering a large range of altitudes and latitudes including Concorde, executive jets, and commercial routes across the globe including polar routes (e.g., Dyer et al., 1990, 2009; Clewer et al., 2019). Regular flights of improved SAIRA units are planned to commence in April 2024 under the UK SWIMMR programme. Measurements from flights with Liulin detectors have also been made in Czech Republic, France (e.g., Bottollier-Depois et al., 2012, 2019) etc. (Yasuda et al., 2020). Although there is currently no operational solution for continuous measurements, it is advisable for the community to initiate the establishment of a database that consolidates all these available measurements.

3.5. Radiation environment models relevant to total dose

Because TID/DDD is a long-term cumulative degradation, the environment models required for total dose analyses are for long term space climatological (as opposed to space weather) models of trapped protons, trapped electrons and solar protons. These radiation sources contribute almost all the total dose exposure for levels of typical shielding used with electronic and photonic components. Since a heavy ion's contribution (either trapped or solar or galactic cosmic rays) is negligible for TID and DDD, the space radiation environments relevant for TID and DDD are trapped particles in planetary magnetic fields and SEPs. Here in this section, we list models available for trapped particles and SEP fluence models (Table 10). The TID/DDD environment models are called climatology models, not space weather models because of the time scale involved. More details of each model can be found in Jun et al. (2024).

4. Gaps and recommendations

While the G3 Cluster is influenced by solar activity and galactic cosmic rays from beyond the solar system, the focus here lies on identifying and addressing gaps within its domain. However, it's crucial to recognize that gaps within the solar and heliospheric clusters are critically important for space weather weather forecasting in general. Challenges associated with space weather forecasting have been emphasized and investigated by the broad community including works by Zheng (2013), Morley (2020), Leka

(2022), Mannucci et al. (2023), Linton et al. (2023), Temmer et al. (2023), Georgoulis et al. (2024), Guo et al. (2024) and many others.

While previous studies, such as Vourlidas et al. (2023), have undertaken gap analysis efforts titled 'The NASA Space Weather Science and Observation Gap Analysis' for the whole Sun-Earth system, the following analyses offer a more comprehensive and synergistic examination of gaps pertinent to the G3 Cluster where it involves diverse communities including scientists, engineers, operators, various end-users, and policymakers working together to reach a higher level of excellence collectively.

4.1. Common gaps across the board

- Data assimilative capabilities are urgently needed to improve all space environment models.
- There is a great need to conduct impact (user needs) – driven model validation efforts, which is a crucial process for research to operation transition.
- Observations for the near-Earth radiation and space plasma environment are still lacking in general (with limited spatial and energy range coverage), including those of direct measurements of space weather effects.
- There is lack of a central depot for space environment models and lack of central depot for all effects tools/catalogs (this review together with Jun et al. (2024) aim to fill some of the gaps).
- Continuous communications/education between the science community (space environment) and the end user community are still much needed, particularly in what the science community can better help with the user community.
- There is lack of tailored/orbit (or region) specific products with better granularity (again emphasizes the need for continuous dialogue/communications between different communities)
- The community needs to keep in mind to have channels for knowledge capture and transfer.
- The ever-present challenge lies in the need for an anomaly database that records various effects experienced by space hardware, electronics, aviation-related systems, crews, and passengers.

4.2. Recommendations for filling the common gaps

4.2.1. Addressing observation needs

- One possible solution for filling the observational gaps is to develop and/or procure low-cost, low-power consumption, and compact sensor suites and fly them on all future missions including smallsats (Millan et al., 2019; Spence et al., 2022) to measure and quantify space weather impacts (Zheng et al., 2023) in addition to the primary instrumentation. Boyd et al. (2023) demonstrates even low-accuracy data are still helpful for anomaly resolution. Major observational gaps are:
  - Heavy ions – high energy SEPs for spacecraft anomaly resolution and for aviation safety (and human safety in space). Corti et al., 2023 have identified energy gaps of SEP measurements (Fig. 1 in the paper) and recommend distributed detector networks at multiple locations. While hundreds MeV and above particles pose radiation risks to aviation industry and manned missions, >30 MeV SEPs can already cause radiation effect concerns on space hardware. Improving the current situation calls for the development of uncomplicated, lightweight, and low-power consumption instruments designed for the measurement of SEPs, encompassing energy ranges >300 MeV, while maintaining uncertainties below 30 %.
  - Low energies and cold plasma is still poorly understood and under-measured that is critical for scientific understanding and for surface charging analysis.
  - Need impact measurements (charging, radiation effects, etc.) on more modern/recent spacecraft/spacecraft hardware.
- We should make full use of the OSSE (Observing System Simulation Experiment) for optimizing future measurements and strategic planning.
- Commercial data buys have been proposed as a potential solution for obtaining critically needed data to improve current space weather products and capabilities. However, the actual value or feasibility of this approach have yet to be examined. It is advisable to leverage OSSE in the evaluation process (in addition to other considerations) before such purchases.
- Data calibration, standardization, and archiving are vital but remain formidable tasks. These processes often suffer from inadequate funding, support, and the appropriate level of recognition.

4.2.2. Addressing users' needs

- To foster better collaboration and user engagement, it is essential to establish and maintain continuous communication and feedback loops between developers of models and/or products (including impact analysis tools) and the end users.
- Improving end user experience and understanding involves developing more comprehensive descriptions and educational materials about the capabilities and limitations of different space weather models and tools. Additionally, increasing awareness among a diverse range of user communities, including the public, stakeholders, and policymakers, and educating them about the effects of space weather on operational systems

Table 10
Models for trapped particles and SEP fluence models.

Models for Trapped Particles			
AE8/AP8	Solar min/solar max	Vette, 1991; Sawyer and Vette, 1976; ESA, 2020	Publicly available
IRENE-AE9/AP9/SPM	Data from variety of source	Ginet et al., 2013; Johnston et al., 2015; O'Brien et al., 2018a	https://www.vdl.afrl.af.mil/programs/ae9ap9/
GREEN	Consists of multiple models	Sicard et al., 2018, 2019	https://www.trad.fr/en/space/omere-software/ publicly available
OMEP-EOR	Dedicated to short-duration missions solar array degradations by 1–10 MeV protons	Brunet et al., 2021	https://www.trad.fr/en/space/omere-software/ publicly available
SEP Proton Fluence Model			
JPL model	>10 to >100 MeV energy range, Cumulative mission fluence	King, 1974; Jun et al., 2007; Feynman et al., 2002	
ESP Model	>1 to >300 MeV the maximum entropy principle & log normal distribution	Xapsos et al., 1998, 1999, 2000, 2004	
SAPPHIRE Model	Monte Carlo-based approach	Crosby et al., 2015; Jiggens et al., 2018a, 2018b	

and society is crucial. Furthermore, knowledge capture and transfer initiatives must be established to ensure the proper transition of our heritage and legacy, especially in the areas of impact testing, mitigation, and prevention, to new generations.

- In the development of data assimilative capabilities for modeling all space environments, it is essential to foster collaboration with Earth Science and other relevant communities, given their experience.
- The community should keep advocating for the anomaly database mentioned above – always a challenge and a desired resource.
- We should keep pushing forward the community's effort in impact-driven model validation and assessment, which is crucially needed. One short-term goal is to expand various scoreboard activities for both scientific research and practical applications.
- To better help users, it is essential to create specialized tools and products tailored to specific orbits and regions, offering a more granular approach, including various LEO orbits (such as for proliferated LEO constellations (O'Brien, 2021)), MEO (Medium Earth Orbit), GEO, with fine distinctions.
- Centralized repositories/depots should be set up to facilitate convenient access to all models with adequate information.
- A system science approach should be implemented to transcend various ISWAT clusters and to extend its application across different domains.
- Interdisciplinary and transdisciplinary work and collaboration should be promoted.
- Machine learning should be leveraged for improvement of model boundary conditions and for optimization of stand-alone models (Bortnik and Camporeale, 2021).

4.2.3. Multi-purpose impact-driven model validation efforts

Due to its important roles in bridging different communities together and in providing assessment of model capabilities, a brief description on what has been done regarding 'Multi-Purpose Impact-Driven Model validation efforts' is provided below. Such validation effort should be one of the priorities from both science and end-user perspectives, with dedicated funding support.

All the above models have strengths and limitations. Validation of model performance remains to be done both for science and space weather application purposes. We recommend continuous and devoted assessments be conducted to compare these models and quantify their errors/uncertainties. Based on that, users can decide which, if any, they may want to use or perhaps take an ensemble approach. Previous efforts aiming to connect the research community with user communities have identified the Essential Space Environment Quantities (ESEQs) that are relevant for different space weather impacts resulting from different space radiation and plasma populations (Zheng et al., 2019; Meier et al., 2018; Yu et al., 2019b). The ESEQs have been carefully chosen, directly related to corresponding impact-driven anomalies or translatable into impacts (see Table 11, updated from Zheng et al. (2019)). Such multi-purpose model validation efforts remain immensely lacking and are the first steps needed in transitioning any model into operations.

While our event/time period selections are mostly space weather impact driven, coordinated efforts with other model validation studies (even those more research-focused) in different domains (such as G1 (Opgenoorth et al., 2024), G2, and H clusters) are strongly recommended and will also be carried out with overlapping time intervals.

More science-research focused model validation efforts are recommended to take somewhat novel approaches

(in addition to the conventional ways) such as validating a model performance from a system-wise response/behavior perspective (Delzanno and Borovsky, 2022) instead of just performing model and data comparisons for one variable alone. We should answer the question "Do model simulations behave in the same manner as the modeled system does?" instead of the standard validation question "How well do simulations reproduce spacecraft data?"

4.3. Gaps and recommendations from each impact perspective

Below we provide gaps and recommendations from each impact perspective. Those have been mentioned in the common theme above will be omitted.

4.3.1. Relevant to surface charging

Cold plasma population, including its ion composition, is not well measured or understood. But it is critical for plasma waves, ring current and radiation belt particle dynamics and is a critical element for surface charging.

The cold populations are poorly understood, partly due to the scarcity of proper observations and challenges for measuring them. Yet cold plasma plays important roles in generating different types of waves and controlling wave characteristics (e.g., Ripoll et al., 2023). For example, it affects chorus and EMIC (electromagnetic ion cyclotron) wave-particle interactions, controls ULF radial diffusion, dictates the location of hiss versus chorus waves, and reduces chances of spacecraft charging when the abundance of cold plasma is high. Cold plasma serves as an important mediator for ring current and radiation belt dynamics. The cold plasma density in the near-Earth region is a critical parameter for global space weather models, known to affect global magnetospheric dynamics. Its global impacts are reviewed in Delzanno et al. (2021).

Other critical gaps for ring current population include (1) tail/plasma sheet connections (seed population); (2) wave effects.

Here are some recommendations for the next 5–10 years.

1. We need carry out more user-oriented model validation (including participation of different types of models and newly developed ones). Such model validation efforts will help identify modeling inadequacy and directions for improvement.
2. Modeling the space environment relevant to surface charging from a system perspective is critically needed.
3. Improving the measurement, understanding, and modeling of the cold plasma population is essential, as mentioned above.
4. A better understanding of daylight charging and its signature is needed. We need to have a better grasp whether surface charging is an issue for LEO assets.

4.3.2. Relevant to internal charging

Major gaps in Understanding the Radiation Belt Environment include:

- There is still lack of a quantitative understanding of the tail/plasma sheet connections (source/seed population) with radiation belt dynamics.
- The lack of a quantitative understanding of nonlinear wave-particle interactions, particularly with respect to large amplitude waves, time-domain structures, and Alfven waves, poses a significant challenge in understanding the 'killer' electrons contributing to internal charging.
- Gaps exist in our understanding and accurate modeling of rapid fluctuations in radiation belt electron dynamics, especially when involving shock impingement as studied by Yue et al. (2017), Zong et al. (2021), and Zong (2022), dynamic tail reconfiguration, and other related phenomena.

Observational gaps:

- To advance our understanding of spacecraft charging effects and their impact on space hardware, it is crucial to conduct missions akin to SCATHA (Spacecraft Charging AT High Altitudes) launched in 1978. The SCATHA mission (McPherson et al., 1975), known for its comprehensive measurements of charging effects and satellite material responses, as well as simultaneous observations of electrons and ions within the energy range of 1 to 10^7 electron volts (eV), remains a cornerstone of our knowledge of satellite charging in this field. In essence, there is a pressing need for more direct measurements to assess space weather's influence on space hardware, a viewpoint advocated by Zheng et al. (2023).
- Global coverage of 300 keV–10 MeV electron flux with on-orbit sensor data, to close gaps in MEO and for HEO. Data buys from commercial satellites could alleviate some of the problems (e.g., GPS)
- Ready to use tools/algorithms to connect LEO (proliferated LEO) measurements to GTO (Geosynchronous Transfer Orbit)

4.3.3. Relevant to SEEs

There remain large gaps in understanding the environment that results in SEEs, especially in the near-Earth region.

SEPs (one major source for SEEs) in the near-Earth region

- Limited observations
- Not well-characterized

Table 11
Essential Space Environment Quantities (ESEQs): their corresponding impacts and temporal scales.

Impacts	Impact Quantity	ESEQ	Time Scales
Surface Charging	>10 keV e- flux	>10 keV e- flux; Te; Ne	seconds
Internal Charging	>100 fA/cm^2 (100 mils)	1 MeV and > 2 MeV e- flux	24-hour, 72hr averaged
Single Event Effects	SEE rate (100 mils)	>30 MeV p + flux	5-min, daily, weekly (worst)
Total Dose in orbit and in the atmosphere	Dose in Silicon (100 mils; 4 mils)	30–50 MeV p + flux; >1.5 MeV e- flux 1–10 MeV p+	5-min, Hourly, Daily, weekly, yearly
Aviation	Dose rate in aircraft (D-index) and single event rates in avionics	>300 MeV p + flux; spectral parameter (power law with rigidity)	5-min, Hourly

- Access to the region depends on geomagnetic activities/-magnetic field (rigidity cutoff)

More details on the recommendations of SEPs can be found in Guo et al., 2024 (this issue).

Specification of SEPs in the Magnetosphere

- Developing a unified and accurate SEP model/or well-validated model(s) for the magnetosphere remains as a major gap. Notably, results from Leske et al. (2001) demonstrate that even a modest 5° equatorward shift in the average geomagnetic cutoff can result in more than a 2.5-fold increase in the duration during which the ISS is situated within the polar cap, thus exposed to heightened levels of energetic particles.
- There is great need to model the space environment relevant to SEPs in geospace from a system perspective. Scientists working on SEPs in the solar and heliospheric physics domain should work together with scientists (far fewer) working in the magnetospheric domain.
- Observations at different altitudes/longitudes are important to see transport of SEP.
- Ground-based observations (such as neutron monitors) about SEP including GLE at different latitudes are essential to monitor SEP variations.

4.3.4. Relevant to radiation effects at aviation altitudes

- Developing a strategy for continuous measurements and identifying the regions that need those measurements are essential. These measurements serve a dual purpose: first, to enhance the quality of model inputs, particularly in terms of energy spectra, and second, to facilitate robust model validation.
- We should strive to increase measurements on multi-platforms (balloons, airplanes, ISS, etc.), especially during SEP events. Efforts include:
- Characterizing radiation measuring instruments
- Defining standards of radiation monitoring at aviation altitudes.
- Developing data assimilative capabilities
- We should take advantage of ensemble modeling as it is good for helping define the uncertainties in the system.
- We should increase our efforts in the realm of model validation, a task of utmost importance. This is exemplified by the situation in the International Civil Aviation Organization (ICAO) space weather advisory centers, where different aviation radiation effects models are employed, yet these models exhibit significant discrepancies and lack consensus with each other.
- Aviation products must shift towards an impact-based approach, such as the D-scale introduced by Meier and Matthiä (2014), rather than relying on an intensity-based framework like the S-scale. This transition should ensure that these products are user-friendly and feature uniform color schemes for consistency across the various product types.
- When issuing aviation related data products, it is essential to include, at the very least, two critical parameters: (i) the dose rate in silicon, (ii) the dose rate in tissue, and (iii) neutron fluxes for SEE rates.

Various considerations on how to improve space weather observations and modeling for aviation radiation are provided and discussed in Bain et al. (2023).

4.3.5. Relevant to total dose

Gaps and recommendations in terms of total dose effects are provided in Jun et al. (2024). As the environment models that are used for total dose assessment are all empirical, one critical need and recommendation is to make more measurements and at orbits where data are even more sparse. Other gaps and recommendations include agreeing upon a unified statistical approach in building models as different methods can lead to a factor 3–5 difference in mission fluence estimate. While current practice in assessing total dose effects ignores geomagnetic shielding (worst-case scenario), such magnetic shielding should be included for more accurate and realistic environment estimates in the future.

5. Summary

The G3 cluster is very complex. It includes a wide variety of particles covering a wide range of energies where they may be involved with a wealth of physical processes, this review focuses on space weather impact aspects of

these populations in terms of science and applications. While some detailed recommendations are mentioned above, here we just stress a few key points. The near-Earth radiation and plasma region should be studied and modeled using a systems approach and as one component of a large and connected system. Global linkages with other regions/ISWAT clusters should always be kept in mind. Another critical need is multi-purpose model validation efforts that facilitate and help accelerate R2O2R (Research-to-Operations and Operations-to-Research) activities. Continued dialog and interactions among science, operations, engineering, and other user communities is also crucial. Seeking innovative ways of carrying out measurements and filling data gaps is desired. Machine learning/AI (Artificial Intelligence) and open science platform/culture should be explored and optimized (e.g., Camporeale, 2019; Bortnik and Camporeale, 2021; Camporeale et al., 2022b) to push progress forward.

CRediT authorship contribution statement

Yihua Zheng: Writing – review & editing, Writing – original draft, Visualization, Resources, Project administration, Methodology, Investigation, Formal analysis, Conceptualization. **Insoo Jun:** Writing – review & editing, Writing – original draft, Resources, Project administration, Conceptualization. **Weichao Tu:** Writing – review & editing, Writing – original draft, Resources, Methodology, Investigation, Conceptualization. **Yuri Shprits:** Writing – review & editing, Writing – original draft, Investigation, Data curation, Conceptualization. **Wousik Kim:** Writing – review & editing, Writing – original draft, Methodology, Conceptualization. **Daniel Matthiä:** Writing – review & editing, Writing – original draft, Resources, Conceptualization. **Matthias M. Meier:** Writing – review & editing, Writing – original draft, Validation, Investigation, Formal analysis, Conceptualization. **W. Kent Tobiska:** Writing – review & editing, Writing – original draft, Methodology, Conceptualization. **Yoshizumi Miyoshi:** Writing – review & editing, Conceptualization. **Vania K. Jordanova:** Writing – review & editing, Writing – original draft, Resources, Conceptualization. **Natalia Y. Ganushkina:** Writing – original draft, Conceptualization. **Valeriy Tenishev:** Writing – review & editing. **T.P. O'Brien:** Writing – review & editing, Conceptualization. **Antoine Brunet:** Writing – review & editing, Writing – original draft, Conceptualization. **Vincent Maget:** Writing – original draft, Investigation, Conceptualization. **Jingnan Guo:** Writing – review & editing, Investigation, Conceptualization. **Dedong Wang:** Writing – review & editing, Writing – original draft, Conceptualization. **Richard B. Horne:** Writing – original draft, Investigation. **Sarah Glauert:** Validation, Resources, Conceptualization. **Bernhard Haas:** Resources, Investigation. **Alexander Y. Drozdov:** .

Declaration of competing interest

The authors declare that they have no known competing financial interests or personal relationships that could have appeared to influence the work reported in this paper.

Acknowledgement

Y. Zheng benefits from discussions from different COSPAR/ISWAT meetings, the G3 Cluster meetings and teleconferences. She acknowledges thought-provoking presentations, discussions, and roadmap activities from the 2017 and 2022 SEESAWs (Space Environment Engineering and Science Applications Workshops). Space Weather Prediction Testbed 2022 Aviation Exercise and Experiment was also useful. Part of the research described in this paper was carried out at the Community Coordinated Modeling Center located at NASA Goddard Space Flight Center with its major funding source from NASA. The work done at the Jet Propulsion Laboratory was under a contract with NASA (80NM0018D0004) and that at the University of Michigan was partly funded by NASA grants #NNX17AI48G, #80NSSC20K0353, and NSF grant #1663770. The contributions by N. Ganushkina were also partly supported by the Academy of Finland (grant 339329). RBH was supported by Natural Environment Research Council (NERC) grant NE/V00249X/1 (SafeRisk) and NERC National Public Good activity grant NE/R016445/1. Contributions by W. Tu were partially supported by NASA Grants 80NSSC21K1312 and 80NSSC21K2008. A. Y. Drozdov was partially supported by NASA Grant 80NSSC23K0656. D. Wang acknowledges the support from the Deutsche Forschungsgemeinschaft (DFG) through the project WA 4323/5-1. D. Wang, Y. Shprits and B. Haas acknowledge support from the European Union's Horizon 2020 research and innovation programme under grant agreement No. 637302 (PAGER). We extend our gratitude to the reviewers and the Editor Dr. Shea for dedicating their time and for providing valuable and constructive feedback that has greatly contributed to enhancing the overall quality of the paper.

Appendix A. Acronyms

In the order of their appearance

SEE	Single Event Effects
GCR	Galactic Cosmic Ray
SEP	Solar Energetic Particle
G3	Near-Earth Radiation and Plasma Environment of the Coupled Geospace System
COSPAR	Committee On Space Research
ISWAT	International Space Weather Action Teams
CME	Coronal Mass Ejection
TD	Total Dose
LEO	Low Earth Orbit
PCA	polar Cap Absorption
HF	High Frequency
NOx	Nitrogen Oxides
HOx	Hydrogen Oxides
IESD	Internal ElectroStatic Discharge
LET	Linear Energy Transfer
EEE	Electrical, Electronic, or Electromechanical
SAA	South Atlantic Anomaly
PAMELA	Payload for Antimatter Matter Exploration and Light-nuclei Astrophysics
MBU	MultiBit Upset
MCU	MultiCell Upset
ASICS	Application Specific Integrated Circuits
SEB	Single Event Burnout
MOSFET	Metal-Oxide-Semiconductor Field-Effect Transistor
SPEs	Solar Particle Events
ICRP	International Commission on Radiological Protection
EU	European Union
FAA	Federal Aviation Administration
MEA	More Electric Aircraft
TID	Total Ionizing Dose
MOS	Metal-Oxide-Semiconductor
SiO2	Silicon Dioxide
DDD	Displacement Damage Dose
CCD	Charge-Coupled Device
THEMIS	Time History of Events and Macroscale Interactions during Substorms
MMS	Magnetospheric MultiScale
RAM-SCB	Ring current-Atmosphere interactions Model (RAM) with Self-Consistent B field (SCB)
CIR/SIR	Corotating Interaction Region/Stream Interaction Region
ENA	Energetic Neutral Atom
MHD	Magnetohydrodynamics
GICs	Geomagnetically Induced Currents
LFM	Lyon-Fedder-Mobarry
BBFs	Bursty Bulk Flows

(*continued*)

SEE	Single Event Effects
DFs	Dipolarization Fronts
GAMERA	Grid Agnostic MHD for Extended Research Applications
CHIMP	Conservative Hamiltonian Integrator for Magnetospheric Particles
IMF	Interplanetary Magnetic Field
ANGIE3D	AuburN Global hybrId codE in 3-D
CIMI	Comprehensive Inner Magnetosphere-Ionosphere
SAPS	Sub-Auroral Polarization Streams
SAID	Sub-Auroral Ion Drift
FACs	Field-Aligned Currents
RCM	Rice Convection Model
MAGE	Multiscale Atmosphere-Geospace Environment
CGS	Center for Geospace Storms
TIEGCM	Thermosphere Ionosphere Electrodynamics General Circulation Model
REMIX	RE-developed Magnetosphere-Ionosphere Coupler/Solver
MSM	Magnetospheric Specification Model)
MSFM	Magnetospheric Specification and Forecast Model
VERB4D	Versatile Electron Radiation Belt-4D
IMPTAM	Inner Magnetosphere Particle Transport and Acceleration model
GEO	geostationary orbit
Fok-RC	Fok Ring Current
Fok – RBE	Fok Radiation Belt Environment
SWMF	Space Weather Modeling Framework
iSWA	integrated Space Weather Analysis
CCMC	the Community Coordinated Modeling Center
PAGER	Prediction of Adverse effects of Geomagnetic storms and Energetic Radiation – PAGER
SHIELDS	Space Hazards Induced near Earth by Large, Dynamic Storms
EnKF	Ensemble Kalman Filter
RMS	Root Mean Square
EMIC	Electromagnetic Ion Cyclotron
SEA	Superposed Epoch Analysis
NOAA	National Oceanic and Atmospheric Administration
POES	Polar-orbiting Operational Environmental Satellite
ULF	Ultra Low Frequency
GEM	Geospace Environment Modeling
MLT	Magnetic Local Time
VLF	Very Low Frequency
ELFIN	Electron Losses and Fields Investigation
RBC	Radiation Belt Content

(*continued*)

SEE	Single Event Effects
BAS-RBM	British Antarctic Survey – Radiation Belt Model
SaRIF	Satellite RIsk prediction and radiation Forecast
DREAM	Dynamic Radiation Environment Assimilation Model
CRRES	Combined Release and Radiation Effects Satellite
RB-FAN	Radiation Belt Forecast And Nowcast activity
REFM	Relativistic Electron Forecast Model
SWPC	Space Weather Prediction Center
NICT	National Institute of Information and Communications Technology
ORIENT-R	Outer RadIation belt Electron Neural net model for Relativistic electrons
ORIENT-M	Outer Radiation belt Electron Neural net model for Medium
NARMAX	Nonlinear AutoRegressive Moving Average models with eXogenous input
SHELLS	Specifying High
SEAES-FC	Space Environment Anomalies Expert System – Flow Chart
RB-Daily-E	The Radiation Belt Daily Average Electron flux model
CXD	Combined X-ray Dosimeter
SINP MSU	Skobeltsyn Institute of Nuclear Physics of Moscow State University
IRENE	International Radiation Environment Near Earth
GREEN	Global Radiation Earth Environment)
5DRBM-e	5 Dimensional Radiation Belt Model for electrons
ANNs	Artificial Neural Networks
CREME	Cosmic Ray Effects on Micro-Electronics
ISO	International Standards Organization
BON 2020	Badhwar-O'Neill 2020
AMS-02	Alpha Magnetic Spectrometer
CRIS	Cosmic Ray Isotope Spectrometer
DLR	German Aerospace Center
ESP	Emission of Solar Protons
SAPPHIRE	Solar Accumulated and Peak Proton and Heavy Ions Radiation Environment
VESPER	Virtual Enhancements-Solar Proton Event Radiation
AMPS	Adaptive Mesh Particle Simulator
SPAM	Solar Particle Access to the Magnetosphere
ISS	International Space Station
CIDs	Cardiac Implanted Devices
GLE	Ground Level Enhancement
CARI	Civil Aeromedical Research Institute
MCNPX	Monte Carlo N-Particle Extended
ISO	International Standard Organization

(*continued*)

SEE	Single Event Effects
WASAVIES	WArning System for AVIation Exposure to Solar Energetic Particles
PHITS	Particle and Heavy Ion Transport code System
NAIRAS	Nowcast of Aerospace Ionization RAdiation System
TRP	Trapped Protons
AU	Astronomical Unit
CISM	Center for Integrated Space weather Modeling
HZETRN	High-Charge-and-Energy (HZE) TRaNsport computer program
RoR	Run-on-Request
PANDOCA	Professional AviatioN DOse CAlculator
SOLARDOS	Assessment of the Radiation Exposure due to Solar Particle Events at Aircraft Altitude
JAM	Jet AA Microscopic Transport Model
JQMD	Jaeri Quantum Molecular Dynamics
IGRF	International Geomagnetic Reference Field
SIEVERT	Système d'information et d'évaluation par vol de l'exposition au rayonnement cosmique dans les transports aériens (in English "System for Information and In-Flight Assessment of Cosmic Radiation Exposure in Air Transportation")
EPCARD	European Program Package for the Calculation of Aviation Route Doses
AVIDOS	Aviation Dosimetry – Software Package for European Accredited Aviation Dosimetry
MAIRE+	The new Model for Atmospheric Ionising Radiation Effects
MOSWOC	Met Office Space Weather Operations Center
QARM	the QinetiQ Atmospheric Radiation Model
ICAO	International Civil Aviation Organization
ARMAS	Automated Radiation Measurements for Aerospace Safety
COTS	Commercial-Off-The-Shelf
OSSE	Observing System Simulation Experiment
MEO	Medium Earth Orbit
ESSQs	Essential Space Environment Quantities
SCATHA	Spacecraft Charging AT High Altitudes
GTO	Geosynchronous Transfer Orbit
R2O2R	Research-to-Operations and Operations-to-Research
AI	Artificial Intelligence

References

Adriani, O., Barbarino, G.C., Bazilevskaya, G.A., et al., 2015. Trapped proton fluxes at low Earth orbits measured by the PAMELA

experiment. Astrophys. J. 799, L4. https://doi.org/10.1088/2041-8205/799/1/L4.

Adriani, O., Barbarino, G.C., Bazilevskaya, G.A., Bellotti, R., Boezio, M., Bogomolov, E.A., Bongi, M., Bonvicini, V., Bottai, S., Bruno, A., et al., 2016. PAMELA's measurements of geomagnetic cutoff variations during the 14 December 2006 storm. Space Weather 14, 210–220. https://doi.org/10.1002/2016SW001364.

Agostinelli, S., Allison, J., Amako, K., Apostolakis, J., Araujo, H., Arce, P., et al., 2003. GEANT4-a simulation toolkit. Nucl. Instrum. Methods Phys. Res. Sect. A-Accelerat. Spectromet. Detect. Associated Equipment 506 (3), 250–303. https://doi.org/10.1016/S0168-9002(03)01368-8.

Aguilar, M., Ali Cavasonza, L., Ambrosi, G., Arruda, L., Attig, N., Barao, F., Barrin, L., Bartoloni, A., Başeğmez-du Pree, S., Bates, J., Battiston, R., Behlmann, M., Beischer, B., Berdugo, J., Bertucci, B., Bindi, V., de Boer, W., Bollweg, K., Borgia, B., Boschini, M., Bourquin, M., Bueno, E., Burger, J., Burger, W., Burmeister, S., Cai, X., Capell, M., Casaus, J., Castellini, G., Cervelli, F., Chang, Y., Chen, G., Chen, H., Chen, Y., Cheng, L., Chou, H., Chouridou, S., Choutko, V., Chung, C., Clark, C., Coignet, G., Consolandi, C., Contin, A., Corti, C., Cui, Z., Dadzie, K., Dai, Y., Delgado, C., Della Torre, S., Demirköz, M., Derome, L., Di Falco, S., Di Felice, V., Díaz, C., Dimiccoli, F., von Doetinchem, P., Dong, F., Donnini, F., Duranti, M., Egorov, A., Eline, A., Feng, J., Fiandrini, E., Fisher, P., Formato, V., Freeman, C., Galaktionov, Y., Gámez, C., García-López, R., Gargiulo, C., Gast, H., Gebauer, I., Gervasi, M., Giovacchini, F., Gómez-Coral, D., Gong, J., Goy, C., Grabski, V., Grandi, D., Graziani, M., Guo, K., Haino, S., Han, K., Hashmani, R., He, Z., Heber, B., Hsieh, T., Hu, J., Huang, Z., Hungerford, W., Incagli, M., Jang, W., Jia, Y., Jinchi, H., Kanishev, K., Khiali, B., Kim, G., Kirn, T., Konyushikhin, M., et al., 2021. The Alpha Magnetic Spectrometer (AMS) on the international space station: Part II – Results from the first seven years. Physics Reports 894, 1–116 https://doi.org/10.1016/j.physrep.2020.09.003.

Allen, J., 2010. The Galaxy 15 anomaly: Another satellite in the wrong place at a critical time. Space Weather 8. https://doi.org/10.1029/2010SW000588.

Allison, J., Amako, K., Apostolakis, J., Araujo, H., Dubois, P.A., Asai, M., et al., 2006. Geant4 developments and applications. IEEE Trans. Nucl. Sci. 53, 270–278. https://doi.org/10.1109/TNS.2006.869826.

Allison, J., Amako, K., Apostolakis, J., Arce, P., Asai, M., Aso, T., et al., 2016. Recent developments in GEANT4. Nucl. Instrum. Methods Phys. Res. Sect. A-Accelerat. Spectromet. Detect. Associated Equipment 835, 186–225. https://doi.org/10.1016/j.nima.2016.06.125.

Allison, H.J., Shprits, Y.Y., 2020. Local heating of radiation belt electrons to ultra-relativistic energies. Nat. Commun. 11, 4533.

Allison, H.J., Shprits, Y.Y., Zhelavskaya, I.S., Wang, D., Smirnov, A.G., 2021. Gyroresonant wave-particle interactions with chorus waves during extreme depletions of plasma density in the Van Allen radiation belts. Science Advances 7 (5), eabc0380 https://doi.org/10.1126/sciadv.abc0380.

Aminalragia-Giamini, S., Sandberg, I., Papadimitriou, C., Daglis, I.A., 2018. Piers Jiggens (2018), The virtual enhancements – solar proton event radiation (VESPER) model. J. Space Weather Space Clim. 8, A06. https://doi.org/10.1051/swsc/2017040.

Andersson, M., Verronen, P., Rodger, C., et al., 2014. Missing driver in the Sun-Earth connection from energetic electron precipitation impacts mesospheric ozone. Nat. Commun. 5, 5197. https://doi.org/10.1038/ncomms6197.

Antonova, E.E., Stepanova, M., Kirpichev, I.P., Ovchinnikov, I.L., Vorobjev, V.G., Yagodkina, O.I., Riazanseva, M.O., Vovchenko, V. V., Pulinets, M.S., Znatkova, S.S., Sotnikov, N.V., 2018. Structure of magnetospheric current systems and mapping of high latitude magnetospheric regions to the ionosphere. J. Atmos. Sol. Terr. Phys. 177, 103–114. https://doi.org/10.1016/j.jastp.2017.10.013.

Aryan, H., Jacob Bortnik, W., Tobiska, K., Mehta, P., Siddalingappa, R., 2023. Enhanced radiation levels at aviation altitudes and their relationship to plasma waves in the inner magnetosphere. Space Weather, 21e2023SW003477 https://doi.org/10.1029/2023SW003477.

Aseev, N.A., Shprits, Y.Y., Drozdov, A.Y., Kellerman, A.C., 2016. Numerical applications of the advective-diffusive codes for the inner magnetosphere. Space Weather 14, 993–1010. https://doi.org/10.1002/2016SW001484.

Aseev, N.A., Shprits, Y.Y., Wang, D., Wygant, J., Drozdov, A.Y., Kellerman, A.C., Reeves, G.D., 2019. Transport and loss of ring current electrons inside geosynchronous orbit during the 17 March 2013 storm. J. Geophys. Res. Space Phys. 124, 915–933. https://doi.org/10.1029/2018JA026031.

Aseev, N.A., Shprits, Y.Y., 2019. Reanalysis of ring current electron phase space densities using Van Allen Probe observations, convection model, and log-normal Kalman filter. Space Weather 17, 619–638. https://doi.org/10.1029/2018SW002110.

Bailey, D.K., 1964. Polar-cap absorption. Planet. Space-Sci. 12 (5), 495–541. https://doi.org/10.1016/0032-0"33(64)90040-6.

Bain, H.M., Onsager, T.G., Mertens, C.J., Copeland, K., Benton, E.R., Clem, J., Mangeard, P.-S., Green, J.C., Guild, T.B., Tobiska, W.K., Shelton-Mur, K., Zheng, Y., Halford, A.J., Carlson, S., Pulkkinen, A., 2023. Improved space weather observations and modeling for aviation radiation. Front. Astron. Space Sci. 10, 1149014. https://doi.org/10.3389/fspas.2023.1149014.

Baker, D.N., 2021. Wave–particle interaction effects in the Van Allen belts. Earth Planets Space 73, 189. https://doi.org/10.1186/s40623-021-01508-y.

Baker, D.N., McPherron, R.L., Cayton, T.E., Klebesadel, R.W., 1990. Linear prediction filter analysis of relativistic electron properties at 6.6 RE. J. Geophys. Res. 95 (A9), 15133–15140. https://doi.org/10.1029/JA095iA09p15133.

Baker, D.N., Mason, G.M., Mazur, J.E., 2012. A small spacecraft mission with large accomplishments. Eos 93, 325–326. https://doi.org/10.1029/2012EO340001.

Baker, D.N., Jaynes, A.N., Hoxie, V.C., Thorne, R.M., Foster, J.C., Li, X., Fennell, J.F., Wygant, J.R., Kanekal, S.G., Erickson, P.J., Kurth, W., Li, W., Ma, Q., Schiller, Q., Blum, L., Malaspina, D.M., Gerrard, A., Lanzerotti, L.J., 2014. An impenetrable barrier to ultrarelativistic electrons in the Van Allen radiation belts. Nature 515 (7528), 531–534. https://doi.org/10.1038/nature13956.

Baker, D.N., Erickson, P.J., Fennell, J.F., et al., 2018. Space weather effects in the earth's radiation belts. Space Sci. Rev. 214, 17. https://doi.org/10.1007/s11214-017-0452-7.

Balikhin, M.A., Rodriguez, J.V., Boynton, R.J., Walker, S.N., Aryan, H., Sibeck, D.G., Billings, S.A., 2016. Comparative analysis of NOAA REFM and SNB3GEO tools for the forecast of the fluxes of high-energy electrons at GEO. Space Weather 14, 22–31. https://doi.org/10.1002/2015SW001303.

Bao, S., Toffoletto, F., Yang, J., Sazykin, S., Wiltberger, M., 2021. Coupling the Rice convection model-equilibrium to the Lyon-Fedder-Mobarry global magnetohydrodynamic model. J. Geophys. Res.: Space Phys. 126e2020JA028973. https://doi.org/10.1029/2020JA028973.

Beck, P., Bottollier-Depois, J.-F., Bütikofer, R., Flückiger, E. O., Fuller, N., Klein, K.-L., et al., 2021. Comparison of codes assessing radiation exposure at aviation altitudes in case of solar particle events (978-3-943701-27-2). Retrieved from doi: 10.12768/zmq7-bv59.

Beutier, T., Boscher, D., 1995. *A three-dimensional analysis of the electron radiation belt by the Salammbô code*. J. Geophys. Res. 100 (14), 853 https://doi.org/10.1029/94JA03066.

Bortnik, J., Camporeale, E., 2021. Ten ways to apply machine learning in Earth and space sciences. Eos 102. https://doi.org/10.1029/2021EO160257.

Bortnik, J., Thorne, R.M., 2007. The dual role of ELF/VLF chorus waves in the acceleration and precipitation of radiation belt electrons. J. Atmos. Sol. Terr. Phys. 69, 378. https://doi.org/10.1016/j.jastp.2006.05.030.

Boscher, D., Bourdarie, S., Maget, V., Sicard-Piet, A., Rolland, G., Standarovski, D., 2018. High-energy electrons in the inner zone. IEEE

Trans. Nucl. Sci. 65 (8), 1546–1552. https://doi.org/10.1109/TNS.2018.2824543.

Boschini, M.J., Della Torre, S., Gervasi, M., La Vacca, G., Rancoita, P. G., 2022. The transport of galactic cosmic rays in heliosphere: The HelMod model compared with other commonly employed solar modulation models. Adv. Space Res. 70 (9), 2636–2648.

Bottollier-Depois, J.F., Allain, E., Baumont, G., Berthelot, N., Darley, G., Ecrabet, F., Jolivet, T., Lebeau-Livé, A., Lejeune, V., Quéinnec, F., Simon, C., Trompier, F., 2019. The OpenRadiation project: monitoring radioactivity in the environment by and for the citizens. Radioprotection 54 (4), 241–246. https://doi.org/10.1051/radiopro/2019046.

Bottollier-Depois, J.-F., Beck, P., Latocha, M., Mares, V., Matthiä, D., Rühm, W., Wissmann, F., 2012. Comparison of codes assessing radiation exposure of aircraft crew due to galactic cosmic radiation (9279270362). Retrieved from doi: 10.12768/sf0h-7h90.

Bourdarie, S.A., Maget, V.F., 2012. Electron radiation belt data assimilation with an ensemble Kalman filter relying on the Salammbô code. Ann. Geophys. 30, 929–943. https://doi.org/10.5194/angeo-30-929-2012.

Boyd, A., O'Brien, T.P., Cox, J., Larsen, B., 2023. Environment specification accuracy requirements for anomaly resolution in various orbits. Adv. Space Res. https://doi.org/10.1016/j.asr.2023.03.017.

Brandt, P.C., Zheng, Y., Sotirelis, T.S., Oksavik, K., Rich, F.J., 2013. The linkage between the ring current and the ionosphere system. Midlatitude Ionospheric Dyn. Disturb., 135–143 https://doi.org/10.1029/181GM13.

Brunet, A., Sicard, A., Papadimitriou, C., Lazaro, D., Caron, P., 2021. (2021), OMEP-EOR: A MeV proton flux specification model for electric orbit raising missions. J. Space Weather Space Clim. 11, 55. https://doi.org/10.1051/swsc/2021038.

Bruno, A., Bazilevskaya, G.A., Boezio, M., Christian, E.R., Nolfo, G.A. d., Martucci, M., Merge', M., Mikhailov, V.V., Munini, R., Richardson, I.G., Ryan, J.M., Stochaj, S., Adriani, O., Barbarino, G.C., Bellotti, R., Bogomolov, E.A., Bongi, M., Bonvicini, V., Bottai, S., Cafagna, F., Campana, D., Carlson, P., Casolino, M., Castellini, G., Santis, C.D., Felice, V.D., Galper, A.M., Karelin, A.V., Koldashov, S. V., Koldobskiy, S., Krutkov, S.Y., Kvashnin, A.N., Leonov, A., Malakhov, V., Marcelli, L., Mayorov, A.G., Menn, W., Mocchiutti, E., Monaco, A., Mori, N., Osteria, G., Panico, B., Papini, P., Pearce, M., Picozza, P., Ricci, M., Ricciarini, S.B., Simon, M., Sparvoli, R., Spillantini, P., Stozhkov, Y.I., Vacchi, A., Vannuccini, E., Vasilyev, G. I., Voronov, S.A., Yurkin, Y.T., Zampa, G., Zampa, N., 2018. Solar Energetic Particle Events Observed by the PAMELA Mission. Astrophys. J. 862 (2), 97 https://doi.org/10.3847/1538-4357/aacc26.

Bruno, A., Martucci, M., Cafagna, F.S., Sparvoli, R., Adriani, O., Barbarino, G.C., Bazilevskaya, G.A., Bellotti, R., Boezio, M., Bogomolov, E.A., Bongi, M., Bonvicini, V., Campana, D., Carlson, P., Casolino, M., Castellini, G., De Santis, C., Galper, A.M., Koldashov, S.V., Koldobskiy, S., Kvashnin, A.N., Lenni, A., Leonov, A.A., Malakhov, V.V., Marcelli, L., Marcelli, N., Mayorov, A.G., Menn, W., Mergè, M., Mocchiutti, E., Monaco, A., Mori, N., Mikhailov, V.V., Munini, R., Osteria, G., Panico, B., Papini, P., Pearce, M., Picozza, P., Ricci, M., Ricciarini, S.B., Simon, M., Sotgiu, A., Spillantini, P., Stozhkov, Y.I., Vacchi, A., Vannuccini, E., Vasilyev, G.I., Voronov, S.A., Yurkin, Y.T., Zampa, G., Zampa, N., 2021. East–West Proton Flux Anisotropy Observed with the PAMELA Mission. ApJ 919 (114) https://doi.org/10.3847/1538-4357/ac1677.

Camporeale, E., 2019. The challenge of machine learning in Space Weather: Nowcasting and forecasting. Space Weather 17, 1166–1207. https://doi.org/10.1029/2018SW002061.

Camporeale, E., Wilkie, G.J., Drozdov, A.Y., Bortnik, J., 2022a. Data-driven discovery of Fokker-Planck equation for the Earth's radiation belts electrons using Physics-Informed neural networks. Journal of Geophysical Research: Space Physics 127e2022JA030377. https://doi.org/10.1029/2022JA030377.

Camporeale, E., Delouille, V., Berger, T., Murray, S., 2022b. Machine learning helps to solve problems in heliophysics. Eos 103. https://doi.org/10.1029/2022EO225033.

Carpenter, D.L., Anderson, R.R., 1992. An ISEE/whistler model of equatorial electron density in the magnetosphere. J. Geophys. Res. 97 (A2), 1097–1108. https://doi.org/10.1029/91JA01548.

Castillo Tibocha, A.M., de Wiljes, J., Shprits, Y.Y., Aseev, N.A., 2021. Reconstructing the dynamics of the outer electron radiation belt by means of the standard and ensemble Kalman filter with the VERB-3D code. Space Weather 19 (10), e2020SW002672. https://doi.org/10.1029/2020SW002672.

Cervantes, S., Shprits, Y.Y., Aseev, N.A., Drozdov, A.Y., Castillo, A., Stolle, C., 2020. Identifying radiation belt electron source and loss processes by assimilating spacecraft data in a three-dimensional diffusion model. J. Geophys. Res.: Space Phys. 125 (1), e2019JA027514. https://doi.org/10.1029/2019JA027514.

Chen, Y., Morley, S.K., Carver, M.R., 2020. Global prompt proton sensor network: Monitoring solar energetic protons based on GPS satellite constellation. J. Geophys. Res.: Space Phys. 125e2019JA027679. https://doi.org/10.1029/2019JA027679.

Chu, X., Ma, D., Bortnik, J., Tobiska, W.K., Cruz, A., Bouwer, S.D., et al., 2021. Relativistic electron model in the outer radiation belt using a neural network approach. Space Weather 19e2021SW002808. https://doi.org/10.1029/2021SW002808.

Clairand, I., Fuller, N., Bottollier-Depois, J.-F., Trompier, F., 2009a. The SIEVERT system for aircrew dosimetry. Radiat. Prot. Dosim. 136 (4), 282–285. https://doi.org/10.1093/rpd/ncp123.

Clairand, I., Fuller, N., Bottollier-Depois, J.-F., Trompier, F., 2009b. The SIEVERT system for aircrew dosimetry. Radiat. Prot. Dosim. 136 (4), 282–285. https://doi.org/10.1093/rpd/ncp123.

Claudepierre, S.G., O'Brien, T.P., 2020. Specifying high-altitude electrons using low-altitude LEO systems: The SHELLS model. Space Weather 18e2019SW002402. https://doi.org/10.1029/2019SW002402.

Clewer, B.J., Ryden, K.A., Dyer, A.C.R., Hands, A., Jackson, D., 2019. A citizen science network for measurements of atmospheric ionizing radiation levels. Space Weather 17, 877–893. https://doi.org/10.1029/2019SW002190.

Combier, N., Claret, A., Laurent, P., et al., 2017. Improvements of FLUKA calculation of the neutron Albedo. IEEE Trans. Nucl. Sci. 64 (1), 614–621. https://doi.org/10.1109/TNS.2016.2611019.

Copeland, K., 2017. CARI-7A: Development and validation. Radiat. Prot. Dosim. 175 (4), 419–431. https://doi.org/10.1093/rpd/ncw369.

Copeland, K., Parker, D.E., Friedberg, W., 2010. Alpha particles at energies of 10 MeV to 1 TeV: Fluence absorbed dose, equivalent dose, effective dose, and gray equivalent conversion coefficients calculated using Monte Carlo radiation transport code MCNPX 2.7.A. Radiat. Prot. Dosim. 138 (4), 310–319. https://doi.org/10.1093/rpd/ncp271.

Copeland, K., Friedberg, W., Sato, T., Niita, K., 2012. Comparison of fluence-to-dose conversion coefficients for deuterons, tritons, and helions. Radiat. Prot. Dosim. 148 (3), 344–351. https://doi.org/10.1093/rpd/ncr035.

Copeland, K., 2018. MIRA 2017: A CARI-7 Based Solar Radiation Alert System. In Office of Aerospace Medicine Report; DOT/FAA/AM-18/6. Available online: https://www.faa.gov/data_research/research/med_humanfacs/oamtechreports/2010s/media/201806.pdf.

Corti, C., Whitman, K., Desai, R., Rankin, J.S., Strauss, D.T., Nitta, N., Chen, T.Y., 2023. Galactic Cosmic Rays and Solar Energetic Particles in Cis-Lunar Space. Bull. AAS 55 (3). https://doi.org/10.3847/25c2cfeb.2b22d58b.

Crosby, N., Heynderickx, D., Jiggens, P., Aran, A., Sanahuja, B., Truscott, P., et al., 2015. SEPEM: A tool for statistical modeling the solar energetic particle environment. Space Weather 13 (7), 406–426. https://doi.org/10.1002/2013SW001008.

Dachev, T., Semkova, J., Tomov, B., Matviichuk, Y., Dimitrov, P., Koleva, R., Malchev, S., Bankov, N., Shurshakov, V., Benghin, V., Yarmanova, E., Ivanova, O., Häder, D.P., Lebert, M., Schuster, M., Reitz, G., Horneck, G., Uchihori, Y., Kitamura, H., Ploc, O., Cubancak, J., Nikolaev, I., 2015. Overview of the liulin type

instruments for space radiation measurement and their scientific results. Life Sci. Space Res. 4, 92–114. https://doi.org/10.1016/j.lssr.2015.01.005.

Dahmen, N., Brunet, A., Bourdarie, S., Katsavrias, C., Bernoux, G., Doulfis, S., Nasi, A., Papadimitriou, C., Oliveros Fernandez, J., Daglis, I., 2023. Electron radiation belt safety indices based on the SafeSpace modelling pipeline and dedicated to the internal charging risk, EGUsphere [preprint], doi: 10.5194/egusphere-2022-1509.

De Zeeuw, D.L., Sazykin, S., Wolf, R.A., Gombosi, T.I., Ridley, A.J., Tóth, G., 2004. Coupling of a global MHD code and an inner magnetospheric model: Initial results. J. Geophys. Res. 109, A12219. https://doi.org/10.1029/2003JA010366.

Delzanno, G.L., Borovsky, J.E., 2022. The need for a system science approach to global magnetospheric models. Front. Astron. Space Sci. 9808629. https://doi.org/10.3389/fspas.2022.808629.

Delzanno, G.L., Camporeale, E., Moulton, J.D., Borovsky, J.E., MacDonald, E.A., Thomsen, M.F., 2013. CPIC: A curvilinear particle-in-cell code for plasma–material interaction studies. IEEE Trans. Plasma Sci. 41 (12), 3577–3587. https://doi.org/10.1109/TPS.2013.2290060.

Delzanno, G.L., Borovsky, J.E., Henderson, M.G., Lira, P.A.R., Roytershteyn, V., Welling, D.T., 2021. The impact of cold electrons and cold ions in magnetospheric physics. J. Atmos. Sol. Terr. Phys. 220105599. https://doi.org/10.1016/j.jastp.2021.105599.

Denton, R.E., Ofman, L., Shprits, Y.Y., Bortnik, J., Millan, R.M., Rodger, C.J., et al., 2019. Pitch angle scattering of sub-MeV relativistic electrons by electromagnetic ion cyclotron waves. J. Geophys. Res. Space Phys. 124, 5610–5626. https://doi.org/10.1029/2018JA026384.

Desorgher, L., Flückiger, E.O., Gurtner, M., 2006. The planetocosmics geant4 application. In: Paper presented at the 36th COSPAR scientific assembly, vol. 36, p. 2361.

Dobynde, M., Harikumaran, J., Guo, J., Wheeler, P., Galea, M., Buticchi, G., 2023. Cosmic radiation reliability analysis for aircraft power electronics. IEEE Trans. Transp. Electrif. https://doi.org/10.1109/TTE.2023.3278319.

Drozdov, A.Y., Shprits, Y.Y., Usanova, M.E., Aseev, N.A., Kellerman, A.C., Zhu, H., 2017. EMIC wave parameterization in the long-term VERB code simulation. J. Geophys. Res. Space Phys. 122 (8), 8488–8501. https://doi.org/10.1002/2017JA024389.

Drozdov, A.Y., Usanova, M.E., Hudson, M.K., Allison, H.J., Shprits, Y.Y., 2020. The role of hiss, chorus, and EMIC waves in the modeling of the dynamics of the multi-MeV radiation belt electrons. J. Geophys. Res.: Space Phys. 125e2020JA028282. https://doi.org/10.1029/2020JA028282.

Drozdov, A.Y., Allison, H.J., Shprits, Y.Y., Usanova, M.E., Saikin, A., Wang, D., 2022. Depletions of multi-MeV electrons and their association to minima in phase space density. Geophys. Res. Lett. 49e2021GL097620. https://doi.org/10.1029/2021GL097620.

Dyer, C., Hands, A., Lei, F., et al., 2009. Advances in measuring and modeling the atmospheric radiation environment. IEEE Trans. Nucl. Sci. 56 (6), 3415–3422. https://doi.org/10.1109/TNS.2009.2032185.

Dyer, C.S., Sims, A.J., Farren, J., Stephen, J., 1990. Measurements of solar flare enhancements to the single event upset environment in the upper atmosphere (avionics). IEEE Trans. Nucl. Sci. 37 (6), 1929–1937. https://doi.org/10.1109/23.101211.

Dyer, C.S., Lei, F., Hands, A., Truscott, P., 2007. Solar particle events in the QinetiQ Atmospheric Radiation Model. IEEE Trans. Nucl. Sci. 54 (4), 1071–1075. https://doi.org/10.1109/TNS.2007.893537.

Dyer, C.S., Ryden, K.A., Morris, P.A., et al., 2023. The living with a star space environment testbed payload. IEEE Trans. Nucl. Sci. 70 (3), 200–215. https://doi.org/10.1109/TNS.2023.3239734.

Ebihara, Y., Watari, S., Kumar, S., 2021. Prediction of geomagnetically induced currents (GICs) flowing in Japanese power grid for Carrington-class magnetic storms. Earth Planets Space 73, 163. https://doi.org/10.1186/s40623-021-01493-2.

ECSS, European Cooperation for Space Standardization, 2019. Space engineering. Spacecraft charging. ECSS-E-ST-20-06C Rev 1. 15 May 2019.

ECSS, European Cooperation for Space Standardization, 2019. Space engineering. Assessment of space worst case charging handbook. ECSS-E-HB-20-06A. 15 May 2019.

Engel, M.A., Morley, S.K., Henderson, M.G., Jordanova, V.K., Woodroffe, J.R., Mahfuz, R., 2019. Improved simulations of the inner magnetosphere during high geomagnetic activity with the RAM-SCB model. J. Geophys. Res.: Space Phys. 124, 4233–4248. https://doi.org/10.1029/2018JA026260.

EURATOM, 1996. Council Directive 96/29/EURATOM of 13 May 1996 Laying Down the Basic Safety Standards for Protection of the Health of Workers and the General Public against the Dangers Arising from Ionizing Radiation. Off. J. Eur. Communities 159, 10–11.

EURATOM, 2014. Council Directive 2013/59/EURATOM of 5 December 2013 Laying Down the Basic Safety Standards for Protection of the Health of Workers and the General Public against the Dangers Arising from Exposure to Ionizing Radiation, and repealing Directives 89/618/Euratom, 90/641/Euratom, 96/29/Euratom, 97/43/Euratom and 2003/122/Euratom. Off. J. Eur. Communities 57, 1–73.

Federal Aviation Administration, 2014. In-Flight Radiation Exposure; Advisory Circular 120-61B. 2014. Available online: https://www.faa.gov/documentlibrary/media/advisory_circular/ac_120-61b.pdf (accessed on 13 March 2023)

Ferguson, D., Denig, W., Rodriguez, J., 2011. Plasma conditions during the Galaxy 15 anomaly and the possibility of ESD from subsurface charging. In: Proc. 49th AIAA Aerosp. Sci. Meeting, pp. 1–14. https://doi.org/10.2514/6.2011-1061.

Ferrari, A., Sala, P.R., Fasso, A., Ranft, J., 2005. FLUKA: a multi-particle transport code, Report CERN-2005-010, INFN-TC-2005-11, SLAC-R-773. https://doi.org/10.2172/877507, https://doi.org/10.5170/CERN-2005-010.

Feynman, J., Ruzmaikin, A., Berdichevsky, V., 2002. The JPL proton fluence model: An update. J. Atmos. Sol. Terr. Phys. 64 (16), 1679–1686. https://doi.org/10.1016/S1364-6826(02)00118-9.

Filwett, R.J., Jaynes, A.N., Baker, D.N., Kanekal, S.G., Kress, B., Blake, J.B., 2020. Solar energetic proton access to the near-equatorial inner magnetosphere. J. Geophys. Res.: Space Phys. 125e2019JA027584. https://doi.org/10.1029/2019JA027584.

Fiori, R.A.D., Kumar, V.V., Boteler, D.H., Terkildsen, M.B., 2022. Occurrence rate and duration of space weather impacts on high-frequency radio communication used by aviation. J. Space Weather Space Clim. 12 (21). https://doi.org/10.1051/swsc/2022017.

Fok, M.-C., Buzulukova, N.Y., Chen, S.-H., Glocer, A., Nagai, T., Valek, P., Perez, J.D., 2014. The comprehensive inner magnetosphere-ionosphere model. J. Geophys. Res. Space Phys. 119, 7522–7540. https://doi.org/10.1002/2014JA020239.

Fok, M.-C., Kang, S.-B., Ferradas, C.P., Buzulukova, N.Y., Glocer, A., Komar, C.M., 2021. New developments in the comprehensive inner magnetosphere-ionosphere model. J. Geophys. Res. Space Phys. https://doi.org/10.1029/2020JA028987, 126, 4.

Fok, M.-C., Moore, T.E., 1997. Ring current modeling in a realistic magnetic field configuration. Geophys. Res. Lett. 24, 1775–1778. https://doi.org/10.1029/97GL01255.

Fok, M.-C., Horne, R.B., Meredith, N.P., Glauert, S.A., 2008. Radiation Belt environment model: Application to space weather nowcasting. J. Geophys. Res. 113A03S08. https://doi.org/10.1029/2007JA012558.

Forsyth, C., Rae, I.J., Murphy, K.R., et al., 2016. What effect do substorms have on the content of the radiation belts? J. Geophys. Res. Space Phys. 121, 6292–6306. https://doi.org/10.1002/2016JA022620.

Foster, J.C., Erickson, P.J., Baker, D.N., Jaynes, A.N., Mishin, E.V., Fennel, J.F., Li, X., Henderson, M.G., Kanekal, S.G., 2016. Observations of the impenetrable barrier, the plasmapause, and the VLF bubble during the 17 March 2015 storm. J. Geophys. Res. Space Phys. 121, 5537–5548. https://doi.org/10.1002/2016JA022509.

Foster, J., Wygant, J., Hudson, M., Boyd, A., Baker, D., Erickson, P., Spence, H.E., 2015. Shock-induced prompt relativistic elec- tron acceleration in the inner magnetosphere. J. Geophys. Res. Space Phys. 120, 1661–1674. https://doi.org/10.1002/2014JA020642.

Freeman, Jr. J.W., Wolf, R.A., Spiro, R.W., Hausman, B.A., Bales, B.A., Lambour, R., 1994. A real-time magnetospheric specification model: magnetospheric specification & forecast model (MSFM), Final Technical Report & Software Documentation. Report for USAF contract F19628-90-K-0012, Rice University, Houston, TX.

Friedberg, W., Copeland, K., 2003. What Aircrews Should Know about Their Occupational Exposure to Ionizing Radiation, United States. Department of Transportation. Federal Aviation Administration. Office of Aviation. Civil Aerospace Medical Institute, DOT/FAA/AM-03/16, https://rosap.ntl.bts.gov/view/dot/57947.

Friedberg, W., Copeland, K., 2011. Ionizing radiation in Earth's atmosphere and in space near Earth. In Office of Aerospace Medicine Report; DOT/FAA/AM-11/; 2011. https://rosap.ntl.bts.gov/view/dot/20607.

Gabrielse, C., Spanswick, E., Artemyev, A., Nishimura, Y., Runov, A., Lyons, L., et al., 2019. Utilizing the heliophysics/geospace system observatory to understand particle injections: Their scale sizes and propagation directions. J. Geophys. Res. Space Phys. 124, 5584–5609. https://doi.org/10.1029/2018JA025588.

Gabrielse, C., Lee, J.H., Claudepierre, S., Walker, D., O'Brien, P., Roeder, J., et al., 2022. Radiation Belt Daily Average Electron flux model (RB-Daily-E) from the seven-year Van Allen Probes mission and its application to interpret GPS on-orbit solar array degradation. Space Weather 20e2022SW003183. https://doi.org/10.1029/2022SW003183.

Ganushkina, N., 2022. Operational inner magnetosphere particle transport and acceleration model (IMPTAM) for 1–300 keV electrons. Adv. Space Res. https://doi.org/10.1016/j.asr.2022.10.022.

Ganushkina, N.Y., Amariutei, O.A., Shprits, Y.Y., Liemohn, M.W., 2013. Transport of the plasma sheet electrons to the geostationary distances. J. Geophys. Res. Space Phys. 118 (1), 82–98. https://doi.org/10.1029/2012JA017923.

Ganushkina, N.Y., Amariutei, O.A., Welling, D., Heynderickx, D., 2015. Nowcast model for low-energy electrons in the inner magnetosphere. Space Weather 13, 16–34. https://doi.org/10.1002/2014SW001098.

Ganushkina, N., Jaynes, A., Liemohn, M., 2017. Space weather effects produced by the ring current particles. Space Sci. Rev. 212, 1315–1344. https://doi.org/10.1007/s11214-017-0412-2.

Ganushkina, N.Y., Liemohn, M.W., Amariutei, O.A., Pitchford, D., 2014. Low-energy electrons (5–50 keV) in the inner magnetosphere. J. Geophys. Res. Space Phys. 119, 246–259. https://doi.org/10.1002/2013JA019304.

Ganushkina, N.Y., Sillanpää, I., Welling, D.T., Haiducek, J., Liemohn, M., Dubyagin, S., Rodriguez, J.V., 2019. Validation of Inner Magnetosphere Particle Transport and Acceleration Model (IMPTAM) with long-term GOES MAGED measurements of keV electron fluxes at geostationary orbit. Space Weather 17. https://doi.org/10.1029/2018SW002028.

Geletaw, B., Melessew, N., Reeves, G.D., 2023. Performance evaluation of SNB3GEO electrons flux forecasting model using LANL and GOES-13 observations. Adv. Space Res. 71, 6, 2833–2845. https://doi.org/10.1016/j.asr.2022.11.044.

Georgoulis, M.K., Yardley, S.L., Guerra, J.A., et al., 2024. Prediction of solar energetic events impacting space weather conditions. Adv. Space Res. https://doi.org/10.1016/j.asr.2024.02.030.

Gersey, B., Tobiska, W.K., Atwell, W., Bouwer, D., Didkovsky, L., Judge, K., et al., 2020. Beamline and flight comparisons of the ARMAS flight module with the tissue equivalent proportional counter for improving atmospheric radiation monitoring accuracy. Space Weather 18e2020SW002599. https://doi.org/10.1029/2020SW002599.

Ginet, G.P., O'Brien, T.P., Huston, S.L., et al., 2013. AE9, AP9 and SPM: New models for specifying the trapped energetic particle and space plasma environment. Space Sci. Rev. 179, 579–615. https://doi.org/10.1007/s11214-013-9964-y.

Gkioulidou, M., Ukhorskiy, A.Y., Mitchell, D.G., Lanzerotti, L.J., 2016. Storm time dynamics of ring current protons: Implications for the long-term energy budget in the inner magnetosphere. Geophys. Res. Lett. 43, 4736–4744. https://doi.org/10.1002/2016GL068013.

Gkioulidou, M., Ohtani, S., Ukhorskiy, A., Mitchell, D., Takahashi, K., Spence, H., et al., 2019. Low-energy (<keV) O+ ion outflow directly into the inner magnetosphere: Van Allen Probes observations. J. Geophys. Res. Space Phys. 124 (1), 405–419. https://doi.org/10.1029/2018ja025862.

Glauert, S.A., Horne, R.B., Meredith, N.P., 2014a. Three-dimensional electron radiation belt simulations using the BAS Radiation Belt Model with new diffusion models for chorus, plasmaspheric hiss, and lightning-generated whistlers. J. Geophys. Res. Space Phys. 119, 268–289. https://doi.org/10.1002/2013JA019281.

Glauert, S.A., Horne, R.B., Meredith, N.P., 2014b. Simulating the Earth's radiation belts: Internal acceleration and continuous losses to the magnetopause. J. Geophys. Res. Space Phys. 119, 7444–7463. https://doi.org/10.1002/2014JA020092.

Glauert, S.A., Horne, R.B., Meredith, N.P., 2018. A 30-year simulation of the outer electron radiation belt. Space Weather 16, 1498–1522. https://doi.org/10.1029/2018SW001981.

Glauert, S.A., Horne, R.B., Kirsch, P., 2021. Evaluation of SaRIF high-energy electron reconstructions and forecasts. Space Weather 19e2021SW002822. https://doi.org/10.1029/2021SW002822.

Godinez, H.C., Yu, Y., Lawrence, E., Henderson, M.G., Larsen, B., Jordanova, V.K., 2016. Ring current pressure estimation with RAM-SCB using data assimilation and Van Allen Probe flux data. Geophys. Res. Lett. 43. https://doi.org/10.1002/2016GL071646.

Goldstein, J., Burch, J.L., Sandel, B.R., Mende, S.B., Brandt, P., Hairston, M.R., 2005. Coupled response of the inner magnetosphere and ionosphere on 17 April 2002. J. Geophys. Res. 110A03205. https://doi.org/10.1029/2004JA010712.

Gopalswamy, N., Yashiro, S., Akiyama, S., Xie, H., Mäkelä, P., Fok, M.-C., Ferradas, C.P., 2022. What is unusual about the third largest geomagnetic storm of solar cycle 24? J. Geophys. Res.: Space Phys. 127e2022JA030404. https://doi.org/10.1029/2022JA030404.

Green, J. C., O'Brien, T. P., Quin, R., Huston, S., Whelan, P., Reker, N., 2021. The Solar Particle Access Model (SPAM): A New Tool for Monitoring Solar Energetic Particle Impacts to Satellite Operations. AMOS Meeting Technical Papers

Gu, X., Xia, S., Fu, S., Xiang, Z., Ni, B., Guo, J., Cao, X., 2020. Dynamic responses of radiation belt electron fluxes to magnetic storms and their correlations with magnetospheric plasma wave activities. The Astrophysical Journal 891 (2), 127 https://doi.org/10.3847/1538-4357/ab71fc.

Guo, J., Wang, B., Whitman, K., Plainaki, C., Zhao, L., Bain, H.M., Cohen, C., Dalla, S., Dumbovic, M., Janvier, M., Jun, I., Luhmann, J., Malandraki, O.E., Leila Mays, M., Rankin, J.S., Wang, L., Zheng, Y., 2024. Particle radiation environment in the heliosphere: status, limitations, and recommendations. Adv. Space Res. https://doi.org/10.1016/j.asr.2024.03.070.

Haas, B., Shprits, Y.Y., Allison, H.J., Wutzig, M., Wang, D., 2023. A missing dusk-side loss process in the terrestrial electron ring current. Sci. Rep. 13, 970. https://doi.org/10.1038/s41598-023-28093-2.

Hands, A., Lei, F., Ryden, K., Dyer, C., Underwood, C., Mertens, C., 2017. New data and modelling for single event effects in the stratospheric radiation environment. IEEE Trans. Nucl. Sci. 64 (1), 587–595. https://doi.org/10.1109/TNS.2016.2612000.

Hands, A.D.P., Lei, F., Davis, C.S., Clewer, B.J., Dyer, C.S., Ryden, K. A., 2022. A new model for nowcasting the aviation radiation environment with comparisons to in situ measurements during GLEs. Space Weather 20e2022SW003155. https://doi.org/10.1029/2022SW003155.

Hao, Y.X., Zong, Q.-G., Zhou, X.-Z., Rankin, R., Chen, X.R., Liu, Y., et al., 2019. Global-scale ULF waves associated with SSC accelerate magnetospheric ultrarelativistic electrons. J. Geophys. Res. Space Phys. 124, 1525–1538. https://doi.org/10.1029/2018JA026134.

Herrera, D., Maget, V.F., Sicard-Piet, A., 2016. Characterizing magnetopause shadowing effects in the outer electron radiation belt during geomagnetic storms. J. Geophys. Res. Space Phys. 121, 9517–9530. https://doi.org/10.1002/2016JA022825.

Hilmer, R.V., Ginet, G.P., 2000. A magnetospheric specification model validation study: Geosynchronous electrons. J. Atmos. Sol. Terr. Phys. 62 (14), 1275–1294. https://doi.org/10.1016/S1364-6826(00)00100-0.

Hilmer, R.V., Voigt, G.-H., 1995. A magnetospheric magnetic field model with flexible current systems driven by independent physical parameters. J. Geophys. Res. 100 (A4), 5613–5626. https://doi.org/10.1029/94JA03139.

Hogan, B., Li, X., Zhao, H., Khoo, L., Jaynes, A., Kanekal, S., et al., 2021. Multi-MeV electron dynamics near the inner edge of the outer radiation belt. Geophys. Res. Lett. 48e2021GL095455. https://doi.org/10.1029/2021GL095455.

Horne, R.B., Glauert, S.A., Meredith, N.P., Boscher, D., Maget, V., Heynderickx, D., Pitchford, D., 2013. Space weather impacts on satellites and forecasting the Earth's electron radiation belts with SPACECAST. Space Weather 11. https://doi.org/10.1002/swe.20023.

Horne, R.B., Glauert, S.A., Kirsch, P., Heynderickx, D., Bingham, S., Thorn, P., et al., 2021. The satellite risk prediction and radiation forecast system (SaRIF). Space Weather 19e2021SW002823. https://doi.org/10.1029/2021SW002823.

Hua, M., Bortnik, J., Ma, Q., 2022a. upper limit of outer radiation belt electron acceleration driven by Whistler-Mode Chorus waves. Geophys. Res. Lett. https://doi.org/10.1029/2022GL099618, 49, 15.

Hua, M., Bortnik, J., Chu, X., 2022b. Homayon Aryan, Qianli Ma, Unraveling the critical geomagnetic conditions controlling the upper limit of electron fluxes in the earth's outer radiation belt. Geophys. Res. Lett. https://doi.org/10.1029/2022GL101096.

Huba, J.D., Sazykin, S., Coster, A., 2017. SAMI3-RCM simulation of the 17 March 2015 geomagnetic storm. J. Geophys. Res. Space Phys. 122, 1246–1257. https://doi.org/10.1002/2016JA023341.

Hudson, M., Jaynes, A., Kress, B., Li, Z., Patel, M., Shen, X.-C., et al., 2017. Simulated prompt acceleration of multi-Mev electrons by the 17 March 2015 interplanetary shock. J. Geophys. Res. Space Phys. 122, 10036–10046. https://doi.org/10.1002/2017JA024445.

ICRP, 1990. Recommendations of the International Commission on Radiological Protection, ICRP Publication 60. Ann. ICRP 21 (1–3), 1–201.

ICRP, 2007. The 2007 Recommendations of the International Commission on Radiological Protection. Ann. ICRP 37 (2–4), 1–332.

ICRP, 2010. Conversion coefficients for radiological protection quantities for external radiation exposures. ICRP Publication 116. Ann. ICRP 40 (2–5), 1–257. https://doi.org/10.1016/j.icrp.2011.10.001.

International Organization for Standardization (ISO), 2004. Space Environment (Natural and Artificial)—Galactic Cosmic Ray Model, Standard, International Organization for Standardization, Geneva, Switzerland. Retrieved from https://www.iso.org/standard/76594.html.

Jaggi, R.K., Wolf, R.A., 1973. Self-consistent calculation of the motion of a sheet of ions in the magnetosphere. J. Geophys. Res. 78 (16), 2852–2866. https://doi.org/10.1029/JA078i016p02852.

Jang, E.J., Yue, C., Zong, Q.G., Fu, S.Y., Fu, H.B., 2021. The effect of non-storm time substorms on the ring current dynamics. Earth Planet. Phys. 5 (3), 251–258. https://doi.org/10.26464/epp2021032, eepp2021032.

JAXA, JERG-2-211A, 2012. Revision A, Design Standard, Spacecraft Charging and Discharging. Japan Aerospace Exploration Agency, 10 May 2012.

Jaynes, A.N., Baker, D.N., Singer, H.J., et al., 2015. Source and seed populations for relativistic electrons: Their roles in radiation belt changes. J. Geophys. Res. Space Phys. 120, 7240–7254. https://doi.org/10.1002/2015JA021234.

Jiggens, P., Varotsou, A., Truscott, P., Heynderickx, D., Lei, F., Evans, H., Daly, E., 2018a. The solar accumulated and peak proton and heavy ion radiation environment (SAPPHIRE) model. IEEE Trans. Nucl. Sci. 65 (2), 698–711. https://doi.org/10.1109/TNS.2017.2786581.

Jiggens, P., Heynderickx, D., Sandberg, I., Truscott, P., Raukunen, O., Vainio, R., 2018b. Updated model of the solar energetic proton environment in space. J. Space Weather Space Clim. 8, A31. https://doi.org/10.1051/swsc/2018010.

Johnston, W.R., O'Brien, T.P., Huston, S.L., Guild, T.B., Ginet, G.P., 2015. Recent updates to the AE9/AP9/SPM radiation belt and space plasma specification model. IEEE Trans. Nucl. Sci. 62, 2760–2766. https://doi.org/10.1109/TNS.2015.2476470.

Jordanova, V.K., Kozyra, J.U., Nagy, A.F., Khazanov, G.V., 1997. Kinetic model of the ring current-atmosphere interactions. J. Geophys. Res.: Space Phys. 102 (A7), 14279–14291. https://doi.org/10.1029/96JA03699.

Jordanova, V.K., Zaharia, S., Welling, D.T., 2010. Comparative study of ring current development using empirical, dipolar, and self-consistent magnetic field simulations. J. Geophys. Res.: Space Phys. 115. https://doi.org/10.1029/2010JA015671. A00J11, 1–17.

Jordanova, V.K., Tu, W., Chen, Y., Morley, S.K., Panaitescu, A.-D., Reeves, G.D., Kletzing, C.A., 2016. RAM-SCB simulations of electron transport and plasma wave scattering during the October 2012 "double-dip" storm. J. Geophys. Res. Space Phys. 121, 8712–8727. https://doi.org/10.1002/2016JA022470.

Jordanova, V.K., Delzanno, G.L., Henderson, M.G., Godinez, H.C., Jeffery, C.A., et al., 2018. Specification of the near-Earth space environment with SHIELDS. J. Atm. Sol.-Terr. Phys. 177, 148–159. https://doi.org/10.1016/j.jastp.2017.11.006.

Jordanova, V., Ilie, R., Chen, M., 2020. Ring Current Investigations: The Quest for Space Weather Prediction. Elsevier. doi: https://doi.org/10.1016/C2017-0-03448-1.

Jordanova, V.K., Morley, S.K., Engel, M.A., et al., 2022. The RAM-SCB model and its applications to advance space weather forecasting. Adv. Space Res. https://doi.org/10.1016/j.asr.2022.08.077.

Jun, I., Kim, W., Zheng, Y., et al., 2024. Radiation Environment Pathways to Impacts: Radiation Effects, Relevant Environment Models, and Future Needs. Advances in Space Research https://doi.org/10.1016/j.asr.2024.03.079.

Jun, I., Swimm, R., Ruzmaikin, A., Feynman, J., Tylka, A., Dietrich, W., 2007. Statistics of solar energetic particle events: Fluences, durations, and time intervals. Adv. Space Res. 40 (3), 304–312. https://doi.org/10.1016/j.asr.2006.12.019.

Kalegaev, V., Kaportseva, K., Myagkova, I., Shugay, Yu., Vlasova, N., Barinova, W., Dolenko, S., Eremeev, V., Shiryaev, A., 2022. Medium-term prediction of the fluence of relativistic electrons in geostationary orbit using solar wind streams forecast based on solar observations. Adv. Space Res. https://doi.org/10.1016/j.asr.2022.08.033.

Kanekal, S., Miyoshi, Y., 2021. Dynamics of the terrestrial radiation belts: a review of recent results during the VarSITI (Variability of the Sun and Its Terrestrial Impact) era, 2014–2018. Prog. Earth Planet. Sci. 8, 35. https://doi.org/10.1186/s40645-021-00413-y.

Kataoka, R., Sato, T., Kubo, Y., Shiota, D., Kuwabara, T., Yashiro, S., Yasuda, H., 2014. Radiation dose forecast of WASAVIES during ground-level enhancement. Space Weather 12 (6), 380–386. https://doi.org/10.1002/2014SW001053.

Keesee, A.M., Buzulukova, N., Mouikis, C., Scime, E.E., 2021. Mesoscale structures in Earth's magnetotail observed using energetic neutral atom imaging. Geophys. Res. Lett. 48e2020GL091467. https://doi.org/10.1029/2020GL091467.

Kepko, L., Viall, N.M., 2019. The source, significance, and magnetospheric impact of periodic density structures within stream interaction regions. J. Geophys. Res. Space Phys. 124, 7722–7743. https://doi.org/10.1029/2019JA026962.

Kilpua, E.K.J., Hietala, H., Turner, D.L., Koskinen, H.E.J., Pulkkinen, T.I., Rodriguez, J.V., Reeves, G.D., Claudepierre, S.G., Spence, H.E., 2015. Unraveling the drivers of the storm time radiation belt response. Geophys. Res. Lett. 42, 3076–3084.

Kilpua, E.K.J., Turner, D.L., Jaynes, A.N., Hietala, H., Koskinen, H.E.J., Osmane, A., Palmroth, M., Pulkkinen, T.I., Vainio, R., Baker, D., Claudepierre, S.G., 2019. Outer Van Allen radiation belt response to interacting interplanetary coronal mass ejections. J. Geophys. Res. (Space Phys.) 124 (3), 1927–1947. https://doi.org/10.1029/2018JA026238.

Kim, K.-C., Shprits, Y., Subbotin, D., Ni, B., 2011. Understanding the dynamic evolution of the relativistic electron slot region including

radial and pitch angle diffusion. J. Geophys. Res. 116, A10214. https://doi.org/10.1029/2011JA016684.

Kim, K.-C., Shprits, Y., 2013. Long-term relativistic radiation belt electron responses to GEM magnetic storms. J. Atmos. Sol. Terr. Phys. 100–101, 59–67. https://doi.org/10.1016/j.jastp.2013.04.007.

King, J.H., 1974. Solar proton fluences for 1977–1983 space missions. J. Spacecr. Rocket 11 (6), 401–408. https://doi.org/10.2514/3.62088.

Kistler, L.M., Mouikis, C.G., Spence, H.E., et al., 2016. The source of O+ in the storm time ring current. J. Geophys. Res. Space Phys. 121, 5333–5349. https://doi.org/10.1002/2015JA022204.

Koi, T., Asai, M., Wright, D., Niita, K., Nara, Y., Amako, K., Sasaki, T., 2003. Interfacing the JQMD and JAM nuclear reaction codes to Geant4, SLAC-PUB 9978.

Koller, J., Chen, Y., Reeves, G.D., et al., 2007. Identifying the radiation belt source region by data assimilation. J. Geophys. Res. 112, A06244. https://doi.org/10.1029/2006JA012196.

Koons, H.C., Majur, J.E., Selesnick, R.S., Blake, J.B., Fennell, J.F., Roeder, J.L., Anderson, P.C., 2000. The Impact of the Space Environment on Space Systems, Proceedings of the 6th Spacecraft Charging Conference. November 2-6, 1998. AFRL Science Center, Hanscom AFB, MA, USA, p. 7–11, 1998sct..conf....7K

Koskinen, H.E.J., Kilpua, E.K.J., 2022. Dynamics of the Electron Belts. In: Physics of Earth's Radiation Belts. Astronomy and Astrophysics Library. Springer, Cham. https://doi.org/10.1007/978-3-030-82167-8_7.

Krall, J., Fok, M.-C., Huba, J.D., Glocer, A., 2023. Stormtime ring current heating of the ionosphere and plasmasphere. J. Geophys. Res.: Space Phys. 128e2022JA030390. https://doi.org/10.1029/2022JA030390.

Kress, B.T., Mertens, C.J., Wiltberger, M., 2010. Solar energetic particle cutoff variations during the 29–31 October 2003 geomagnetic storm. Space Weather 8, S05001. https://doi.org/10.1029/2009SW000488.

Kress, B.T., Hudson, M.K., Perry, K.L., Slocum, P.L., 2004. Dynamic modeling of geomagnetic cutoff for the 23–24 November 2001 solar energetic particle event. Geophysical Research Letters 31, L04808. https://doi.org/10.1029/2003GL018599.

Kress, B.T., Hudson, M.K., Selesnick, R.S., Mertens, C.J., Engel, M., 2015. Modelling geomagnetic cutoffs for space weather applications. J. Geophys. Res. Space Phys. 120, 5694–5702. https://doi.org/10.1002/2014JA020899.

Kryakunova, O.N., Belov, A.V., Yakovets, A.F., Abunin, A.A., Tsepakina, I.L., Seifullina, B.B., Abunina, M.A., Nikolayevskiy, N.F., Shlyk, N.S., 2023. A statistical relationship between the fluence of magnetospheric relativistic electrons and interplanetary and geomagnetic characteristics. Adv. Space Res. https://doi.org/10.1016/j.asr.2022.08.067.

Kurita, S., Miyoshi, Y., Shiokawa, K., Higashio, N., Mitani, T., Takashima, T., et al., 2018. Rapid loss of relativistic electrons by EMIC waves in the outer radiation belt observed by Arase, Van Allen Probes, and the PWING ground stations. Geophys. Res. Lett. 45, 12720–12729. https://doi.org/10.1029/2018GL080262.

Latocha, M., Beck, P., Rollet, S., 2009. AVIDOS—a software package for European accredited aviation dosimetry. Radiat. Prot. Dosim. 136 (4), 286–290. https://doi.org/10.1093/rpd/ncp126.

Lei, F., Clucas, S., Dyer, C., Truscott, P., 2004. An atmospheric radiation model based on response matrices generated by detailed Monte Carlo simulations of cosmic ray interactions. IEEE Trans. Nucl. Sci. 51 (6), 3442–3451. https://doi.org/10.1109/tns.2004.839131.

Lei, F., Hands, A., Clucas, S., Dyer, C., Truscott, P., 2006. Improvement to and Validations of the QinetiQ Atmospheric Radiation Model (QARM). IEEE Trans. Nucl. Sci. 53 (4), 1851–1858. https://doi.org/10.1109/TNS.2006.880567.

Lejosne, S., Allison, H.J., Blum, L.W., Drozdov, A.Y., Hartinger, M.D., Hudson, M.K., Jaynes, A.N., Ozeke, L., Roussos, E., Zhao, H., 2022. Differentiating between the leading processes for electron radiation belt acceleration. Front. Astron. Space Sci. 9896245. https://doi.org/10.3389/fspas.2022.896245.

Lejosne, S., Kollmann, P., 2020. Radiation belt radial diffusion at earth and beyond. Space Sci. Rev. 216, 19. https://doi.org/10.1007/s11214-020-0642-6.

Leka, K.D., 2022. Solar Flare Forecasting: where we stand as the activity cycle looms, The Third Triennial Earth-Sun Summit (TESS), held 8-11 August, 2022 in Bellevue/Seattle, WA. Bull. AAS 54(7), 2022n7i111ap01., 2022tess.conf111a01

Leske, R.A., Mewaldt, R.A., Stone, E.C., von Rosenvinge, T.T., 2001. Observations of geomagnetic cutoff variations during solar energetic particle events and implications for the radiation environment at the Space Station. J. Geophys. Res. 106 (A12), 30011–30022. https://doi.org/10.1029/2000JA000212.

Li, X., 2004. Variations of 0.7–6.0 MeV electrons at geosynchronous orbit as a function of solar wind. Space Weather 2, S03006. https://doi.org/10.1029/2003SW000017.

Li, Z., Engel, M., Hudson, M., Kress, B., Patel, M., Qin, M., Selesnick, R., 2021b. Solar energetic proton access to the inner magnetosphere during the September 7–8, 2017 event. J. Geophys. Res.: Space Phys. 126e2021JA029107. https://doi.org/10.1029/2021JA029107.

Li, X., Selesnick, R.S., Zhao, H., Baker, D.N., Blake, J.B., Temerin, M. A., 2021. Source, loss, and transport of energetic particles deep inside earth's magnetosphere (L <4), Magnetosp. Sol. Syst. 0, 323–334.

Li, W., Hudson, M.K., 2019. Earth's Van Allen radiation belts: From discovery to the Van Allen Probes Era. J. Geophys. Res. Space Phys. 124, 8319–8351. https://doi.org/10.1029/2018JA0doi25940.

Li, W., Shprits, Y.Y., Thorne, R.M., 2007. Dynamic evolution of energetic outer zone electrons due to wave-particle interactions during storms. J. Geophys. Res. 112, A10220. https://doi.org/10.1029/2007JA012368.

Li, W., Ma, Q., Thorne, R.M., Bortnik, J., Kletzing, C.A., Kurth, W.S., Hospodarsky, G.B., Nishimura, Y., 2015. Statistical properties of plasmaspheric hiss derived from Van Allen Probes data and their effects on radiation belt electron dynamics. J. Geophys. Res. Space Phys. 120, 3393–3405. https://doi.org/10.1002/2015JA021048.

Li, X., Temerin, M., Baker, D.N., Reeves, G.D., Larson, D., 2001. Quantitative prediction of radiation belt electrons at geostationary orbit based on solar wind measurements. Geophys. Res. Lett. 28 (9), 1887–1890. https://doi.org/10.1029/2000GL012681.

Li, X., Xiang, Z., Zhang, K., Khoo, L., Zhao, H., Baker, D.N., Temerin, M.A., 2020. New insights from long-term measurements of inner belt protons (10s of MeV) by SAMPEX, POES, Van Allen Probes, and simulation results. J. Geophys. Res.: Space Phys. 125e2020JA028198. https://doi.org/10.1029/2020JA028198.

Li, L.Y., Yu, J., Cao, J.B., Yang, J.Y., Li, X., Baker, D.N., Reeves, G.D., Spence, H., 2017. Roles of whistler mode waves and magnetosonic waves in changing the outer radiation belt and the slot region. J. Geophys. Res. Space Phys. 122, 5431–5448. https://doi.org/10.1002/2016JA023634.

Lin, D., Sorathia, K., Wang, W., Merkin, V., Bao, S., Pham, K., et al., 2021a. The role of diffuse electron precipitation in the formation of subauroral polarization streams. J. Geophys. Res.: Space Phys. 126 (12), e2021JA029792. https://doi.org/10.1029/2021JA029792.

Lin, Y., Wang, X.Y., Fok, M.-C., Buzulukova, N., Perez, J.D., Cheng, L., Chen, L.-J., 2021b. Magnetotail-inner magnetosphere transport associated with fast flows based on combined global-hybrid and CIMI simulation. J. Geophys. Res.: Space Phys. 126e2020JA028405. https://doi.org/10.1029/2020JA028405.

Lin, D., Wang, W., Merkin, V.G., Huang, C., Oppenheim, M., Sorathia, K., et al., 2022. Origin of dawnside subauroral polarization streams during major geomagnetic storms. AGU Adv. 3e2022AV000708. https://doi.org/10.1029/2022AV000708.

Linton, M.G., Antiochos, S.K., Barnes, G., Fan, Y., Liu, Y., Lynch, B.J., Afanasyev, A.N., Nick Arge, C., Burkepile, J., Cheung, M.C.M., Dahlin, J.T., DeRosa, M.L., Giuliana de Toma, C., DeVore, R., Fisher, G.H., Henney, C.J., Jones, S.I., Karpen, J.T., Kazachenko, M. D., Leake, J.E., Török, T., Welsch, B.T., 2023. Recent progress on understanding coronal mass ejection/flare onset by a NASA living with

a star focused science team. Adv. Space Res. https://doi.org/10.1016/j.asr.2023.06.045.

Lorenzato, L., Sicard, A., Bourdarie, S., 2012. A physical model for electron radiation belts of Saturn. J. Geophys. Res. 117, A08214. https://doi.org/10.1029/2012JA017560.

Lozinski, A.R., Horne, R.B., Glauert, S.A., Del Zanna, G., Claudepierre, S.G., 2021a. Modeling inner proton belt variability at energies 1 to 10 MeV using BAS-PRO. J. Geophys. Res.: Space Phys. 126e2021JA029777. https://doi.org/10.1029/2021JA029777.

Lozinski, A.R., Horne, R.B., Glauert, S.A., Del Zanna, G., Albert, J.M., 2021b. Optimization of radial diffusion coefficients for the proton radiation belt during the CRRES era. J. Geophys. Res.: Space Phys. 126e2020JA028486. https://doi.org/10.1029/2020JA028486.

Lyon, J.G., Fedder, J.A., Mobarry, C.M., 2004. The Lyon–Fedder–Mobarry (LFM) global MHD magnetospheric simulation code. J. Atmos. Sol. Terr. Phys. 66 (15–16), 1333–1350. https://doi.org/10.1016/j.jastp.2004.03.020.

Ma, D., Chu, X., Bortnik, J., Claudepierre, S.G., Tobiska, W.K., Cruz, A., et al., 2022. Modeling the dynamic variability of sub-relativistic outer radiation belt electron fluxes using machine learning. Space Weather 20e2022SW003079. https://doi.org/10.1029/2022SW003079.

Ma, D., Bortnik, J., Chu, X., Claudepierre, S.G., Ma, Q., Kellerman, A., 2023. Opening the black box of the radiation belt machine learning model. Space Weather 21e2022SW003339. https://doi.org/10.1029/2022SW003339.

Maget, V., Bourdarie, S., Rolland, G., 2013. Characterizing solar energetic particles access to any Earth-space location. IEEE Trans. Nucl. Sci. 60 (4), 2404–2410. https://doi.org/10.1109/TNS.2012.2233756.

Maget, V., Papadimitriou, C., Sandberg, I., Bourdarie, S., Glover, A., Evans, H., Keil, R., 2022. Assessing objective performances of nowcast-forecast framework in the context of the ESA radiation belt forecast and nowcast activity. In: 44th COSPAR Scientific Assembly, vol. 44, p. 3447.

Maliniemi, V., Arsenovic, P., Seppälä, A., Nesse Tyssøy, H., 2022. The influence of energetic particle precipitation on Antarctic stratospheric chlorine and ozone over the 20th century. Atmos. Chem. Phys. 22, 8137–8149. https://doi.org/10.5194/acp-22-8137-2022.

Mann, I.R., Ozeke, L.G., Murphy, K.R., Claudepierre, S.G., Turner, D. L., Baker, D.N., et al., 2016. Explaining the dynamics of the ultra-relativistic third Van Allen radiation belt. Nat Phys 12 (10), 978–983. https://doi.org/10.1038/nphys3799.

Mann, I.R., Ozeke, L.G., 2016. How quickly, how deeply, and how strongly can dynamical outer boundary conditions impact Van Allen radiation belt morphology? J. Geophys. Res. Space Phys. 121, 6. https://doi.org/10.1002/2016ja022647.

Mannucci, A., Bortnik, J., Cid, C., Gulyaeva, T., Liu, H., McGranaghan, R., Verkhoglyadova, O., 2023. The future of space weather prediction and forecasting. Bull. AAS 55 (3). https://doi.org/10.3847/25c2cfeb.3ea9f658.

Maruyama, N., Richmond, A.D., Fuller-Rowell, T.J., Codrescu, M.V., Sazykin, S., Toffoletto, F.R., Spiro, R.W., Millward, G.H., 2005. Interaction between direct penetration and disturbance dynamo electric fields in the storm-time equatorial ionosphere. Geophys. Res. Lett. 32, L17105. https://doi.org/10.1029/2005GL023763.

Matthiä, D., Heber, B., Reitz, G., Meier, M., Sihver, L., Berger, T., Herbst, K., 2009a. Temporal and spatial evolution of the solar energetic particle event on 20 January 2005 and resulting radiation doses in aviation. J. Geophys. Res.-Space Phys. 114. https://doi.org/10.1029/2009ja014125.

Matthiä, D., Heber, B., Reitz, G., Sihver, L., Berger, T., Meier, M., 2009b. The ground level event 70 on December 13th, 2006 and related effective doses at aviation altitudes. Radiat. Prot. Dosim. 136 (4), 304–310. https://doi.org/10.1093/Rpd/Ncp141.

Matthiä, D., Berger, T., Mrigakshi, A.I., Reitz, G., 2013. A ready-to-use galactic cosmic ray model. Adv. Space Res. 51, 329–338. https://doi.org/10.1016/j.asr.2012.09.022.

Matthiä, D., Meier, M.M., Reitz, G., 2014. Numerical calculation of the radiation exposure from galactic cosmic rays at aviation altitudes with the PANDOCA core model. Space Weather 12 (3), 161–171. https://doi.org/10.1002/2013sw001022.

Maus, S., Macmillan, S., Chernova, T., Choi, S., Dater, D., Golovkov, V., et al., 2005. The 10th-generation international geomagnetic reference field. Geophys. J. Int. 161 (3), 561–565. https://doi.org/10.1111/j.1365-246X.2005.02641.x.

McCracken, K.G., Shea, M.A., Smart, D.F., 2023. A high time-resolution analysis of the Ground-Level Enhancement (GLE) of 23 February 1956 in terms of the CSHKP standard flare model. Adv. Space Res. 72 (8), 2023. https://doi.org/10.1016/j.asr.2023.06.049.

McPherson, D.A., Cauffman, D.P., Schober, W., 1975. Spacecraft Charging at High Altitudes – The Scatha Satellite Program. In: 1975 IEEE International Symposium on Electromagnetic Compatibility, San Antonio, TX, USA, pp. 1–1. https://doi.org/10.1109/ISEMC.1975.7567816.

Meier, M.M., Berger, T., Jahn, T., et al., 2023. Impact of the South Atlantic Anomaly on radiation exposure at flight altitudes during solar minimum. Sci Rep 13, 9348. https://doi.org/10.1038/s41598-023-36190-5.

Meier, M.M., Matthiä, D.A., 2014. (2014), space weather index for the radiation field at aviation altitudes. J. Space Weather. Space Clim. 4, A13.

Meier, M.M., Copeland, K., Matthiä, D., Mertens, C.J., Schennetten, K., 2018. First steps toward the verification of models for the assessment of the radiation exposure at aviation altitudes during quiet space weather conditions. Space Weather 16, 1269–1276. https://doi.org/10.1029/2018SW001984.

Meier, M.M., Copeland, K., Klöble, K.E.J., Matthiä, D., Plettenberg, M. C., Schennetten, K., Wirtz, M., Hellweg, C.E., 2020. Radiation in the atmosphere—A hazard to aviation safety? Atmosphere 11 (12), 1358. https://doi.org/10.3390/atmos11121358.

Meier, M.M., Matthiä, D., 2019. Dose assessment of aircrew: the impact of the weighting factors according to ICRP 103. J. Radiol. Prot. 39 (3), 698. https://doi.org/10.1088/1361-6498/ab178d.

Meierbachtol, C.S., Svyatskiy, D., Delzanno, G.L., Vernon, L.J., Moulton, J.D., 2017. An electrostatic particle-in-cell code on multi-block structured meshes. J. Comput. Phys. 350, 796–823. https://doi.org/10.1016/j.jcp.2017.09.016.

Merkin, V.G., Lyon, J.G., 2010. Effects of the low-latitude ionospheric boundary condition on the global magnetosphere. J. Geophys. Res. 115, A10202. https://doi.org/10.1029/2010JA015461.

Merkin, V.G., Panov, E.V., Sorathia, K., Ukhorskiy, A.Y., 2019. Contribution of bursty bulk flows to the global dipolarization of the magnetotail during an isolated substorm. J. Geophys. Res. Space Phys. 124, 8647–8668. https://doi.org/10.1029/2019JA026872.

Mertens, C.J., Tobiska, W.K., 2021. Space Weather Radiation Effects on High-Altitude/-Latitude Aircraft. In: Anthea J. Coster, Philip J. Erickson, Louis J. Lanzerotti, Yongliang Zhang, Larry J. Paxton (Eds.), Space Weather Effects and Applications, Geophysical Monograph Series. https://doi.org/10.1002/9781119815570.ch4.

Mertens, C.J., Kress, B.T., Wiltberger, M., Blattnig, S.R., Slaba, T.C., Solomon, S.C., Engel, M., 2010. Geomagnetic influence on aircraft radiation exposure during a solar energetic particle event in October 2003. Space Weather 8, S03006. https://doi.org/10.1029/2009SW000487.

Mertens, C.J., Meier, M.M., Brown, S., Norman, R.B., Xu, X., 2013. NAIRAS aircraft radiation model development, dose climatology, and initial validation. Space Weather 11, 603–635. https://doi.org/10.1002/swe.20100.

Mertens, C.J., Gronoff, G.P., Zheng, Y., Petrenko, M., Buhler, J., Phoenix, D., et al., 2023. NAIRAS model run-on-request service at CCMC. Space Weather 21e2023SW003473. https://doi.org/10.1029/2023SW003473.

Métrailler, L., Bélanger, G., Kretschmar, P., Kuulkers, E., Martínez, R.P., Ness, J.-U., Rodriguez, P., Casale, M., Fauste, J., Finn, T., Sanchez, C., Godard, T., Southworth, R., 2019. Data-driven modelling of the

Van Allen Belts: The 5DRBM model for trapped electrons. Adv. Space Res. 64 (9), 1701–1711. https://doi.org/10.1016/j.asr.2019.07.036.

Millan, R.M., von Steiger, R., Ariel, M., Bartalev, S., Borgeaud, M., Campagnola, S., Castillo-Rogez, J.C., Fléron, R., Gass, V., Gregorio, A., et al., 2019. Small satellites for space science: A COSPAR scientific roadmap. Adv. Space Res. 64 (8), 1466–1517. https://doi.org/10.1016/j.asr.2019.07.035.

Minow, J., Jordanova, V.K., Pitchford, D., Ganushkina, N.Y., Zheng, Y., Delzanno, G.L., Jun, I., Kim, W., 2024. ISWAT Spacecraft Surface Charging Review Paper, ASR, AISR-D-23-00139

Mironova, I.A., Aplin, K.L., Arnold, F., et al., 2015. Energetic particle influence on the earth's atmosphere. Space Sci. Rev. 194, 1–96. https://doi.org/10.1007/s11214-015-0185-4.

Mishev, A., Panovska, S., Usoskin, I., 2023. Assessment of the radiation risk at flight altitudes for an extreme solar particle storm of 774 AD. J. Space Weather Space Clim. 13, 22. https://doi.org/10.1051/swsc/2023020.

Miyoshi, Y., & Kataoka, R., 2011. Solar cycle variations of outer radiation belt and its relationship to solar wind structure dependences. Journal of Atmospheric and Solar-Terrestrial Physics, 73 (1) https://doi.org/10.1016/j.jastp.2010.09.031.

Miyoshi, Y., Kataoka, R., 2005. Ring current ions and radiation belt electrons during geomagnetic storms driven by coronal mass ejections and corotating interaction regions. Geophys. Res. Lett. 32, L21105. https://doi.org/10.1029/2005GL024590.

Miyoshi, Y., Shinohara, I., Takashima, T., Asamura, K., Higashio, N., Mitani, T., et al., 2018. Geospace exploration project ERG. Earth Planets Space 70, 101. https://doi.org/10.1186/s40623-018-0862-0.

Miyoshi, Y., Shinohara, I., Ukhorskiy, S., et al., 2022. Collaborative research activities of the Arase and Van Allen Probes. Space Sci. Rev. 218, 38. https://doi.org/10.1007/s11214-022-00885-4.

Morley, S.K., 2020. Challenges and opportunities in magnetospheric space weather prediction. Space Weather 18e2018SW002108. https://doi.org/10.1029/2018SGuoW002108.

Mouikis, C.G., Bingham, S.T., Kistler, L.M., Farrugia, C.J., Spence, H. E., Reeves, G.D., et al., 2019. The storm-time ring current response to ICMEs and CIRs using Van Allen Probe Observations. J. Geophys. Res. Space Phys. 124, 9017–9039. https://doi.org/10.1029/2019JA026695.

Murphy, K.R., Mann, I.R., Sibeck, D.G., Rae, I.J., Watt, C.E.J., Ozeke, L.G., et al., 2020. A framework for understanding and quantifying the loss and acceleration of relativistic electrons in the outer radiation belt during geomagnetic storms. Space Weather 18e2020SW002477. https://doi.org/10.1029/2020SW002477.

NASA, 2022. NASA-HDBK-4002B. Mitigating in-space charging effects - a guideline. 07 June 2022.

National Research Council, 2008. Severe space weather events – Understanding societal and economic impacts: A workshop report. Natl. Acad. Press, Washington, D.C., 144 p.

Neal, J.J., Rodger, C.J., Green, J.C., 2013. Empirical determination of solar proton access to the atmosphere: Impact on polar flight paths,. Space Weather 11 https://doi.org/10.1002/swe.20066.

Nénon, Q., Sicard, A., Caron, P., 2018. The rings of Jupiter as seen by the electron and proton radiation belt model Salammbô. Geophys. Res. Lett. 45, 10838–10846. https://doi.org/10.1029/2018GL080157.

Newell, P.T., Sotirelis, T., Wing, S., 2009. Diffuse, monoenergetic, and broadband aurora: The global precipitation budget. J. Geophys. Res. 114, A09207. https://doi.org/10.1029/2009JA014326.

Nitta, N.V., Liu, Y., DeRosa, M.L., et al., 2012. What are special about ground-level events? Space Sci. Rev. 171, 61–83. https://doi.org/10.1007/s11214-012-9877-1.

Nymmik, R.A., Panasyuk, M.I., Suslov, A.A., 1996. Galactic cosmic ray flux simulation and prediction. Adv. Space Res. 17 (2), 19–30. https://doi.org/10.1016/0273-1177(95)00508-C.

O'Brien, T.P., 2009. SEAES-GEO: A spacecraft environmental anomalies expert system for geosynchronous orbit. Space Weather 7, S09003 https://doi.org/10.1029/2009SW000473.

O'Brien, T.P., Johnston, W.R., Huston, S.L., Roth, C.J., Guild, T.B., Su, Y.-J., Quinn, R.A., 2018a. Changes in AE9, AP9-IRENE version 1.5. IEEE Trans. Nucl. Sci. 65 (1), 462–466. https://doi.org/10.1109/TNS.2017.2771324.

O'Brien, T.P., Mazur, J.E., Looper, M.D., 2018b. Solar energetic proton access to the magnetosphere during the 10–14 September 2017 particle event. Space Weather 16, 2022–2037. https://doi.org/10.1029/2018SW001960.

O'Brien, T.P., 2021. Lowering to the Occasion: Meeting Society's Energetic Charged Particle Needs in the Age of Proliferated LEO. Aerospace Report No. ATR-2021-068.

Ogliore, R.C., Mewaldt, R.A., Leske, R.A., Stone, E.C., von Rosenvinge, T.T., 2001. A Direct Measurement of the Geomagnetic Cutoff for Cosmic Rays at Space Station Latitudes Vol. 10, 4112–4114.

Olifer, L., Mann, I.R., Ozeke, L.G., Claudepierre, S.G., Baker, D.N., Spence, H.E., 2021. On the similarity and repeatability of fast radiation belt loss: Role of the last closed drift shell. J. Geophys. Res.: Space Phys. 126e2021JA029957. https://doi.org/10.1029/2021JA029957.

O'Neill, P.M., 2010. Badhwar–O'Neill 2010 Galactic Cosmic Ray Flux Model—Revised. IEEE Trans. Nucl. Sci. 57 (6), 3148–3153. https://doi.org/10.1109/TNS.2010.2083688.

O'Neill, P.M., Golge, S., Slaba, T.C., 2015. Badhwar-O'Neill 2014 galactic cosmic ray flux model description (NASA/TP-2015-218569). NASA Johnson Space Center, Houston, TX.

Opgenoorth, Hermann, J., Robinson, R., et al., 2024. Earth's geomagnetic environment—progress and gaps in understanding, prediction, and impacts. Adv. Space Res. (this issue)

Ozeke, L.G., Mann, I.R., Dufresne, S.K.Y., Olifer, L., Morley, S.K., Claudepierre, S.G., et al., 2020. Rapid outer radiation belt flux dropouts and fast acceleration during the March 2015 and 2013 storms: The role of ULF wave transport from a dynamic outer boundary. J. Geophys. Res. Space Phys. 125e2019JA027179. https://doi.org/10.1029/2019JA027179.

Pandya, M., Bhaskara, V., Ebihara, Y., Reeves, G.D., 2022. L-value and energy dependence of 0.1–50 keV O+, He+, and H+ ions for CME and CIR storms over the entire Van Allen Probes era. J. Geophys. Res.: Space Phys. 127e2022JA030568. https://doi.org/10.1029/2022JA030568.

Pembroke, A., Toffoletto, F., Sazykin, S., Wiltberger, M., Lyon, J., Merkin, V., Schmitt, P., 2012. Initial results from a dynamic coupled magnetosphere-ionosphere-ring current model. J. Geophys. Res. 117, A02211. https://doi.org/10.1029/2011JA016979.

Pham, K.H., Zhang, B., Sorathia, K., Dang, T., Wang, W., Merkin, V., et al., 2022. Thermospheric density perturbations produced by traveling atmospheric disturbances during August 2005 storm. J. Geophys. Res.: Space Phys. 127e2021JA030071. https://doi.org/10.1029/2021JA030071.

Picone, J.M., Hedin, A.E., Drob, D.P., Aikin, A.C., 2002. NRLMSISE-00 empirical model of the atmosphere: Statistical comparisons and scientific issues. J. Geophys. Res.: Space Phys. 107 (A12). https://doi.org/10.1029/2002ja009430, SIA 15-11-SIA 15-16.

Pierrard, V., Botek, E., Ripoll, J.-F., Thaller, S.A., Moldwin, M.B., Ruohoniemi, M., Reeves, G., 2021. Links of the plasmapause with other boundary layers of the magnetosphere: ionospheric convection, radiation belt boundaries, auroral oval. Front. Astron. Space Sci. 2021. https://doi.org/10.3389/fspas.2021.728531.

Pulkkinen, A., Rastätter, L., Kuznetsova, M., Singer, H., Balch, C., Weimer, D., Toth, G., Ridley, A., Gombosi, T., Wiltberger, M., Raeder, J., Weigel, R., 2013. Community-wide validation of geospace model ground magnetic field perturbation predictions to support model transition to operations. Space Weather 11, 369–385. https://doi.org/10.1002/swe.20056.

Qian, L., Burns, A.G., Emery, B.A., Foster, B., Lu, G., Maute, A., Richmond, A.D., Roble, R.G., Solomon, S.C., Wang, W., 2014. The NCAR TIE-GCM. In: J. Huba, R. Schunk and G. Khazanov (Eds.), Modeling the Ionosphere–Thermosphere System. https://doi.org/10.1002/9781118704417.ch7.

Qin, M., Hudson, M., Li, Z., Millan, R., Shen, X., Shprits, Y., et al., 2019a. Investigating Loss of Relativistic Electrons Associated With EMIC Waves at Low L Values on 22 June 2015. J. Geophys. Res. Space Phys. 124 (6), 4022–4036. https://doi.org/10.1029/2018JA025726.

Qin, M., Hudson, M., Kress, B., Selesnick, R., Engel, M., Li, Z., Shen, X., 2019b. Investigation of solar proton access into the inner magnetosphere on 11 September 2017. J. Geophys. Res. Space Phys. 124 (5), 3402–3409. https://doi.org/10.1029/2018JA026380.

Raeder, J., Berchem, J., Ashour-Abdalla, M., 1996. The importance of small scale processes in global MHD simulations: Some numerical experiments. In: Chang, T., Jasperse, J. (Eds.), The Physics of Space Plasma, vol. 14. MIT Cent. for Theoret. Ceo/Cosmo Plasma PHys, Cambridge, Mass, p. 403.

Randall, C.E. et al., 2005. Stratospheric effects of energetic particle precipitation in 2003–2004. Geophys. Res. Lett. 32, L05802. https://doi.org/10.1029/2004GL022003.

Reames, D.V., 2013. The Two Sources of Solar Energetic Particles. Space Sci Rev 175, 53–92 https://doi.org/10.1007/s11214-013-9958-9.

Reeves, G.D., Chen, Y., Cunningham, G.S., Friedel, R.W.H., Henderson, M.G., Jordanova, V.K., Koller, J., Morley, S.K., Thomsen, M.F., Zaharia, S., 2012. Dynamic radiation environment assimilation model: DREAM. Space Weather 10, S03006. https://doi.org/10.1029/2011SW000729.

Reeves, G.D., Friedel, R.H.W., Larsen, B.A., Skoug, R.M., Funsten, H. O., Claudepierre, S.G., Fennell, J.F., Turner, D.L., Denton, M.H., Spence, H.E., Blake, J.B., Baker, D.N., 2016. Energy-dependent dynamics of keV to MeV electrons in the inner zone, outer zone, and slot regions. J. Geophys. Res. 121, 397–412. https://doi.org/10.1002/2015JA021569.

Reiss, M.A., Arge, C.N., Henney, C.J., Klimchuk, J.A., Linker, J.A., Muglach, K., Pevtsov, A.A., Pinto, R.F., Schonfeld, S.J., 2023. Progress and challenges in understanding the ambient solar magnetic field, heating, and spectral irradiance. Adv. Space Res. https://doi.org/10.1016/j.asr.2023.08.039.

Richmond, A., Ridley, E.C., Roble, R.G., 1992. A thermosphere/ionosphere general circulation model with coupled electrodynamics. Geophys. Res. Lett. 19 (6), 601–604. https://doi.org/10.1029/92GL00401.

Ripoll, J.-F., Claudepierre, S.G., Ukhorskiy, A.Y., Colpitts, C., Li, X., Fennell, J., Crabtree, C., 2020. Particle dynamics in the Earth's radiation belts: Review of current research and open questions. J. Geophys. Res.: Space Phys. 125e2019JA026735. https://doi.org/10.1029/2019JA026735.

Ripoll, J.-F., Pierrard, V., Cunningham, G.S., Chu, X., Sorathia, K.A., Hartley, D.P., Thaller, S.A., Merkin, V.G., Delzanno, G.L., De Pascuale, S., Ukhorskiy, A.Y., 2023. Modeling of the cold electron plasma density for radiation belt physics. Front. Astron. Space Sci. https://doi.org/10.3389/fspas.2023.1096595.

Robinson, R.M., Vondrak, R.R., Miller, K., Dabbs, T., Hardy, D., 1987. On calculating ionospheric conductances from the flux and energy of precipitating electrons. J. Geophys. Res. 92 (A3), 2565. https://doi.org/10.1029/JA092iA03p02565.

Rodger, C.J., Clilverd, M.A., Hendry, A.T., Forsyth, C., 2022. Examination of radiation belt dynamics during substorm clusters: Magnetic local time variation and intensity of precipitating fluxes. J. Geophys. Res.: Space Phys. 127e2022JA030750. https://doi.org/10.1029/2022JA030750.

Rose, D.C., Ziauddin, S., 1962. The polar cap absorption effect. Space Sci. Rev. 1, 115–134. https://doi.org/10.1007/BF00174638.

Sadykov, V.M., Kitiashvili, I.N., Tobiska, W.K., Guhathakurta, M., 2020. Radiation data portal: integration of radiation measurements at the aviation altitudes and solar-terrestrial environment observations. Space Weather 19e2020SW002653. https://doi.org/10.1029/2020SW002653.

Saikin, A.A., Shprits, Y.Y., Drozdov, A.Y., Landis, D.A., Zhelavskaya, I. S., Cervantes, S., 2021. Reconstruction of the radiation belts for solar cycles 17–24 (1933–2017). Space Weather 19e2020SW002524. https://doi.org/10.1029/2020SW002524.

Sakaguchi, K., Miyoshi, Y., Saito, S., Nagatsuma, T., Seki, K., Murata, K.T., 2013. Relativistic electron flux forecast at geostationary orbit using Kalman filter based on multivariate autoregressive model. Space Weather 11, 79–89. https://doi.org/10.1002/swe.20020.

Sakaguchi, K., Nagatsuma, T., Reeves, G.D., Spence, H.E., 2015. Prediction of MeV electron fluxes throughout the outer radiation belt using multivariate autoregressive models. Space Weather 13, 853–867. https://doi.org/10.1002/2015SW001254.

Sandhu, J.K., Rae, I.J., Freeman, M.P., Forsyth, C., Gkioulidou, M., Reeves, G.D., et al., 2018. Energization of the ring current by substorms. J. Geophys. Res. Space Phys. 123, 8131–8148. https://doi.org/10.1029/2018JA025766.

Sato, T., Yasuda, H., Niita, K., Endo, A., Sihver, L., 2008. Development of PARMA: PHITS-based analytical radiation model in the atmosphere. Radiat. Res. 170 (2), 244–259. https://doi.org/10.1667/RR1094.1.

Sato, T., Kataoka, R., Yasuda, H., Yashiro, S., Kuwabara, T., Shiota, D., Kubo, Y., 2014. Air shower simulation for WASAVIES: warning system for aviation exposure to solar energetic particles. Radiat. Prot. Dosim. 161 (1–4), 274–278. https://doi.org/10.1093/rpd/nct332.

Sato, T., Kataoka, R., Shiota, D., Kubo, Y., Ishii, M., Yasuda, H., et al., 2018. Real time and automatic analysis program for WASAVIES: Warning system for aviation exposure to solar energetic particles. Space Weather 16, 924–936. https://doi.org/10.1029/2018SW001873.

Sawyer, D.M., Vette, J.I., 1976. Ap-8 trapped proton environment for solar maximum and solar minimum. [AP8MAX and AP8MIN] (No. N-77-18983; NASA-TM-X-72605). National Aeronautics and Space Administration, Greenbelt, MD (USA). Goddard Space Flight Center.

Selesnick, R.S., Baker, D.N., Jaynes, A.N., Li, X., Kanekal, S.G., Hudson, M.K., Kress, B.T., 2014. Observations of the inner radiation belt: CRAND and trapped solar protons. J. Geophys. Res. Space Phys. 119, 6541–6552. https://doi.org/10.1002/2014JA020188.

Shea, M.A., Smart, D.F., 2012. Space Weather and the Ground-Level Solar Proton Events of the 23rd Solar Cycle. Space Sci. Rev. 171 (1–4), 161–188. https://doi.org/10.1007/s11214-012-9923-z.

Shprits, Y.Y., Elkington, S.R., Meredith, N.P., Subbotin, D.A., 2008a. Review of modeling of losses and sources of relativistic electrons in the outer radiation belt I: Radial transport. J. Atmos.Sol.-Terrestr. Phys. 70, 1679–1693. https://doi.org/10.1016/j.jastp.2008.06.008.

Shprits, Y.Y., Drozdov, A.Y., Spasojevic, M., Kellerman, A.C., Usanova, M.E., Engebretson, M.J., et al., 2016. Wave-induced loss of ultra-relativistic electrons in the Van Allen radiation belts. Nat. Commun. 7 (1), 12883. https://doi.org/10.1038/ncomms12883.

Shprits, Y.Y., Angelopoulos, V., Russell, C.T., et al., 2018b. Scientific objectives of electron losses and fields investigation onboard lomonosov satellite. Space Sci. Rev. 214, 25. https://doi.org/10.1007/s11214-017-0455-4.

Shprits, Y.Y., Allison, H.J., Wang, D., Drozdov, A., Szabo-Roberts, M., Zhelavskaya, I., Vasile, R., 2022. A new population of ultra-relativistic electrons in the outer radiation zone. J. Geophys. Res.: Space Phys. 127e2021JA030214. https://doi.org/10.1029/2021JA030214.

Shprits, Y.Y., Horne, R.B., Kellerman, A.C., Drozdov, A.Y., 2018a. The dynamics of Van Allen belts revisited. Nat. Phys. 14 (2), 102–103. https://doi.org/10.1038/nphys4350.

Shprits, Y., Subbotin, D., Ni, B., Horne, R., Baker, D., Cruce, P., 2011. Profound change of the near-Earth radiation environment caused by solar superstorms. Space Weather 9, S08007. https://doi.org/10.1029/2011SW000662.

Shprits, Y., Kellerman, A., Kondarashov, D., Subbotin, D., 2013b. Application of a new data operator-splitting data assimilation technique to the 3-D VERB diffusion code and CRRES measurements. Geophys. Res. Lett. 40, 4998–5002. https://doi.org/10.1002/grl.50969.

Shprits, Y.Y., Subbotin, D.A., Meredith, N.P., Elkington, S.R., 2008b. Review of modeling of losses and sources of relativistic electrons in the outer radiation belt II: Local acceleration and loss. J. Atmos. Sol. Terr. Phys. 70 (14), 1694–1713. https://doi.org/10.1016/j.jastp.2008.06.014.

Shprits, Y.Y., Menietti, J.D., Gu, X., Kim, K.C., Horne, R.B., 2012. Gyroresonant interactions between the radiation belt electrons and whistler mode chorus waves in the radiation environments of Earth, Jupiter, and Saturn: A comparative study. J. Geophys. Res. 117, A11216. https://doi.org/10.1029/2012JA018031.

Shprits, Y.Y., Subbotin, D., Drozdov, A., Usanova, M.E., Kellerman, A., Orlova, K., et al., 2013a. Unusual stable trapping of the ultrarelativistic electrons in the Van Allen radiation belts. Nat. Phys. 9 (11), 699–703. https://doi.org/10.1038/nphys2760.

Shprits, Y.Y., Kellerman, A.C., Drozdov, A.Y., Spence, H.E., Reeves, G. D., Baker, D.N., 2015. Combined convective and diffusive simulations: VERB-4D comparison with 17 March 2013 Van Allen Probes observations. Geophys. Res. Lett. 42, 9600–9608. https://doi.org/10.1002/2015GL065230.

Shprits, Y.Y., Vasile, R., Zhelavskaya, I.S., 2019. Nowcasting and predicting the Kp index using historical values and real-time observations. Space Weather 17, 1219–1229. https://doi.org/10.1029/2018SW002141.

Sicard, A., Boscher, D., Bourdarie, S., Lazaro, D., Standarovski, D., Ecoffet, R., 2018. GREEN: the new Global Radiation Earth ENvironment model (beta version). Ann. Geophys. 36, 953–967. https://doi.org/10.5194/angeo-36-953-2018.

Sicard, A., Boscher, D., Lazaro, D., Bourdarie, S., Standarovski, D., Ecoffet, R., 2019. New Model for the Plasma Electrons Fluxes (Part of GREEN Model). IEEE Trans. Nucl. Sci. 66 (7), 1738–1745. https://doi.org/10.1109/TNS.2019.2923005.

Sicard, A., Maget, V., Lazaro, D., Balcon, N., Ecoffet, R., 2022. GREEN upper envelope model for energetic electrons. IEEE Trans. Nucl. Sci. 69 (7), 1533–1540. https://doi.org/10.1109/TNS.2022.3157399.

Sinnhuber, M., Funke, B., 2020. Chapter 9 – Energetic electron precipitation into the atmosphere. In: Jaynes, A.N., Usanova, M.E. (Eds.), The Dynamic Loss of Earth's Radiation Belts, Elsevier, 2020, Pages 279-321, ISBN 9780128133712. https://doi.org/10.1016/B978-0-12-813371-2.00009-3.

Simpson, J.A., 1983. Elemental and Isotopic Composition of the Galactic Cosmic Rays. Annual Review of Nuclear and Particle Science 33 https://doi.org/10.1146/annurev.ns.33.120183.001543.

Slaba, T.C., Whitman, K., 2020. The Badhwar-O'Neill 2020 GCR model. Space Weather 18e2020SW002456. https://doi.org/10.1029/2020SW002456.

Smart, D.F., Shea, M.A., 2001. A comparison of the tsyganenko model predicted and measured geomagnetic cutoff latitudes. Advances in Space Research 28 (12) https://doi.org/10.1016/S0273-1177(01)00539-7.

Smart, D.F., Shea, M.A., 2003. The space-developed dynamic vertical cutoff rigidity model and its applicability to aircraft radiation dose. Advances in Space Research 32 (1) https://doi.org/10.1016/S0273-1177(03)90376-0.

Smart, D.F., Shea, M.A., 2005. A review of geomagnetic cutoff rigidities for Earth-orbiting spacecraft. Adv. Space Res. 36 (10), 2012–2020. https://doi.org/10.1015/j.asr.2004.09.015.

Sorathia, K.A., Ukhorskiy, A.Y., Merkin, V.G., Fennell, J.F., Claudepierre, S.G., 2018. Modeling the depletion and recovery of the outer radiation belt during a geomagnetic storm: Combined MHD and test particle simulations. J. Geophys. Res. Space Phys. 123, 5590–5609. https://doi.org/10.1029/2018ja025506.

Smart, D.F, &Shea, M.A, 2009. Fifty years of progress in geomagnetic cutoff rigidity determinations. Advances in Space Research 44 (10) https://doi.org/10.1016/j.asr.2009.07.005.

Sorathia, K.A., Merkin, V.G., Panov, E.V., Zhang, B., Lyon, J.G., Garretson, J., et al., 2020. Ballooning-interchange instability in the near-Earth plasma sheet and auroral beads: Global magnetospheric modeling at the limit of the MHD approximation. Geophys. Res. Lett. 47e2020GL088227. https://doi.org/10.1029/2020GL088227.

Sorathia, K.A., Michael, A., Merkin, V.G., Ukhorskiy, A.Y., Turner, D. L., Lyon, J.G., Garretson, J., Gkioulidou, M., Toffoletto, F.R., 2021. The role of mesoscale plasma sheet dynamics in ring current formation. Front. Astron. Space Sci. https://doi.org/10.3389/fspas.2021.761875, 8.

Spence, H.E., Caspi, A., Bahcivan, H., Nieves-Chinchilla, J., Crowley, G., Cutler, J., Fish, C.a., Jackson, D., Jorgensen, T.M., Klumpar, D., Li, X., Mason, J.P., Paschalidis, N., Sample, J., Smith, S., Swenson, C.M., Woods, T.N., 2022. Achievements and lessons learned from successful small satellite missions for space weather-oriented research. Space Weather. https://doi.org/10.1029/2021SW003031.

Störmer, C., 1955. The Polar Aurora. Oxford Univ. Press, London, England.

Subbotin, D.A., Shprits, Y.Y., 2012. Three-dimensional radiation belt simulations in terms of adiabatic invariants using a single numerical grid. J. Geophys. Res. 117, A05205. https://doi.org/10.1029/2011JA017467.

Subbotin, D.A., Shprits, Y.Y., Ni, B., 2011. Long-term radiation belt simulation with the VERB 3-D code: Comparison with CRRES observations. J. Geophys. Res. 116, A12210. https://doi.org/10.1029/2011JA017019.

Swiger, B.M., Liemohn, M.W., Ganushkina, N.Y., Dubyagin, S.V., 2022. Energetic electron flux predictions in the near-Earth plasma sheet from solar wind driving. Space Weather 20e2022SW003150. https://doi.org/10.1029/2022SW003150.

Takahashi, N., Seki, K., Fok, M.-C., Zheng, Y., Miyoshi, Y., Kasahara, S., et al., 2021. Relative contribution of ULF waves and whistler-mode chorus to the radiation belt variation during the May 2017 storm. J. Geophys. Res.: Space Phys. 126e2020JA028972. https://doi.org/10.1029/2020JA028972.

Temmer, M., Scolini, C., Richardson, I.G., Heinemann, S.G., Paouris, E., Vourlidas, A., Zhuang, B., 2023. CME propagation through the heliosphere: Status and future of observations and model development. Adv. Space Res. https://doi.org/10.1016/j.asr.2023.07.003.

Tenishev, V., Borovikov, D., Combi, M.R., Sokolov, I., Gombosi, T., 2018. Toward development of the energetic particle radiation nowcast model for assessing the radiation environment in the altitude range from that used by the commercial aviation in the troposphere to LEO, MEO, and GEO, AIAA 2018-3650. 2018 Atmospheric and Space Environments Conference. June 2018, doi: https://doi.org/10.2514/6.2018-3650.

Tenishev, V., Shou, Y., Borovikov, D., Lee, Y., Fougere, N., Michael, A., Combi, M.R., 2021. Application of the Monte Carlo method in modeling dusty gas, dust in plasma, and energetic ions in planetary, magnetospheric, and heliospheric environments. J. Geophys. Res.: Space Phys. 126e2020JA028242. https://doi.org/10.1029/2020JA028242.

Thaller, S., Ripoll, J.-F., Nishimura, T., Erickson, P., 2022. Editorial: Coupled feedback mechanisms in the magnetosphere-ionosphere system. Front. Astron. Space Sci. 9, 1011217. https://doi.org/10.3389/fspas.2022.1011217.

Thorne, R.M., 2010. Radiation belt dynamics: The importance of wave-particle interactions. Geophys. Res. Lett. 37, L22107. https://doi.org/10.1029/2010GL044990.

Thorne, R., Li, W., Ni, B., et al., 2013. Rapid local acceleration of relativistic radiation-belt electrons by magnetospheric chorus. Nature 504, 411–414. https://doi.org/10.1038/nature12889.

Thorne, R.M., O'Brien, T.P., Shprits, Y.Y., Summers, D., Horne, R.B., 2005. Timescale for MeV electron microburst loss during geomagnetic storms. J. Geophys. Res. 110, A09202. https://doi.org/10.1029/2004JA010882.

Tobiska, W.K. et al., 2016. Global real-time dose measurements using the Automated Radiation Measurements for Aerospace Safety (ARMAS) system. Space Weather 14, 1053–1080. https://doi.org/10.1002/2016SW001419.

Tobiska, W.K., Atwell, W., Beck, P., Benton, E., Copeland, K., Dyer, C., Gersey, B., Getley, I., Hands, A., Holland, M., Hong, S., Hwang, J., Jones, B., Malone, K., Meier, M.M., Mertens, C., Phillips, T., Ryden, K., Schwadron, N., Wender, S.A., Wilkins, R., Xapsos, M.A., 2015. Advances in Atmospheric Radiation Measurements and Modeling Needed to Improve Air Safety. Space Weather 13, 202–210. https://doi.org/10.1002/2015SW001169.

Tobiska, W.K., Didkovsky, L., Judge, K., Weiman, S., Bouwer, D., Bailey, J., et al., 2018. Analytical representations for characterizing the global aviation radiation environment based on model and measurement databases. Space Weather 16, 1523–1538. https://doi.org/10.1029/2018SW001843.

Toffoletto, F., Sazykin, S., Spiro, R., et al., 2003. Inner magnetospheric modeling with the Rice Convection Model. Space Sci. Rev. 107, 175–196. https://doi.org/10.1023/A:1025532008047.

Tu, W., Cunningham, G.S., Chen, Y., Henderson, M.G., Camporeale, E., Reeves, G.D., 2013. Modeling radiation belt electron dynamics during GEM challenge intervals with the DREAM3D diffusion model. J. Geophys. Res. Space Phys. 118, 6197–6211. https://doi.org/10.1002/jgra.50560.

Tu, W., Cunningham, G.S., Chen, Y., Morley, S.K., Reeves, G.D., Blake, J.B., Baker, D.N., Spence, H., 2014. Event-specific chorus wave and electron seed population models in DREAM3D using the Van Allen Probes. Geophys. Res. Lett. 41, 1359–1366. https://doi.org/10.1002/2013GL058819.

Tu, W., Li, W., Albert, J.M., Morley, S.K., 2019a. Quantitative assessment of radiation belt modeling. J. Geophys. Res. Space Phys. 124, 898–904. https://doi.org/10.1029/2018JA026414.

Tu, W., Xiang, Z., Morley, S.K., 2019b. Modeling the magnetopause shadowing loss during the June 2015 dropout event. Geophys. Res. Lett. 46, 9388–9396. https://doi.org/10.1029/2019GL084419.

Turner, D.L., Kilpua, E.K.J., Hietala, H., Claudepierre, S.G., O'Brien, T. P., Fennell, J.F., et al., 2019. The response of Earth's electron radiation belts to geomagnetic storms: Statistics from the Van Allen Probes era including effects from different storm drivers. Journal of Geophysical Research: Space Physics 124 (2), 1013–1034 https://doi.org/10.1029/2018JA026066.

Tylka, A.J., Adams, J.H., Boberg, P.R., Brownstein, B., Dietrich, W.F., Flueckiger, E.O., Petersen, E.L., Shea, M.A., Smart, D.F., Smith, E. C., 1997. CREME96: A revision of the cosmic ray effects on microelectronics code. IEEE Trans. Nucl. Sci. 44, 2150–2160. https://doi.org/10.1109/23.659030.

Tyssøy, H.N., Stadsnes, J., 2015. Cutoff latitude variation during solar proton events: Causes and consequences. J. Geophys. Res. 120 https://doi.org/10.1002/2014JA020508.

Usanova, M.E., Drozdov, A., Orlova, K., Mann, I.R., Shprits, Y., Robertson, M.T., et al., 2014. Effect of EMIC waves on relativistic and ultrarelativistic electron populations: Ground-based and Van Allen Probes observations. Geophysical Research Letters 41 (5), 1375–1381 https://doi.org/10.1002/2013GL059024.

Usoskin, I.G., Kovaltsov, G.A., 2021. Mind the gap: New precise 14C data indicate the nature of extreme solar particle events. Geophys. Res. Lett. 48e2021GL094848. https://doi.org/10.1029/2021GL094848.

van Hazendonk, C.M., Heino, E., Jiggens, P.T.A., Taylor, M.G.G.T., Partamies, N., Mulders, H.J.C., 2022. Cutoff latitudes of solar proton events measured by GPS satellites. J. Geophys. Res.: Space Phys. 127e2021JA030166. https://doi.org/10.1029/2021JA030166.

Vette, J. I. (1991). The AE-8 Trapped Electron Model Environment, 91-24, NSSDC/WDC-A-R&S.

Vigorito, C.F., Vernetto, S., Bedogni, R., Calamida, A., Castro Campoy, A.I., Fontanilla, A., Russo, L., Cirilli, S., Miranda, P., Subieta Vasquez, M.A., 2023. SAMADHA neutron spectrum and cosmic ray dose rate measurements at 5200 m in the SAA region. In: 38th International Cosmic Ray Conference (ICRC2023) - Solar & Heliospheric Physics (SH), vol. 444. https://doi.org/10.22323/1.444.1254.

Varotsou, A., Boscher, D., Bourdarie, S., Horne, R.B., Meredith, N.P., Glauert, S.A., Friedel, R.H., 2008. Three-dimensional test simulations of the outer radiation belt electron dynamics including electron-chorus resonant interactions. J. Geophys. Res. 113 https://doi.org/10.1029/2007JA012862.

Vourlidas, A., Turner, D., Biesecker, D., et al., 2023. The NASA Space Weather Science and Observation Gap Analysis. Adv. Space Res. https://doi.org/10.1016/j.asr.2023.06.046.

Wang, D., Shprits, Y.Y., 2019. On how high-latitude chorus waves tip the balance between acceleration and loss of relativistic electrons. Geophys. Res. Lett. 46, 7945–7954. https://doi.org/10.1029/2019GL082681.

Wang, D., Shprits, Y.Y., Zhelavskaya, I.S., Effenberger, F., Castillo, A., Drozdov, A.Y., et al., 2020. The effect of plasma boundaries on the dynamic evolution of relativistic radiation belt electrons. J. Geophys. Res.: Space Phys. 125e2019JA027422. https://doi.org/10.1029/2019JA027422.

Welling, D.T., Jordanova, V.K., Zaharia, S.G., Glocer, A., Toth, G., 2011. The effects of dynamic ionospheric outflow on the ring current. J. Geophys. Res. 116, A00J19. https://doi.org/10.1029/2010JA015642.

Whitman, K., Egeland, R., Richardson, I.G., et al., 2023. Review of Solar Energetic Particle Models. Adv. Space Res. 72 (12). https://doi.org/10.1016/j.asr.2022.08.006.

Wolf, R.A., Spiro, R.W., Sazykin, S., Toffoletto, F.R., Yang, J., 2016. Forty-Seven Years of the Rice Convection Model. In: C.R. Chappell, R.W. Schunk, P.M. Banks, J.L. Burch and R.M. Thorne (Eds.), Magnetosphere-Ionosphere Coupling in the Solar System. https://doi.org/10.1002/9781119066880.ch17.

Wolf, R.A., Harel, M., Spiro, R.W., Voigt, G.-H., Reiff, P.H., Chen, C.-K., 1982. Computer simulation of inner magnetospheric dynamics for the magnetic storm of July 29, 1977. J. Geophys. Res. 87 (A8), 5949–5962. https://doi.org/10.1029/JA087iA08p05949.

Wu, Q., Wang, W., Lin, D., Huang, C., Zhang, Y., 2022. Penetrating electric field simulated by the MAGE and comparison with ICON observation. J. Geophys. Res.: Space Phys. 127e2022JA030467. https://doi.org/10.1029/2022JA030467.

Xapsos, M., Barth, J., Stassinopoulos, E., Burke, E., Gee, G., 1999. Space environmental effects: Model for Emission of Solar Protons (ESP)—Cumulative and worst-case event fluences. Retrieved from https://ntrs.nasa.gov/citations/20000021506.

Xapsos, M., Summers, G., Barth, J., Stassinopoulos, E., Burke, E., 2000. Probability model for cumulative solar proton event fluences. (vol. 47, p. 486–490). https://doi.org/10.1109/23.856469.

Xapsos, M., Summers, G., Burke, E., 1998. Probability model for peak fluxes of solar proton events. IEEE Trans. Nucl. Sci. 45 (6), 2948–2953. https://doi.org/10.1109/23.736551.

Xapsos, M., Stauffer, C., Gee, G., Barth, J., Stassinopoulos, E., McGuire, R., 2004. Model for solar proton risk assessment. IEEE Trans. Nucl. Sci. 51 (6), 3394–3398. https://doi.org/10.1109/TNS.2004.839159.

Xu, W., Marshall, R.A., Tobiska, W.K., 2021. A method for calculating atmospheric radiation produced by relativistic electron precipitation. Space Weather 19e2021SW002735. https://doi.org/10.1029/2021SW002735.

Yang, J., Toffoletto, F.R., Wolf, R.A., Sazykin, S., 2015. On the contribution of plasma sheet bubbles to the storm-time ring current injection. J. Geophys. Res. Space Phys. https://doi.org/10.1029/2015JA021398.

Yasuda, H., Sato, T., Yonehara, H., Kosako, T., Fujitaka, K., Sasaki, Y., 2011. Management of cosmic radiation exposure for aircraft crew in Japan. Radiat. Prot. Dosim. 146, 123–125. https://doi.org/10.1093/rpd/ncr133.

Yasuda, H., Yajima, K., Sato, T., 2020. Investigation of using a long-life electronic personal dosimeter for monitoring aviation doses of frequent flyers. Radiat. Meas. 134 (2020), 106309. https://doi.org/10.1016/j.radmeas.2020.106309.

Young, S.L., Kress, B.T., 2016. How accurately can we map SEP observations using L*? American Geophysical Union, Fall General Assembly 2016, abstract id.SM11C-2160, 2016AGUFMSM11C2160Y.

Young, S., Alcala, C., Puhl-Quinn, P., Jeffries, T., 2021. Analysis of a Simple Liouville Theory Based Approach to SEP Hazard Specification, AGU Fall Meeting 2021, held in New Orleans, LA, 13-17 December 2021, id. SM45C-2280. Bibcode: 2021AGUFMSM45C2280Y.

Yu, Y., Jordanova, V.K., Ridley, A.J., Albert, J.M., Horne, R.B., Jeffery, C.A., 2016. A new ionospheric electron precipitation module coupled with RAM-SCB within the geospace general circulation model. J.

Geophys. Res. Space Phys. 121, 8554–8575. https://doi.org/10.1002/2016JA022585.

Yu, Y., Liemohn, M.W., Jordanova, V.K., Lemon, C., Zhang, J., 2019a. Recent advancements and remaining challenges associated with inner magnetosphere cross-energy/population interactions (IMCEPI). J. Geophys. Res. Space Phys. 124, 886–897. https://doi.org/10.1029/2018JA026282.

Yu, Y., Rastätter, L., Jordanova, V.K., Zheng, Y., Engel, M., Fok, M.-C., Kuznetsova, M.M., 2019b. Initial results from the GEM challenge on the spacecraft surface charging environment. Space Weather 17. https://doi.org/10.1029/2018SW00203.

Yu, Y., Cao, J., Pu, Z., et al., 2022. Meso-scale electrodynamic coupling of the earth magnetosphere-ionosphere system. Space Sci. Rev. 218, 74. https://doi.org/10.1007/s11214-022-00940-0.

Yue, C., Chen, L., Bortnik, J., Ma, Q., Thorne, R.M., Angelopoulos, V., Spence, H.E., 2017. The characteristic response of whistler mode waves to interplanetary shocks. J. Geophys. Res. Space Phys. 122, 10047–10057. https://doi.org/10.1002/2017JA024574.

Yue, C., Bortnik, J., Li, W., Ma, Q., Wang, C.-P., Thorne, R.M., et al., 2019. Oxygen ion dynamics in the Earth's ring current: Van Allen Probes observations. J. Geophys. Res. Space Phys. 124, 7786–7798. https://doi.org/10.1029/2019JA026801.

Zhang, B., Brambles, O.J., 2021. Polar Cap O+ Ion Outflow and Its Impact on Magnetospheric Dynamics. American Geophysical Union (AGU), pp. 83–114. Chap. 5. https://doi.org/10.1002/9781119815617.ch5.

Zhang, X.-J., Angelopoulos, V., Mourenas, D., Artemyev, A., Tsai, E., Wilkins, C., 2022a. Characteristics of electron microburst precipitation based on high-resolution ELFIN measurements. J. Geophys. Res.: Space Phys. 127e2022JA030509. https://doi.org/10.1029/2022JA030509.

Zhang, X.-J., Artemyev, A., Angelopoulos, V., Tsai, E., Wilkins, C., Kasahara, S., Mourenas, D., Yokota, S., Keika, K., Hori, T., Miyoshi, Y., Shinohara, I., 2022b. Ayako Matsuoka, Superfast precipitation of energetic electrons in the radiation belts of the Earth. Nat. Commun. 13 (1). https://doi.org/10.1038/s41467-022-29291-8.

Zhang, B., Sorathia, K.A., Lyon, J.G., Merkin, V.G., Garretson, J.S., Wiltberger, M., 2019. Gamera: A three-dimensional finite-volume Mhd solver for non-orthogonal curvilinear geometries. ApJS 244, 20. https://doi.org/10.3847/1538-4365/ab3a4c.

Zhao, H., Li, X., Baker, D.N., Claudepierre, S.G., Fennell, J.F., Blake, J. B., Larsen, B.A., Skoug, R.M., Funsten, H.O., Friedel, R.H.W., et al., 2016. Ring current electron dynamics during geomagnetic storms based on the Van Allen Probes measurements. J. Geophys. Res. Space Phys. 121, 3333–3346. https://doi.org/10.1002/2016JA022358.

Zhao, H., Baker, D.N., Li, X., Malaspina, D.M., Jaynes, A.N., Kanekal, S.G., 2019a. On the acceleration mechanism of ultrarelativistic electrons in the center of the outer radiation belt: A statistical study. J. Geophys. Res. Space Phys. 124, 8590–8599. https://doi.org/10.1029/2019JA027111.

Zhao, H., Ni, B., Li, X., Baker, D.N., Johnston, W.R., Zhang, W., et al., 2019b. Plasmaspheric hiss waves generate a reversed energy spectrum of radiation belt electrons. Nat. Phys. 15 (4), 367–372. https://doi.org/10.1038/s41567-018-0391-6.

Zhelavskaya, I.S., Aseev, N.A., Shprits, Y.Y., 2021. A combined neural network- and physics-based approach for modeling plasmasphere dynamics. J. Geophys. Res.: Space Phys. 126e2020JA028077. https://doi.org/10.1029/2020JA028077.

Zhelavskaya, I., Shprits, Y.Y., Spasojević, M., 2017. Empirical modeling of the plasmasphere dynamics using neural networks. J. Geophys. Res. Space Phys. 122 (11), 11227–11244. https://doi.org/10.1002/2017JA024406.

Zheng, Y., 2013. Improving CME forecasting capability: An urgent need. Space Weather 11, 641–642. https://doi.org/10.1002/2013SW001004.

Zheng, Y., Fok, M.-C., Khazanov, G.V., 2003. A radiation belt-ring current forecasting model. Space Weather 1 (3), 1013. https://doi.org/10.1029/2003SW000007.

Zheng, Y., Zhang, Y., Kozyra, J.U., Albert, J., Bortnik, J., Gallagher, D. L., Kessel, R.L., 2009. Toward an integrated view of inner magnetosphere and radiation belts. J. Atmos. Sol.-Terrestr. Phys. 71 (16), 1613. https://doi.org/10.1016/j.jastp.2009.04.013.

Zheng, Y., Kuznetsova, M.M., Pulkkinen, A.A., Maddox, M.M., Mays, M.L., 2015. Research-based monitoring, prediction, and analysis tools of the spacecraft charging environment for spacecraft users. IEEE Trans. Plasma Sci. 43 (11), 3925–3932. https://doi.org/10.1109/TPS.2015.2479575.

Zheng, Y., Ganushkina, N.Y., Jiggens, P., Jun, I., Meier, M., Minow, J.I., et al., 2019. Space radiation and plasma effects on satellites and aviation: Quantities and metrics for tracking performance of space weather environment models. Space Weather 17, 1384–1403. https://doi.org/10.1029/2018SW002042.

Zheng, Y., Xapsos, M., Jun, I., O'Brien, T.P., Parker, L., Kim, W., Rowland, D., 2023. Recommending low-cost compact space environment and space weather effects sensor suites for NASA missions. Bull. AAS 55 (3). https://doi.org/10.3847/25c2cfeb.be388308.

Zhou, R., Ni, B., Fu, S., Teng, S., Tao, X., Hu, Z., et al., 2022. Global distribution of concurrent EMIC waves and magnetosonic waves: A survey of Van Allen Probes observations. J. Geophys. Res.: Space Phys. 127e2021JA030093. https://doi.org/10.1029/2021JA030093.

Zong, Q.-G., 2022. Magnetospheric response to solar wind forcing: ultra-low-frequency wave–particle interaction perspective. Ann. Geophys. 40, 121–150. https://doi.org/10.5194/angeo-40-121-2022.

Zong, Q., Rankin, R., Zhou, X., 2017. The interaction of ultra-low-frequency Pc3-5 waves with charged particles in Earth's magnetosphere. Rev. Mod. Plasma Phys. 1, 10. https://doi.org/10.1007/s41614-017-0011-4.

Zong, Q.-G., Yue, C., Fu, S.-Y., 2021. shock induced strong substorms and super substorms: Preconditions and associated oxygen ion dynamics. Space Sci. Rev. 217 (2). https://doi.org/10.1007/s11214-021-00806-x.

Oak Ridge National Laboratory (ORNL). Monte Carlo N-Particle Transport Code System for Multiparticle and High Energy Applications (MCNPX 2.7.0) RSICC code package C740 (2011), developed at Los Alamos National Laboratory (available from the Radiation Safety Information Computational Center at ORNL, Oak Ridge, TN).

ESA, 2020. ECSS-E-ST-10-04C Rev.1 – Space environment (15 June 2020) | European Cooperation for Space Standardization (No. ECSS-E-ST-10-04C Rev.1).